



University of HUDDERSFIELD

University of Huddersfield Repository

Thwaites, Laura Elizabeth Anne

A comparison of microwave and induction heating in the study of complex metal oxides

Original Citation

Thwaites, Laura Elizabeth Anne (2020) A comparison of microwave and induction heating in the study of complex metal oxides. Masters thesis, University of Huddersfield.

This version is available at <http://eprints.hud.ac.uk/id/eprint/35334/>

The University Repository is a digital collection of the research output of the University, available on Open Access. Copyright and Moral Rights for the items on this site are retained by the individual author and/or other copyright owners. Users may access full items free of charge; copies of full text items generally can be reproduced, displayed or performed and given to third parties in any format or medium for personal research or study, educational or not-for-profit purposes without prior permission or charge, provided:

- The authors, title and full bibliographic details is credited in any copy;
- A hyperlink and/or URL is included for the original metadata page; and
- The content is not changed in any way.

For more information, including our policy and submission procedure, please contact the Repository Team at: E.mailbox@hud.ac.uk.

<http://eprints.hud.ac.uk/>

A comparison of microwave and induction heating in the study of
complex metal oxides

by

Laura Elizabeth Anne Thwaites



University of
HUDDERSFIELD

A thesis submitted to the University of Huddersfield in partial
fulfilment of the requirements for the degree of Master of
Philosophy

Department of Chemical Sciences
The University of Huddersfield

January 2020

Copyright Statement

- i. The author of this thesis (including any appendices and/ or schedules to this thesis) owns any copyright in it (the “Copyright”) and s/he has given The University of Huddersfield the right to use such Copyright for any administrative, promotional, educational and/or teaching purposes.
- ii. Copies of this thesis, either in full or in extracts, may be made only in accordance with the regulations of the University Library. Details of these regulations may be obtained from the Librarian. Details of these regulations may be obtained from the Librarian. This page must form part of any such copies made.
- iii. The ownership of any patents, designs, trademarks and any and all other intellectual property rights except for the Copyright (the “Intellectual Property Rights”) and any reproductions of copyright works, for example graphs and tables (“Reproductions”), which may be described in this thesis, may not be owned by the author and may be owned by third parties. Such Intellectual Property Rights and Reproductions cannot and must not be made available for use without permission of the owner(s) of the relevant Intellectual Property Rights and/or Reproductions.

Contents

Acknowledgments.....	6
Abstract	7
Chapter 1	9
1.0. Introduction	9
1.1 Thermal analysis	9
1.1.1. Current methods of Thermal analysis.....	9
1.1.2 Microwave Thermal Analysis (MWTA).....	10
1.1.3 Microwave Heating.....	11
1.1.4 Multi-mode cavities	14
1.1.5 Single mode cavities	16
1.2 Induction Heating (IH).....	17
1.2.1 Introduction	17
1.2.2 Induction heating in industry.....	19
1.3 Materials to be investigated	20
1.3.1 Rock salt (Halite).....	20
1.3.2 Transition Metal oxides (TMOs)	21
1.3.3 Perovskites	22
1.3.4 Double perovskites.....	25
1.3.5 Disordered and tilted perovskite structures	27
1.4 Dielectrics.....	28
1.5 Electrical and magnetic properties.....	29
1.5.1 Ferro- and ferrimagnetism.....	30
1.5.2 Para- and Diamagnetism.....	31
1.6 Magnetic and electrical properties of perovskite systems	32
1.6.1 Behaviour of perovskites	32
1.6.2 Electron Doping of perovskites.....	34
1.7 Objectives	35
Chapter 2.....	37
2.0 Experimental.....	37
2.1 Sample Synthesis.....	37
2.1.1 NiO-MgO solid solution	37
2.1.2 $\text{Sr}_2\text{FeMo}_{1-x}\text{W}_x\text{O}_6$	37
2.1.3 $\text{Sr}_{2-x}\text{La}_x\text{FeMoO}_6$	38
2.1.4 $\text{Sr}_2\text{CrMo}_{1-x}\text{W}_x\text{O}_6$	39
2.2 Characterisation of synthesised compounds.....	41
2.2.1 NiO-MgO solid series	41
2.2.2 $\text{Sr}_2\text{FeMo}_{1-x}\text{W}_x\text{O}_6$	43
2.2.3 $\text{Sr}_{2-x}\text{La}_x\text{FeMoO}_6$	46

2.2.4 Sr ₂ CrMo _{1-x} W _x O ₆	47
Chapter 3.....	48
3.0 Thermal methods of analysis	48
3.1 Thermogravimetric Analysis (TGA).....	48
3.2 Differential Thermal Analysis (DTA).....	48
3.3. Differential Scanning Calorimetry (DSC).....	49
3.4. Microwave Thermal Analysis (MWTA).....	50
3.2.1 Microwave heating	51
3.2.2 Microwave heating theory	51
3.4. Induction heating	54
3.4.1. Introduction	54
3.4.2 Theory of Induction heating.....	54
Chapter 4.....	56
4.0 Instrumentation	56
4.1 Non-thermal methods of characterisation	56
4.1.1 X-ray	56
4.1.2 X-ray Powder Diffraction (XRPD)	56
4.2 Microwave (MW).....	58
4.2.1 MWTA basic cells	58
4.2.2 New MWTA cells for E- and H- analysis.....	59
4.3 Explanation of microwave thermogram.....	61
4.3.1 MWTA method development.....	67
4.3.2 Limitations.....	68
4.4. Induction heater (IH).....	68
4.4.1. Introduction	68
4.4.2 Induction heater for thermal analysis.....	68
4.4.3 IHTA Sample holder development.....	70
4.4.4 IHTA Method development.....	72
Chapter 5.....	76
5.0 Results and Discussion.....	76
5.1 MWTA Introduction.....	76
5.2 Preparation.....	76
5.3 MWTA initial testing.....	76
5.4 Metal oxide microwave susceptibility.	78
5.5. Specific Metal Oxides	82
5.5.1 Nickel Oxide (NiO)	82
5.5.2 Manganese Oxide (MnO)	85
5.5.3 Zinc Oxide (ZnO)	86
5.5.4 Magnesium oxide (MgO).....	88
5.6 Comparison of metal oxides.	90

5.7 Induction Heater	93
5.7.1 Introduction	93
5.7.2 Explanation of Induction thermogram	93
5.7.3 IHTA standards – Iron oxides	97
5.8 IHTA of Metal Oxides	99
5.8.1 Nickel Oxide (NiO)	100
5.8.2 Copper Oxide (CuO)	101
5.8.3 Manganese oxide (Mn ₂ O ₃ and MnO ₂)	101
5.8.4 Lead oxide, zirconium dioxide and titanium dioxide (PbO, ZrO ₂ and TiO ₂)	102
5.9 Ni _{1-x} Mg _x O Rock salt	103
5.10 Perovskites (ABX ₃)	104
5.10.1 MWTA	104
5.10.2 IHTA Perovskites (ABX ₃)	110
5.11 Double Perovskites (ABB'X ₆)	112
5.11.1 MWTA Sr ₂ FeMo _{1-x} W _x O ₆	112
5.11.2 Sr ₂ CrMo _{1-x} W _x O ₆	115
5.11.3 Sr _{2-x} La _x FeMoO ₆	118
5.12 IHTA	121
5.12.1 Sr ₂ FeMo _x W _{1-x} O ₆	121
5.12.2 Sr ₂ CrMo _{1-x} W _x O ₆ series	124
5.12.3 Sr _{2-x} La _x FeMoO ₆	127
Chapter 6	132
6.0 Conclusions and Further Work	132
6.1 Conclusion	132
6.1.1 MWTA	132
6.1.2 IHTA	132
6.2 Further work	133
7.0 References	136

Acknowledgments

I would like to thank my supervisors, Dr. Lisa J. Gillie and Dr. Gareth M.B. Parkes for their continued patience while I have completed this thesis. They have been continually supportive throughout this research and have fought especially hard for me to be able to complete the work. Thanks also go to Gage Ashton for his help with the electronic side to the research and the technical drawings for the instrumentation.

I also thank my family, Mark has been a rock from the moment I decided to go to University and especially throughout my PhD. Always pushing me on and motivating me to continue, even when I thought I had given everything, he always found the extra push I needed. My children, Elizabeth, William and the newest member, Meredith, for making me realise that anything is possible, and for cheering me up when things didn't quite go to plan. My parents, for always being supportive and proud, every step of the way.

Recognition goes to all the other Postgraduates and Postdocs with whom I shared an office with during my time as a PhD student, in particular Dr. Rebecca Fennessy, Dr Alessandro Sinopoli, Dr. Baljinder Uppal and Dr. Samantha Bullock, without whom I would not have got this far.

To all I have mentioned, and to those I have not, from the bottom of my heart, Thank you.

Abstract

Although microwave and induction (magnetic) heating are widely used in industry, their potential as a tool for thermal analysis has not been fully studied. Microwave thermal analysis (MWTA), which uses a frequency of 2.45 GHz and was partly developed at the University of Huddersfield, has been successfully applied to a range of materials but research in this area has focussed primarily on the electrical (E-field) component of the electromagnetic wave with the magnetic component (H-field) being less studied. There is little previous research in the use of induction heating (utilising alternating magnetic fields at a frequency of around 150 kHz) for thermal analysis.

This work describes the adaptations made to the existing MWTA to allow for controlled magnetic heating and the development of IHTA (Induction Heating Thermal Analysis). The techniques were applied to a selection of compounds from simpler metal oxides to complex perovskite systems which were synthesised and characterised as part of this research.

The metal oxides and perovskite systems used were purchased from Sigma Aldrich and Fischer. The more complex systems (double perovskites) were synthesised *via* either a solid solution (dissolution in solvent) route or solid-state route (grinding with acetone) and then calcined at high temperatures. These are discussed in detail in Chapter 2. Chapter 3 outlines the changes made to the MWTA instrument and the development of the IHTA including sample cells available.

Chapters 4 and 5 discuss the results of this research. The instrumentation and method development are discussed in Chapter 4. Chapter 5 discusses how the adaptations made to the existing MWTA were successful and magnetic heating can be seen in several of the samples. This informed the decision of which samples were most likely to heat within the IHTA instrument. The IHTA showed promising results with numerous samples, as magnetic heating was evident, although some samples that had coupled well on the MWTA showed negligible coupling with the IHTA, suggesting a difference in the manner of heating taking place.

The simpler metal oxides behaved in a similar manner on both the MWTA and the IHTA and these were also used for Curie point determination and, in the case of $\text{Fe}_2\text{O}_3/\text{Fe}_3\text{O}_4$, the initial testing for percentage composition. It was also discovered that with manganese oxides, Mn_2O_3 heated better in the IHTA than the microwave, while MnO_2 heated better in the MWTA. This also lends itself to the conclusion that another type of interaction is taking place, as it is possible the E-field in the MWTA may contribute to the coupling of the sample.

The $\text{Sr}_{2-x}\text{La}_x\text{FeMoO}_6$ samples show similar power profiles, suggesting that even though the MWTA and IHTA have different input powers (2.45 GHz and 125kHz respectively), the power required to heat the samples increases at a similar rate throughout each experiment. This may allow the user to directly compare the two thermograms.

The results indicate that IHTA has the potential to be used as a complimentary thermal analysis technique alongside DSC/DTA and MWTA and is particularly suitable for materials that exhibit major changes in magnetic properties such as Curie points. However, the approach is still in its infancy and more work, particularly surround characterisation of Curie temperatures is still required. Further analysis into the more complex perovskite systems with current techniques to observe similar changes with the IHTA would be beneficial for development of the instrumentation.

Chapter 1

1.0. Introduction

Current methods for investigating magnetic and electrical properties of various compounds are expensive. The SQUID (super-conducting quantum interference device) magnetometer, used to measure extremely subtle magnetic fields, is an expensive instrument to purchase and to continue to run, which makes it inaccessible to many academic institutions and small companies within industry. Departments that do have access to this type of instrument can charge researchers from other companies or institutions to enable them to investigate their samples, which is also an expense that many researchers cannot warrant spending. The magnetic behaviour may be subtle, which prevents researchers gaining a preliminary insight as to whether it would be pertinent to send their samples for testing. In addition to magnetic field testing, impedance spectroscopy measures the dielectric properties of a material as a function of frequency. While this instrumentation is relatively accessible for most users it can be time consuming and there may not be any conductivity to measure. The aim of this thesis is to investigate the potential of novel instrumentation to measure magnetic and electrical properties of functional ceramic materials, while allowing these instruments to be accessible for more users. To help validate this instrumentation, various ceramic materials with well characterised properties have been examined. These materials consist of metal oxides, rock salt solid solution series, perovskites and double perovskites. The structure and properties of these materials increases in complexity, and they were specifically chosen because of their magnetic and electrical properties. It is also hoped it will be possible to track changes in properties using these instruments.

1.1 Thermal analysis

Thermal analysis is the measure of physical properties of a sample as a function of temperature. The simplest method is thermogravimetry – measuring the change in mass of a sample as a function of temperature. There are many commercially available instruments for thermal analysis, all encompassing different techniques. This thesis examines the use of a new method of thermal analysis – Induction Heating Thermal Analysis (IHTA) and also the adaptations of Microwave Thermal Analysis (MWTA) to examine the magnetic and electrical properties of functional ceramic materials.

1.1.1. Current methods of Thermal analysis

Current methods of thermal analysis include, differential thermal analysis (DTA), differential scanning calorimetry (DSC) and thermogravimetric analysis (TGA). DTA and DSC are both closely related methods. DTA measures a temperature difference between a sample and a thermally inert reference sample, when they are heated under the same program. There

are two methods of DSC: power compensation, where the sample and reference are kept at the same temperature and the heat added, which compensates for heat loss or gain due to an exothermic or endothermic reaction, is recorded. With heat flux, the same rate of heating is applied to both the reference and the sample and the difference in heat flow from the furnace is proportional to the temperature difference between them. TGA measures the mass of a sample as a function of temperature and is one of the most commonly used methods of thermal analysis.¹⁻³ These methods of thermal analysis are further discussed in Chapter 3.

1.1.2 Microwave Thermal Analysis (MWTA)

Microwaves are electromagnetic waves in the frequency band from 300 MHz (3×10^8 cycles s^{-1}) to 300 GHz (3×10^{11} cycles s^{-1}). 1 GHz to 30 GHz is used for radar and telecommunications industries. In order to prevent interference, industrial and domestic microwave heaters usually operate at 900 MHz or 2.45 GHz.⁴ Industrial microwave processing is performed at frequencies set aside for this particular use, specifically 915 MHz, 2.45 GHz, 5.8 GHz and 24.124 GHz.⁵

Electromagnetic waves and therefore microwaves, were first discovered by Hertz in 1888.⁶ The existence of an electromagnetic wave system had previously been theorised by Maxwell in 1864, which later became known as Maxwell's Equations, and it was upon this work that Hertz was able to prove the existence of the electromagnetic wave. Fig. 1.1 Depicts the current electromagnetic spectrum

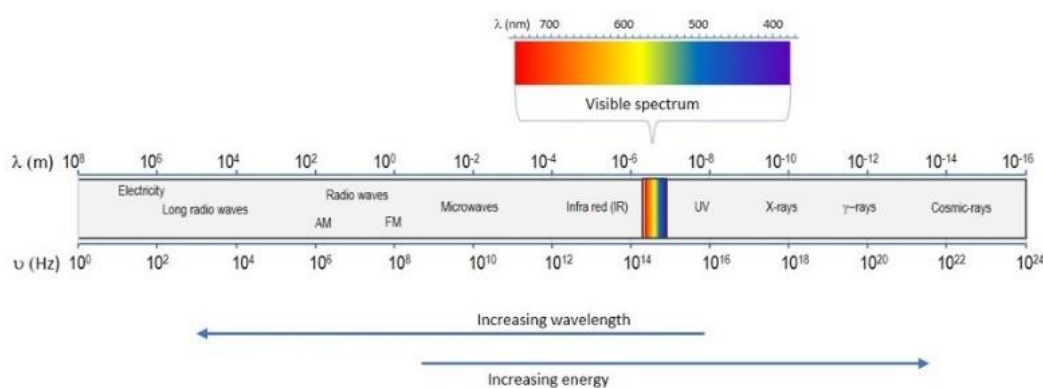


Fig.1.1 Current electromagnetic spectrum

During experiments performed in 1935,⁷ it was discovered that radio waves could be bounced off aircraft and the echo picked up by a receiving station. This enabled the determination of the bearing and distance of the aircraft. This technology was henceforth known as RAdio Detection And Ranging system, more commonly known by its acronym –

RADAR. RADAR was instrumental in the Allied victory of the Second World War, but due to lack of resources, Britain struggled to produce the amount of magnetron tubes needed for the war effort. A contract with Raytheon, USA, was awarded for them to supply the magnetrons.⁸

Raytheon engineer, Percy Spencer discovered microwave cooking by accident when a chocolate bar, which was in his pocket, began to melt when he was in front of an active magnetron.⁹ A further experiment using popcorn kernels followed, and when they popped in the bag while held in front of the magnetron, a new appliance was soon on its way.

1.1.3 Microwave Heating

When a material directly interacts with electromagnetic energy, microwave heating is the result. There are several parameters that determine the magnitude to which a material is heated by microwave energy, the most important are the dielectric properties of the material.¹⁰ Polar liquids are readily heated *via* frictional heating which is shown in fig 1.2. Frictional heating occurs when polar molecules, such as H₂O, attempt to follow the electromagnetic (EM) field. The constant movement of the molecules as the dipoles attempt to realign themselves with the EM-field causes heating of the sample. Materials such as silica glass are relatively transparent to microwaves, therefore no heating occurs. Microwave heating can have many benefits over conventional heating for suitable systems, such as rapid heating and cooling (the thermal lag is avoided), temperature gradients across the sample may be reduced and in some cases, enhanced reaction times.¹¹

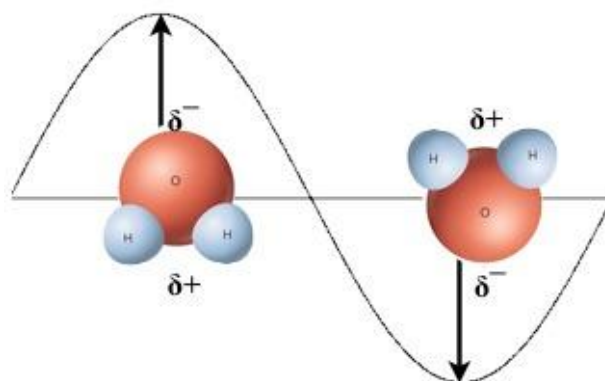


Fig. 1.2 The rotation of water molecules under the influence of the electric field component in an electromagnetic wave. (Black arrows represent electric field.)¹²

Another form of microwave heating is known as Ohmic heating, and occurs within a solid, where there are no polar liquid groups. The electrons (charge carriers) are dragged through the material as they try to follow the alternating EM field (Fig.1.3). This results in the sample being heated. In order for Ohmic heating to occur, the dielectric properties of the material are important. If the microwaves do not affect the material so that the electrons are moved through it, no heating will occur. The distance the charges are moved is dependant on the material, as the resistance of the material is what allows heating to occur – the higher the resistance, the harder it is for a current to flow and the more heat is produced.¹³

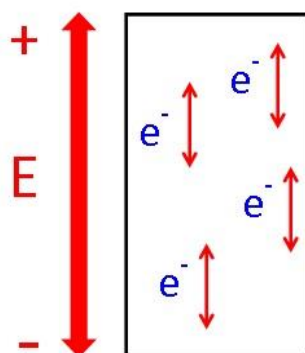


Fig. 1.3 Visual representation of Ohmic heating. The electrons are dragged back and forth within the material trying to follow the alternating field.

Dielectric materials are insulators that have a high polarisability (further detail in section 3.2.2.1 pg. 53) when subjected to an electric field. This determines the response of a material when an external field is applied. When a material is subjected to microwave radiation, the extent to which it heats depends on the dielectric constant (ϵ') and the dielectric loss factor (ϵ'').¹⁴ Dielectric properties will be discussed in more detail in section 1.3.

A number of studies¹⁵⁻²⁴ have investigated the use of microwaves for both analytical and synthetic purposes. A selection of these studies, encompassing topics as varied as drying of materials to measuring dielectric losses, are discussed below. These studies also highlight previous research using microwaves and they have specifically investigated different metal oxides, which leads on to the research discussed in this thesis. As early as the 1960s, microwaves were being utilised as a form of analysis into the properties of different materials. Rupprecht and Bell¹⁵ used microwaves to look at the microwave losses in pure and doped SrTiO₃, as a function of frequency and temperature. The frequency range being used at that time was between 3 and 36 kMc s⁻¹(Kilo-Mega-cycles/second), which equates to 3 – 36 GHz. It was found that temperature and frequency had a large effect on SrTiO₃, especially when there were lattice imperfections within the structure. These lattice

imperfections improved with annealing (calcining) temperature (as expected) and were found to directly affect the microwave losses in the experiment *i.e.* as lattice imperfections decreased, the loss tangent ($\tan\delta$) also decreased.

Research by Standish¹⁶ focussed on the effects of particle size on the heating and drying, using microwave energy, of different oxides. Al_2O_3 and Fe_3O_4 were both studied, and it was discovered that the drying of Al_2O_3 was influenced by the particle size, with the fine particle size heating better than the coarse particles. For Fe_3O_4 , the drying was independent of both particle size and moisture content. However, coarse samples heated better than fine samples, the exact opposite of the Al_2O_3 sample. Crane *et al.*²⁰ also investigated how particle size affected microwave coupling with metals and metal oxides, using Al metal and Fe_2O_3 in the micron and submicron range. Two different particle sizes of each substance were heated in a microwave at a frequency of 3.3 GHz, for 60 seconds each. The temperature change was recorded after the 60 seconds. It was discovered that reducing the particle size of Fe_2O_3 enhanced microwave absorption as a result of the increased surface area, whereas with Al metal, reduced particle size reduced microwave absorption. The ratio of particle radius to skin depth has increased significance than particle size alone for conductive materials, but for the non-metal oxides, the increase in the effective conductivity and surface area in microwave absorption are an important parameter.²⁰ The distance from the exterior to the electromagnetic field, to the point where the field strength reduces to 36.8% of its value at the surface is known as skin depth, or penetration depth (as described by Crane *et al.*).

The focus of research by Tanaka *et al.*^{17,18} was microwave heating in the magnetic component of the electromagnetic field, which is of interest for this research. The work was theoretical but it was found that Fe_3O_4 should heat well in the H-field (magnetic field) as it is highly magnetic. Tanaka theorised that the heating taking place would be in response to the magnetisation to microwaves originating from electron spins residing in the unfilled 3d shell. It was also postulated that heating would continue above the T_C , as each electron spin would still be able to respond to the alternating H-field.^{17,18} Hayashi *et al.*¹⁹ studied this very theory experimentally, investigating Fe_3O_4 in both the E-field (electrical field) and H-field of the electromagnetic wave. The researchers examined particle size and relative density of the Fe_3O_4 . It was found that the microwave absorption increased as the relative density increased, but that the absorption was not dependent on the particle size. The notion that there should be a difference between heating in the E-field maximum and H-field maximum seemed to be inconclusive.

In 1985, Karmazsin *et al.*²¹ used microwaves for thermal analysis. Using differential thermal analysis (DTA), Karmazsin found that it was possible to study even weakly absorbing materials such as CaSO₄, as phase changes were evident. The research also showed that dehydration peaks could be observed with CaHPO₄·2H₂O, and that this occurred at lower temperatures than conventional heating. With thermodilatometry, this was also the case, where previously unnoticed phase changes could be seen when using the microwave. The changes were also much more evident than in differential thermal analysis.^{21,22} Parkes *et al.*²³ have also investigated microwaves for thermal analysis. Using a single-mode wave guide and a frequency of 2.45 GHz, different heating modes were used to analyse materials known to undergo a phase change. The research showed that when compared to a conventional thermal analysis, DSC, the temperature profiles obtained from the MWTA instrument were very similar to analysis using DSC. The constant power mode allows a fixed power level between 0 and 300 W, and the sample temperature is measured as a function of time. The linear power mode allows the power ramp at a preset rate (e.g. 2 W min⁻¹). This method monitors sample temperature as a function of power. With the linear heating method, the power is altered to maintain a preset heating rate. Ramp rates, either heating or cooling can be set. Like Karmazsin, Parkes *et al.*^{23,24} found that melting, dehydration and other phase changes could be observed using the aforementioned methods.

The Parkes microwave thermal analysis instrumentation will be discussed further in Chapter 3.

1.1.4 Multi-mode cavities

A cavity contains the microwaves during heating and there are two widely used cavities; the most common is the multi-mode cavity which is used in domestic microwave ovens. These work by launching microwaves along a short waveguide, into the path of a stirrer which reflects the waves onto the sides of the cavity. The cavity walls are metal, and the waves are randomly reflected onto the object to be heated. With domestic microwave ovens the object is usually rotated to increase the chances of the object interacting with the waves (fig. 1.4).²⁵

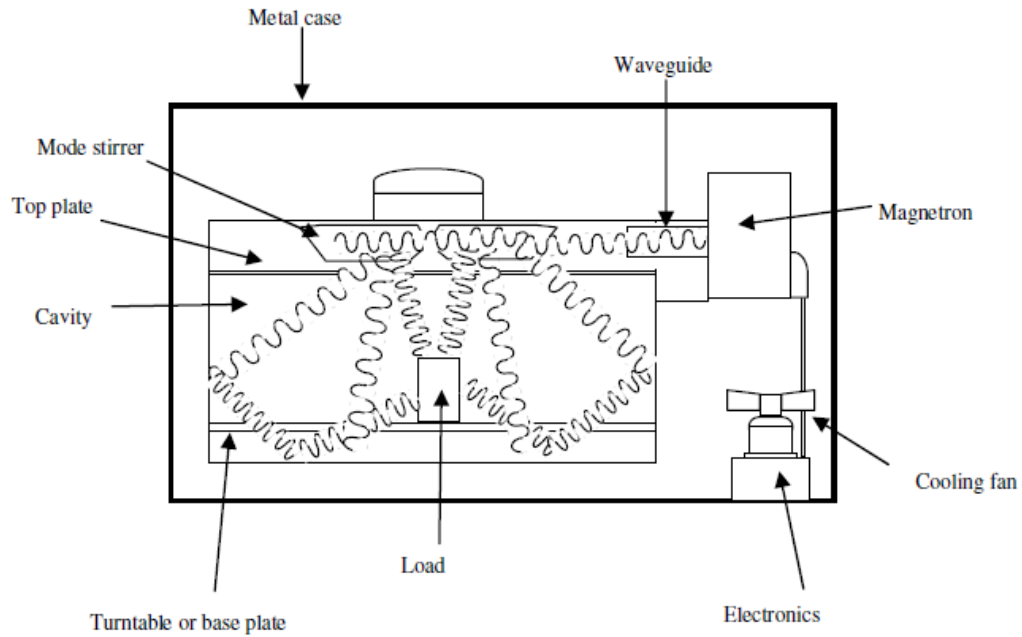


Fig. 1.4 Cross section of a multi-mode cavity (domestic microwave).²⁵

Domestic microwave ovens usually have simple power controls which have on/off cycles in seconds and are based on pulse modulation. The power cannot be adjusted rapidly or accurately enough for thermal analysis due to the inconsistent interaction of the wave and sample, along with the time between switching cycles.²⁵ The second cavity utilised in microwave heating is the single mode cavity which is discussed in more depth in section 1.1.5 over leaf.

1.1.5 Single mode cavities

Unlike a multimode cavity, a single mode cavity forces a dominant wave to propagate. The result of this is that set points of maxima and minima are formed. The advantage of this is that it allows an object to constantly interact with the wave as it can always be placed in the position of the propagating waves' maximum.⁵ A schematic of a single mode cavity microwave is shown in fig.1.5

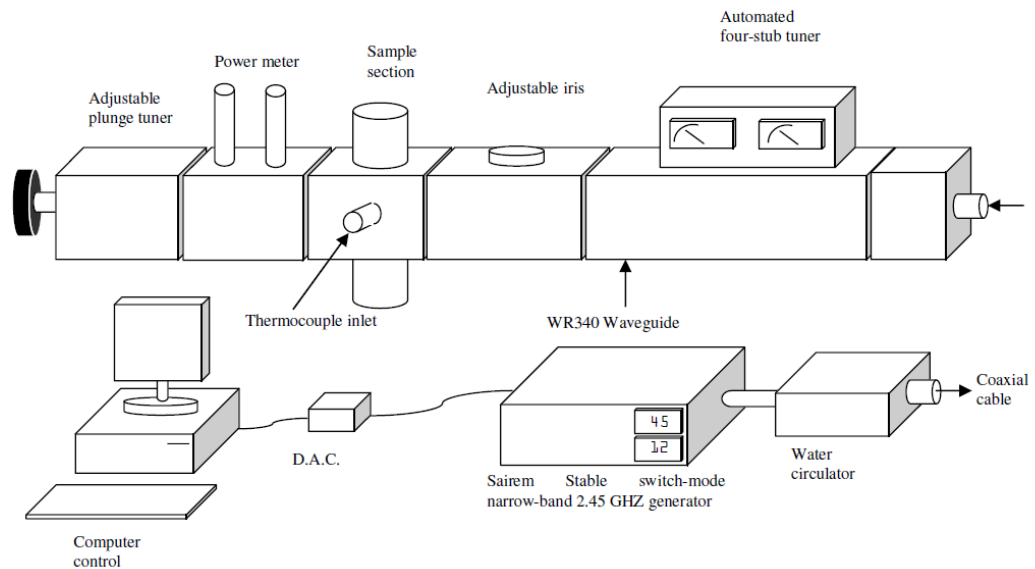


Fig. 1.5 Schematic of single mode cavity MWTA equipment²⁵.

The electric component (E_y) and magnetic component (H_x) are perpendicular to each other, which is the case for all EM waves, with both being in phase. An illustration of an EM wave is shown in fig. 1.6.

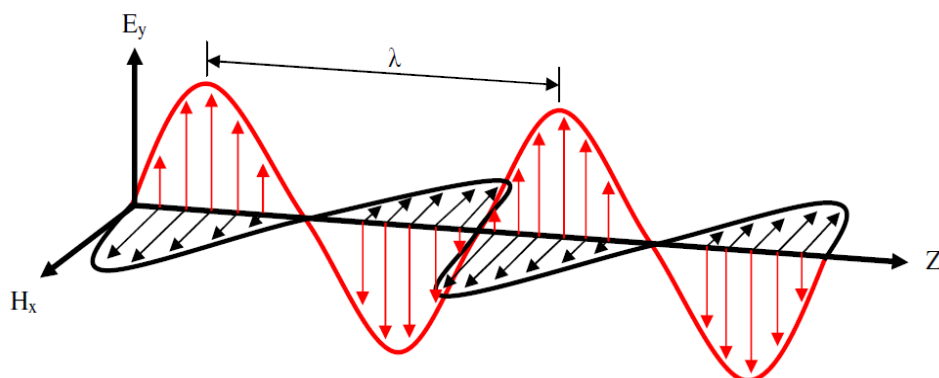


Fig. 1.6 Electromagnetic propagation – E_y the electrical component along the y-axis, H_x , the magnetic component along the x-axis, direction of propagation along the z-axis, and λ is the wavelength.²⁵

In a rectangular waveguide, the electromagnetic radiation is polarised with the electric field strongest in the centre, and the magnetic field strongest near the edges of the waveguide, seen in fig.1.7. This phenomenon is further discussed in Chapter 3 as the precise location of the E- and H-fields within the waveguide is fundamental to the research presented here.

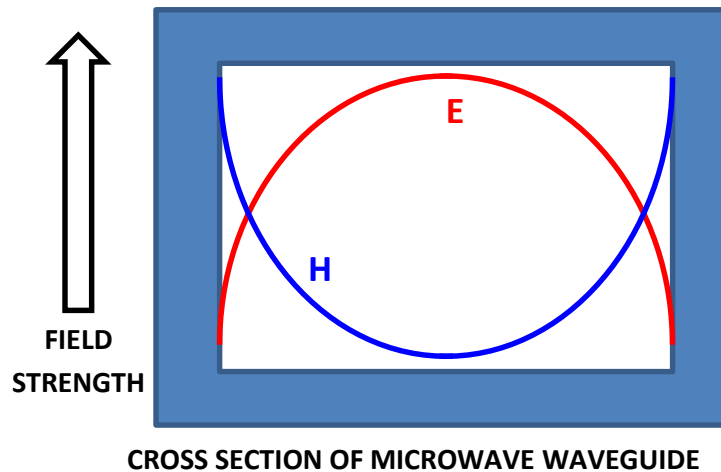


Fig. 1.7 Microwave waveguide cross-section illustrating the different field strengths.

1.2 Induction Heating (IH)

1.2.1 Introduction

In 1831, English physicist Michael Faraday discovered the basis for induction heating after experimenting in his laboratory with two coils of wire wrapped around an iron core.^{26,27} Faraday concluded that a changing magnetic field can produce an electric current.

Induction heating is a way of heating a metal part without any physical contact. In most common heating methods, heat is applied directly to the part to be heated. With induction heating, the heat is induced within the material itself with the use of a circulating electrical current.²⁸ Faraday's Law plays a large part in induction heating theory and explains how a current is induced within a sample. A power supply sends an alternating current (a/c) through an inductor (copper coil) and the part to be heated (sample) is placed inside the inductor. This current creates an alternating magnetic field and when the sample is placed within the inductor, an electrical current is induced within the sample. Fig. 1.8 shows a basic induction heating setup. Depending on the resistance of the sample, varying degrees of heating can take place.

The inductor serves as the transformer primary, and the sample is the secondary. When the metal part is placed within the inductor and enters the magnetic field, eddy currents are induced within the sample (fig 1.9).²⁸

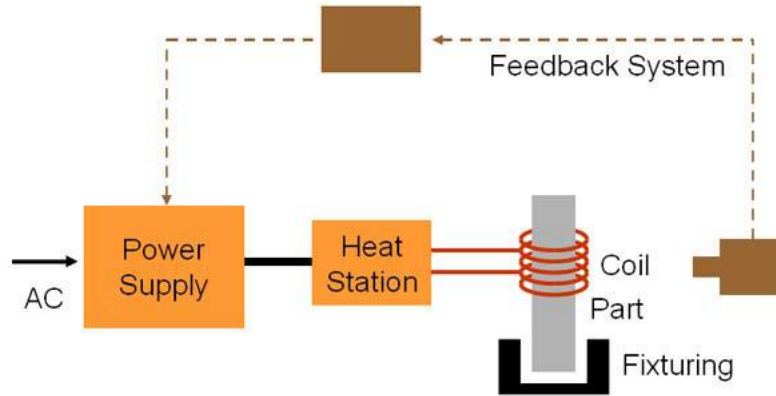


Fig. 1.8 Basic induction heater set-up²⁹

As shown in fig 1.9, these eddy currents flow against the electrical resistivity of the metal, generating precise and localised heating within the sample without any physical contact. Heating occurs in magnetic and non-magnetic materials, and is referred to as the 'Joule Effect', which refers to Joules first law (Eqn. 1). Secondly, heating is induced in magnetic materials as hysteresis; an internal friction that is created when magnetic parts pass through the inductor.²⁸

$$Q \propto I^2 \cdot R \quad (\text{Eqn. 1})$$

Where the amount of heat released (Q) is proportional to the square of the current (I) multiplied by the resistance (R).

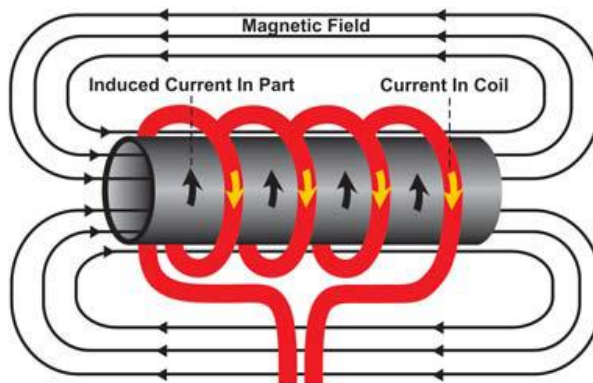


Fig. 1.9. Induction coil with central sample and induced magnetic field²⁹

The rate of heating in the sample is dependent on several factors: -

- The frequency of the induced current
- The intensity of the induced current
- The specific heat capacity (ability to absorb heat) of the material
- The magnetic permeability of the material
- The resistance of the material to the flow of current

The sample has to be a poor conductor of electricity so that the relationships between the frequency of the EM-field that produces the eddy currents, and the properties of the sample, can be satisfied.³⁰ Although induction heating relies on the materials resistance to the flow of electric current resulting in heating, those that are also magnetic such as nickel and steel, may also benefit from hysteresis losses³⁰ (hysteresis heating).²⁸ As the samples are being heated, the magnetic field causes the magnetic dipoles to oscillate as the magnetic poles change their orientation every cycle, and a minor amount of heat is produced due to friction. If a material is heated above its T_c , hysteresis ceases to contribute to any further heating, as the material becomes non-magnetic.^{28,30}

1.2.2 Induction heating in industry

Induction heating has been utilised in the metal processing industry due to high productivity and repeatability. This method of heating is also more energy efficient which lowers production costs within the industrial sector. Iron has a crystalline body-centred cubic (BCC) structure at temperatures below 912 °C. Above this temperature there is an allotropic transformation to face-centred cubic (FCC). The change in structure as the iron reaches its T_c results in the iron becoming paramagnetic, which in turn causes the rise in temperature to slow down, or stop. Rudnev *et al.*²⁶ discussed the heating interruptions as iron reaches 4 critical temperatures. The first interruption is at 768 °C, which is the T_c of iron. At 912 °C it undergoes a second interruption as the iron undergoes an allotropic transformation from BCC to FCC. As the iron undergoes a second transition at 1392 °C the heating is interrupted again and halts completely at the melting point (1528-1538 °C).²⁶ While temperatures to this level are not discussed further in this research, it is interesting to note that the use of induction heating for industrial purposes can define the T_c of iron due to the fact that the loss of its magnetic properties affects heating of the sample.

1.3 Materials to be investigated

In this work, the materials used to investigate the capabilities of the thermal analysis techniques to be described in Chapter 3 were metal oxides. These oxides were primarily of rock-salt, perovskite and double perovskite structural type. These materials were chosen particularly because of their magnetic and electrical properties, specifically their magnetisation and conductivity, allowing the material to couple well within the H-field and E-field of the electromagnetic field in the microwave cavity. The MWTA instrument will be used to determine the coupling capability of these materials which will then enable a decision as to which materials will be investigated in the induction heater. The materials have been well characterised in previous studies.^{31–44}

1.3.1 Rock salt (Halite)

Halite (rock salt) is the mineral form of solid sodium chloride (NaCl), which is better known as table salt. It is an ionic compound and Na and Cl are arranged in a cubic 'chequerboard' type pattern and is a FCC arrangement with respect to the anions. The larger chloride ions (1.67 Å) are arranged in a cubic array, whereas the smaller sodium ions (1.16 Å) fill the octahedral voids between them. Fig. 1.10 shows the NaCl arrangement, where the coordination number of each ion is 6; each anion is coordinated to 6 cations at the vertices of an octahedron, and each cation is coordinated to 6 anions at the vertices of an octahedron. There are many other compounds which have the same structure as this, and it is known as the 'rock-salt' crystal structure. This structure is more likely to be formed if the cation is smaller than the anion (Na⁺ is smaller than the Cl⁻). The space group of the structure is Fm $\bar{3}$ m (in Hermann-Mauguin notation).

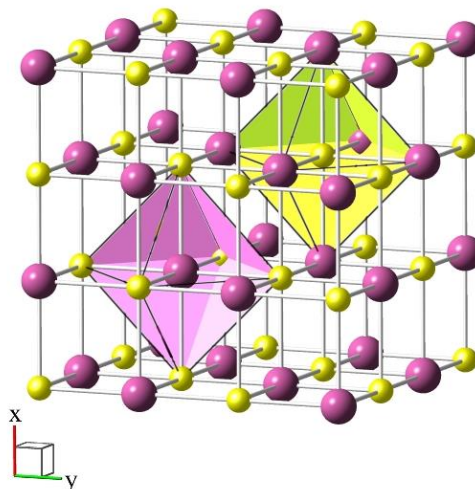


Fig 1.10 NaCl crystal structure - The pink octahedron has a chloride ion in its centre, and the yellow octahedron has a sodium ion at its centre

1.3.2 Transition Metal oxides (TMOs)

Transition metal oxides (TMO's) have undergone an exhaustive amount of research throughout the 20th century.^{18,38,45-54} TMO's have tremendous variations of stoichiometry which are responsible for some of the complexity in structure and the properties associated with these oxides.⁵³ The oxygen content can be a problem, although it is often an added advantage, within many of these oxide samples as it is easily lost or gained during synthesis. The concentration of defects within the compounds can also be very large and can have important consequences for many physical properties observed.⁵³

Bonding in transition metal oxides can vary from ionic (NiO, CoO) to covalent (OsO₄, RuO₄) and metallic bonding (TiO, NbO and ReO). TMO structure can also vary from cubic structure to triclinic. The simple binary oxides, two of which are discussed below, generally have the cubic structure.⁴⁹

Nickel oxide (NiO) and magnesium oxide (MgO) are other examples of ionic compounds which form a rock salt structure.

TMO's can also exhibit a wide range of magnetic and electrical properties⁴⁹ which are outlined in the table below.

Table 1.1 TMO magnetic and electrical properties.⁵⁵

TMO	Structure	Magnetic property	Electrical conductivity
CoO	Rocksalt (NaCl)	Antiferromagnetic (< 289 K)	Semiconducting (200-1500 K)
CrO ₂	Rutile	Ferromagnetic (T _C = 395 K)	Metallic (80 – 575 K)
Cr ₂ O ₃	Corundum	Antiferromagnetic (<308 K)	Semiconducting (300 -1600 K)
Fe ₂ O ₃	Corundum	Antiferromagnetic (T _N ≈ 960 K)	Semiconducting (200 – 1600 K)
Fe ₃ O ₄	Inverse spinel	Ferrimagnetic (T _N ≈ 860 K)	Semiconducting (T<119 K)
MnO	Rocksalt (NaCl)	Antiferromagnetic (T _N 118 K)	Semiconducting (< ~1500 K)
Mn ₂ O ₃	Non-corundum	Paramagnetic (80 K)	Semiconducting (400-1000 K)
Mn ₃ O ₄	Spinel	Ferrimagnetic (T _C = 47 K)	Semiconducting (300 K)
MoO ₃	Layer	Diamagnetic (RT)	Semiconductor (450 K)
NbO ₂	Rutile	Paramagnetic (300 – 1200 K)	Semiconducting (300 K)
NiO	Rocksalt (NaCl)	Antiferromagnetic (T _N ~ 523)	Insulator (300 K)
ReO ₃	Cubic	Pauli-paramagnetic (300 K)	Metallic (300 K)
TiO ₂	Rutile	Diamagnetic (300 K)	Dielectric (300 K)
Ti ₂ O ₃	Corundum	Paramagnetic (300 K)	Insulator (300 K)
VO ₂	Rutile (T < 340 K)	Paramagnetic (1.7 – 400 K)	Semiconducting (T<340 K)
V ₂ O ₃	Corundum (at RT) ⁵⁶	Antiferromagnetic (T _N =154 K)	Metallic (at RT) ⁵⁶
V ₂ O ₅	Layer	Diamagnetic (RT)	Semiconducting (T = 77-450 K)
WO ₃	Monoclinic (RT)	Diamagnetic (77-292 K)	Semiconducting (200 – 400 K)
ZrO ₂	Monoclinic (RT)	Diamagnetic (RT)	Insulating (RT)

1.3.3 Perovskites

1.3.3.1 History

Perovskites are named after Russian mineralogist Lev. A. Perovski who discovered CaTiO_3 . While they are primarily ternary oxides, nitrides and halides and other compositions are also known. Perovskites can undergo structural changes, adopt complex intergrowth structures i.e. Aurivillius phase or can be doped with other ions. Creating subtle distortions within the perovskite lattice can change the properties of these compounds, giving rise to properties such as ferroelectricity, piezoelectricity and colossal magnetoresistance.⁵⁷

1.3.3.2 Structure

A metal ion in an arrangement with an oxide ion to give a cubic close packed (ccp) structure is quite common, especially with divalent metal oxides. e.g. NiO, MgO etc., which are known to have a rock salt structure,⁵⁸ but if one quarter of the oxide ions are replaced by a cation of similar size radius, (alkali, alkaline-earth or rare earth elements), the octahedral voids are reduced to one quarter as they are filled by a small cation. The structure is called perovskite (fig 1.9), and the general composition is ABX_3 , where A is usually a rare earth cation, B is usually a transition metal ion and X is most commonly O^{2-} , but can be replaced with larger anions such as F^- and Cl^- .⁵⁹⁻⁶⁰

Perovskites are a family which have the same crystal structures as CaTiO_3 . In the ideal non-distorted form, the cubic ABX_3 perovskite has eight corner-sharing $[\text{BX}_6]$ octahedra with a central A-cation in the cubo-octahedral position formed at the centre of these octahedra. Fig. 1.11 illustrates two different unit cells of the same crystal structure. The ideal cubic perovskite is not very common but SrTiO_3 is commonly regarded as one of the compounds that is as close as possible to this ideal cubic structure. The perovskites that possess the ideal structure adopt the $\text{Pm}\bar{3}\text{m}$ space group.⁶⁰

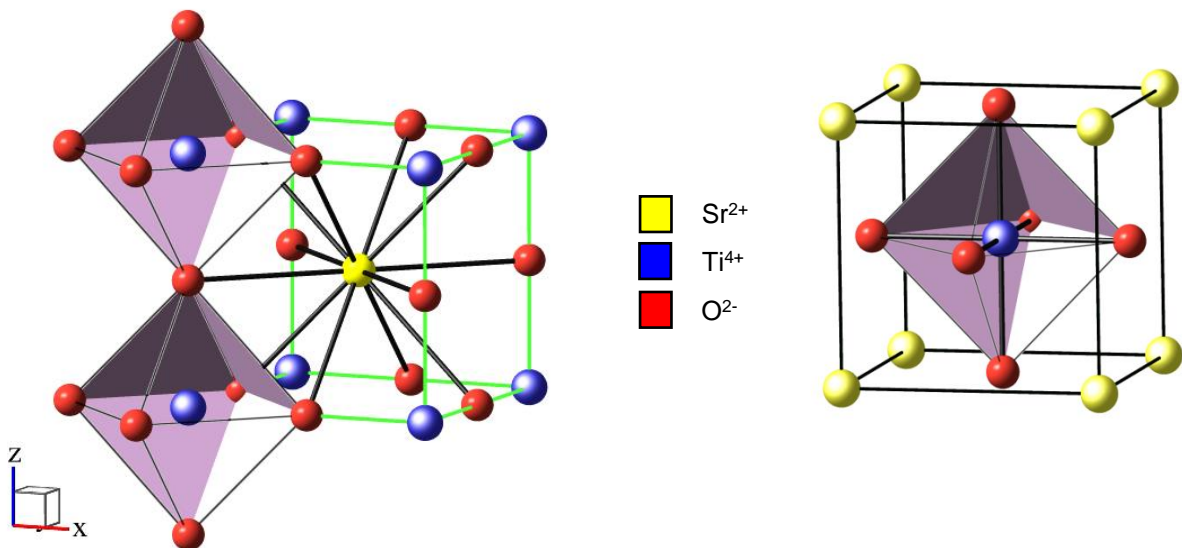


Fig. 1.11 Cubic perovskite structure (SrTiO₃). [TiO₆] corner sharing octahedra and Sr²⁺ in the 12 fold cavities between the octahedra.

Perovskites are one of the most studied forms of the oxides, and distorted perovskites are extremely important for industrial applications as their lack of symmetry gives them unique electrical and magnetic properties.^{34,41,59,61–65} A lot of early research that focussed on perovskites was very much based on characterising the structure and symmetry of the compounds, and went some way to discuss the ferroelectric and ferromagnetic properties exhibited by particular perovskites.^{60,66–70} Matthias in 1954 patented an ‘Electrical device embodying ferroelectric lanthanum-containing substances’. The ferroelectric compounds within the patent were LaGaO₃ and LaAlO₃, and their use described within the patent include devices used as a piezoelectric element and as an electrical transducer.⁷¹ However, the fact that these compounds were ferroelectric was disputed as no proof or description of the properties was given.⁶⁷ These two compounds, among others, have also recently been researched for use as solid oxide fuel cells (SOFC) *via* doping on the A- or B-site.⁷²

Perovskite structures are known to be very diverse, and A and B can be varied, leading to many known compounds with a perovskite type structure. As mentioned earlier, the ideal perovskite structure is very rare, and the distortions are caused by a number of factors - size effects, deviations from the ideal composition and Jahn Teller effect.⁵⁹

The ferroelectric phenomenon was first discovered in 1921 by J.Valasek⁷³ while working on a Rochelle salt ($\text{Na}_2\text{KC}_4\text{H}_4\text{O}_6 \cdot 4\text{H}_2\text{O}$). This was furthered by Von Hippel in 1946 using a perovskite system, BaTiO_3 .⁷⁴

Ferroelectrics exhibit an electrical dipole moment, even in the absence of an electrical field. They also possess a domain of different orientations of electrical polarisation that can be reoriented and brought into alignment by an external electrical field.

PbTiO_3 is a ferroelectric compound. It is commonly synthesised in a solid solution with PbZrO_3 to give the composition $\text{Pb}(\text{Ti}_{0.47}\text{Zr}_{0.53})\text{O}_3$, more commonly known as PZT. Although the PZT solid solution series is known to go through a number of phase changes, with each phase resulting in different properties, PbTiO_3 only undergoes one phase change at 763 K⁷⁵ where it becomes tetragonal. This distortion can be increased by substituting Pb^{2+} with La^{3+} in differing atomic percentages. The results demonstrated the importance of lattice strain on the structure and the resulting property changes.⁷⁵

BaTiO_3 and SrTiO_3 are two of the most widely studied ferroelectric compounds, and are of particular interest for the next generation of electronics and semiconductors in industry.⁷⁶ Along with PZT (discussed above) they are used in different electronics. BaTiO_3 enabled scientists to develop a two-state and electrically switchable device during World War II. These devices were able to encode the 1 and 0 states that were essential for binary computer memories.⁵⁴ PZT was used for ferroelectric random access memory in computers (FeRAM) and there is an 8-kbit FeRAM in every Sony Playstation 2, which consists of PZT. This is possible because of the stability of the ferroelectric crystalline structure at room temperature.⁵⁴

Perovskite nanomaterials have also been investigated for their use in solar electricity applications. Their use in photovoltaic devices has been researched because of their semiconducting and ferroelectric properties. They are also sought after because of the ability for controlled synthesis methods. Dye-sensitised solar cell systems (DSSCs) were developed by Grätzel⁷⁷ and this development shows a lot of promise due to a considerably high energy conversion efficiency combined with low manufacturing costs.⁵⁴

The examples outlined above are of relevance to this research as they are investigated with the MWTA and IHTA instrumentation. They also show that, depending on the composition of the compound, the properties exhibited by the compound can change. This was also investigated within this research.

1.3.4 Double perovskites

Ordered perovskites are derivatives of the simple perovskite structure, formed when either or both of the A and B sites are replaced by other cations. If they are ordered at only one site, the compounds are commonly known as double perovskites. If ordering occurs at both sites the compounds are known as quadruple or complex perovskites.⁶⁰

The perovskite structure has a lot of potential to tolerate a wide range of elements of differing size so the number of possible permutations is quite high and because of their importance in industry as dielectric resonators at microwave frequencies, the majority of studied ordered perovskites tends to be oxide perovskites which exhibit B-site ordering.⁶⁰

Fig 1.12 below shows an ideal double perovskite, with the structure $ABB'O_6$. At the centre of each octahedron, the B/B' site, are transition metal atoms, whose valence states can vary to give +1/+7, +2/+6, +3/+5 and +4/+4. which have arranged themselves in an alternating 'chequerboard' pattern There is an oxygen ion at the vertices of each octahedron and the cation on the 'A' site occupies the interstice between the octahedra. The A cation is usually a alkali earth ion, with a valence state of +2. The most studied are Ca^{2+} , Sr^{2+} , and Ba^{2+} .

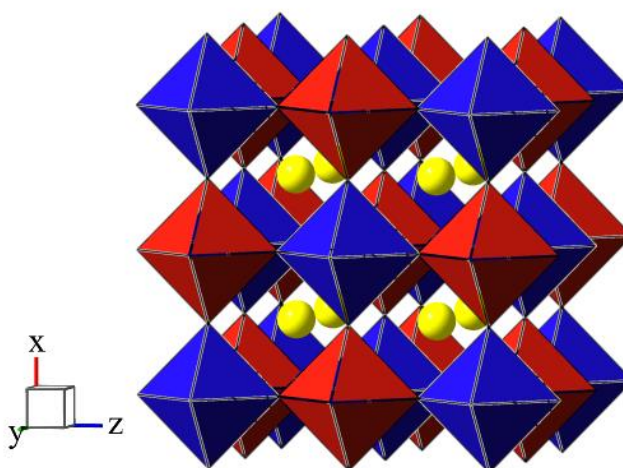


Fig. 1.12 Double perovskite with $ABB'O_6$ structure

Anderson *et al.*⁷⁸ reviewed work on double perovskites up to 1993. nd because the B cations generally determine the physical properties of double perovskites, it was the B cations that were the focus of the review. A central research theme over the years has focussed on changing the size, valence and electronic configurations of constituent ions. These are primarily, the cation charge difference, and secondarily, the cation size difference.⁷⁸ Fig. 1.12 shows the relationship between these two factors.

Previous research into double perovskites, which is outlined below, shows that the compositions chosen for investigation have various magnetic and electrical properties which is pertinent to the research conducted with the MWTA and IHTA instrumentation. These were chosen due to ease of synthesis and the expectation of coupling within the two instruments.

There are numerous $A_2BB'X_6$ structures arising from rock salt cation ordering, combined with simple octahedral tilting,⁷⁹ The cation ordering can have a profound effect on the properties of double perovskites.⁸⁰ Pb based double perovskites (Pb_2ScTaO_6) have dielectric properties that are highly susceptible to differences in the extent of B/B' ordering.⁸¹ Magnetotransport properties (Sr_2FeMoO_6) are extremely sensitive to B/B' disorder and their spin polarisation, therefore half metallicity, degrades as cation order decreases.⁸² $Li_{3x}La_{2/3x}TiO_3$ at room temperature has one of the greatest known conductivities. The ionic conductivity is strongly affected by the degree of ordering at the A-site.⁸³

Perovskite systems have also been found to have magnetoresistive properties. Arulraj⁸⁴ studied the double perovskite system Sr_2CrMoO_6 , after the room temperature magnetoresistive properties of Sr_2FeMoO_6 were discovered by Kobayashi.⁶³ These compounds are both ferrimagnetic with transition temperatures that are above room temperature, but Sr_2CrMoO_6 was found to have lower magnetisation and magnetoresistive properties than Sr_2FeMoO_6 . This is possibly due to the lack of valence compensation, as Cr must always be trivalent, and therefore Mo must always be pentavalent. In the Sr_2FeMoO_6 compound, the Fe can vary between divalent and trivalent states, allowing Mo to vary between pentavalent and hexavalent states. There is some conflicting evidence where $Sr_2CrMo_{1-x}W_xO_6$ is concerned. These properties are sensitive to subtle distortions within the structure, particularly those which arise from octahedral tilting.⁸⁵

1.3.5 Disordered and tilted perovskite structures

There is a large variety of non-cubic structures in existence that are often distorted and have lower symmetry than the cubic structure. The structural distortion usually occurs due to size incompatibility of the three ions and to accommodate the size difference, repulsion between ions within the system (electrostatic forces) causes the distortion.⁸⁶

The degree of distortion within the structure can be predicted using the Goldschmidt tolerance factor, t , (eqn. 2)

Eqn.2.

$$t = \frac{r_A + r_O}{\sqrt{2}(r_B + r_O)}$$

Where: r_A = the radius of the A-cation

r_B = the radius of the B-cation

r_O = the radius of the Oxygen anion

Eqn. 2 only relates to the tolerance factor of a simple perovskite. In the case of complex and ordered perovskites, the average radius of ions on each site is used as more than one ion occupies the A and/or B-sites.⁸⁷

The closer the tolerance factor is to one, the closer the unit cell is to the ideal cubic system. The following rule can be considered for the double perovskite family: for $1.05 > t > 1.00$ the cubic structure is adopted within the $Fm\bar{3}m$ space group, for $1.00 > t > 0.97$, the structure is most probably tetragonal with an $I4/m$ space group and if $t < 0.97$, either a monoclinic ($P2_1/n$) or orthorhombic structure is adopted.

According to Glazer, distortion occurs from displacement of the B-cations ($BaTiO_3$), tilting of the octahedra ($CaTiO_3$) or a combination of both ($NaNbO_3$).^{35,88} The properties of perovskite transition metal oxides, both magnetic and electrical, are known to be affected by these distortions.⁵⁹

1.4 Dielectrics

Von Hippel⁸⁹ states that a dielectric is not so much an insulator, but a broad range of non-metals that should be thought about from the position of their interaction with electric, magnetic and electromagnetic fields.

Dielectrics are materials with a high polarizability, determining the dynamical response of a bound system to external fields. To meet with the requirements for microwave applications, several types of dielectric materials have been investigated.⁹⁰⁻⁹⁴ and, due to their extreme structural and compositional flexibility, those materials with the perovskite structure are some of the most researched (see Section 1.2 for more detailed description of perovskite systems). 1:2 ordered perovskites, $A_3B'B''_2O_9$ and $A_2B'B''O_6$, are some of the compositions that have recently gained attention. A^{2+} is usually an alkaline earth ion, and B'/B'' are usually a transition metal ion with charges varying between B'^{+2}/B''^{+6} and B'^{+3}/B''^{+5} . There have also been instances where B'^{+4}/B''^{+4} (Ba_2CePtO_6) and B'^{+1}/B''^{+7} (Ba_2NaReO_6) have been synthesised.⁶⁰ Compositions studied include double perovskites A_2MgTeO_6 (where $A = Ca^{2+}$, Sr^{2+} and Ba^{2+})⁹⁵, $LaCoMnO_6$ ⁹⁶ and triple perovskites A_3CoNbO_9 (where $A = Ca^{2+}$, Sr^{2+} and Ba^{2+})⁹⁷ and $Sr_3Zn_{1-x}Mg_xNb_2O_9$ ($0 \leq x \leq 1$)⁹⁰.

A material can be heated by subjecting it to high frequency electromagnetic radiation. The ability of the E-field to exert a force on charged particles resulted in the origin of these heating effects. A current is induced if the particles within a material can move freely through it. If the charge carriers are bound to certain regions within that material, then they will move until a counter-force balances them. The net result is dielectric polarisation.

The extent to which a material will heat when subjected to microwave radiation is dependent on two critical factors – the dielectric constant of that material (ϵ') and the dielectric loss factor (ϵ'').^{4,10,14,24} ϵ' relates to a material's ability to polarise in an E-field. ϵ'' is the efficiency with which the energy of electromagnetic radiation can be converted into heat.²³ Both ϵ' and ϵ'' vary with frequency, where ϵ'' reaches a maximum as the dielectric constant falls. The ratio of ϵ' and ϵ'' gives the dielectric loss tangent ($\tan\delta$), shown in Eqn.3.

$$\tan\delta = \frac{\epsilon''}{\epsilon'} \quad \text{Eqn. 3}$$

The dielectric loss factor defines the ability of a material to convert electromagnetic energy into thermal energy at a given temperature and frequency.⁴

The power dissipated by a material that is exposed to microwave radiation can be given by the Maxwell equation (Eqn.4).

$$P = \text{constant} \cdot f \cdot E \cdot \epsilon' \cdot \tan\delta \quad \text{Eqn. 4}$$

Where: P = power density ($W\ m^{-3}$)
 f = applied frequency (Hz)
 E = average electric field component of the microwave energy ($V\ m^{-1}$)

Energy absorption increases with frequency for a constant loss factor, but penetration depth (D_p) falls. The penetration depth for a frequency of 2.45 GHz is in the order of a few centimetres, depending on the loss factor of each individual material.²⁴

Generally, ϵ' decreases with frequency and temperature, but the behaviour of ϵ'' is less regular. The loss factor tends to increase with temperature. This can lead to undesirable consequences, such as thermal runaway, in some materials.²⁵

1.5 Electrical and magnetic properties

Some materials have properties that enable them to be used as sensors, ultrasonic devices, and memory or data storage devices. These materials are called piezoelectric materials, and this title also includes materials that are ferroelectric and non-ferroelectric. Out of thirty-two crystalline classes, twenty of these are piezoelectric. These can be split again into a pyroelectric class and non-pyroelectric class. The pyroelectric classes consist of materials that have a spontaneous electric voltage in response to a temperature change. This group includes ferro- and non-ferroelectric materials. The non-pyroelectric class consists of materials that have a spontaneous electric voltage in response to an application of external stress on the material.

1.5.1 Ferroelectricity

Ferroelectricity refers to the spontaneous polarizability of a material which can be reversed with the application of an external magnetic field.⁹⁸ First discovered in the Rochelle salts in 1921, A. von Hippel later found barium titanate ($BaTiO_3$) exhibited ferroelectrical behaviour in 1944. Currently there are over 250 materials classified as having ferroelectric properties including lead titanate ($PbTiO_3$), lead zirconate titanate (PZT) and lead lanthanum zirconate titanate (PLZT).⁹⁸ The exhibiting of ferroelectric behaviour (the spontaneous polarizability) occurs below the Curie temperature (T_C) and is defined by the crystal symmetry of the material.

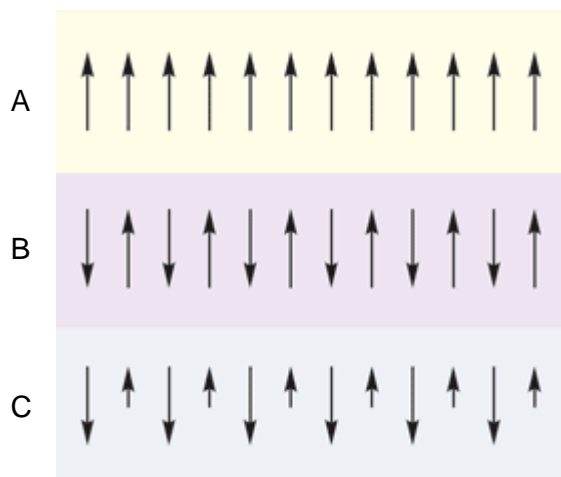
1.5.2 Ferro- and ferrimagnetism

Magnetism is a phenomenon associated with the motion of electric charges. Electric currents and magnetic moments of a material create a magnetic field, which then affects the magnetic fields of other materials. Most materials are affected by magnetic fields, and they can be classified as being ferromagnetic (Fe, Co, Ni), ferrimagnetic (Fe_3O_4), anti-ferromagnetic (NiO, Cr), paramagnetic (Na, Al, Ca etc.), and diamagnetic (N, Cu, Ag, Au) materials, depending on the net degree of magnetisation of individual substances.

A ferromagnetic material possesses a spontaneous magnetic moment (saturation moment) with zero applied magnetic field. The electron spin and the magnetic moment are arranged in a regular manner (Fig. 1.13). They have long-range ordering at the atomic level, where unpaired electron spins align parallel to one another in different domain. The magnetisation within the domain is strong, but in a bulk sample, it is likely to be non-magnetic, as the domains themselves are randomly orientated with respect to one another. A small magnetic field can cause the domains to line up, magnetising the material. Most materials will stay magnetised, to some extent, after being subjected to a magnetic field. This tendency for the materials to 'remember their magnetic history' is known as hysteresis.⁹⁹

All ferromagnets have a maximum temperature where their ferromagnetic properties disappear i.e. above this temperature a ferromagnet becomes paramagnetic. This is known as the Curie temperature (T_C). It is analogous to the Néel temperature (T_N), which is the temperature above which an antiferromagnet becomes paramagnetic. Antiferromagnets have no net magnetic moment, as the electrons spins are aligned oppositely (fig. 1.14), resulting in a net magnetisation of zero.

Another branch of magnetic materials is ferrimagnetism. These magnets are less magnetic than ferromagnets, as the electrons spins are oppositely charged, but the opposing charges are smaller, therefore resulting in an overall net magnetisation.



1.5.3 Para- and Diamagnetism

Diamagnetic materials have completely paired electrons therefore the total spin is 0. These materials are not attracted to a magnetic field and are slightly repelled. In contrast to diamagnetic materials, paramagnetic materials have one or more lone electrons in an orbital and these materials are slightly attracted to a magnetic field and attempt to realign in response to the external applied field. No magnetisation is retained by the material in the absence of a magnetic field. Where d- or f-electrons are involved, stronger magnetic effects can typically be observed, particularly with the lanthanide atoms.¹⁰⁰

1.6 Magnetic and electrical properties of perovskite systems

1.6.1 Behaviour of perovskites

1.6.1.1 ABX₃ system

Oxide perovskites with ferromagnetic behaviour were first reported in 1950 during a study on manganites (AMnO₃: A= divalent or trivalent cation).⁶⁸ Jonker and Van Santen investigated compounds of the general formula A³⁺B³⁺O₃²⁻, and although they found that LaMnO₃ was ferromagnetic at liquid-air temperatures (78 K), LaFeO₃ and LaCrO₃ were not. It was subsequently found that LaMnO₃ was only ferromagnetic when it contained some manganese of a valency higher than three. In order to increase the valency of the Mn, they prepared some mixed crystals of the formula La_{1-x}A_xBO₃, where A= Ca²⁺, Sr²⁺, Ba²⁺, Cd²⁺ and Pb²⁺ and where 0 ≤ x ≤ 1. Ferromagnetic materials were formed when x = 0.2 to 0.4. The physical properties of the materials were found to be closely related to the valence of the manganese, and also to the T_C. In order to explain this they suggested a positive indirect exchange mechanism, now known as superexchange.⁶⁸

Zener interpreted ferromagnetism as arising from the indirect coupling of incomplete *d*-shells *via* the conducting electrons and found a correlation between conductivity and ferromagnetism. As an example of the dependency of ferromagnetism on the conduction electrons, Zener mentioned the difference in the behaviour of the Mn ions in the Heusler alloys (of the type Cu₂MnSn) and in MnCl₂. These compounds are FM and AFM respectively, although the Mn atoms are 40% further apart than in metallic Mn.⁷⁰ Zener introduced indirect coupling through the oxygen ion by means of double exchange.⁶⁹

The discovery by Zener of the double exchange mechanism *via* electron transfer through oxygen orbitals, encouraged further studies on oxide materials that could show ferromagnetism at high temperatures.¹⁰¹

With regards to ferroelectric properties, the most studied perovskites are ones containing Pb and Ba as the A-site cation. The main focus for research with these perovskites is that they are very similar in structure, yet their properties are quite different. Cohen looked at the BaTiO₃ and PbTiO₃ systems to try and what was causing the differences.¹⁰² Their unit cell size is similar, at 64.2 and 63.2 Å³ respectively. Both are paraelectric (non-polar) at high temperatures and have a simple cubic structure – space group *Pm3m*. However, BaTiO₃ undergoes three ferroelectric phase transitions; from cubic to tetragonal at 393 K, from tetragonal to orthorhombic at 278 K and from orthorhombic to rhombohedral at 183 K. In

comparison, PbTiO_3 only undergoes one ferroelectric phase transition from cubic to tetragonal at 766 K.¹⁰²

With the $\text{Pb}(\text{B},\text{B}')\text{O}_3$ and $\text{Ba}(\text{B},\text{B}')\text{O}_3$, the Pb systems are used as relaxor ferroelectric transducers, actuators and multilayer capacitors. The Ba systems are used as dielectric resonator materials, in particular $\text{Ba}(\text{Zn}_{1/3}\text{Ta}_{2/3})\text{O}_3$.⁸¹ B-site order has been found to be essential to obtain the relaxor properties in the Pb systems, but the dielectric quality factor degrades by orders of magnitude if there is any disorder in the Ba systems. Burton *et al.* compared the two systems, and found that the long-range coulombic interactions that drive the ordering with the Ba system weren't present in the Pb systems. In the Pb systems, hybridisation between the Pb 6s and O 2p states causes competition between long- and short-range many body interactions, which is why the Pb based systems disorder at lower temperatures.

1.6.1.2 $\text{ABB}'\text{X}_6$ systems

In 1961, ferrimagnetic behaviour in a double perovskite was reported by Longo and Ward.¹⁰³ This behaviour occurred in a rhenium based double perovskite above room temperature. Subsequent experiments further explored Re-based double perovskites, and their electrical and magnetic properties.^{103,104} It was discovered during these studies, that B cation ordering could be attributed to the large charge difference between them. This finding caused an increase in research on different B-site cations in double perovskites. It was also at this stage that Longo and Ward postulated the use of Mo^{5+} and Os^{6+} for use as cations, in combination with a divalent cation, to increase the charge difference. Although it was suggested that the use of other elements could yield similar results, Longo and Ward continued to study the Rhenium compounds as this was where other research had had the most success.^{103,104}

In 1962, Patterson *et al.*¹⁰⁵ looked at oxides with the perovskite structure containing Mo^{5+} and W^{5+} . It had previously been found that with paramagnetic B cations of different magnetic moment in neighbouring B-sites, the compound should exhibit ferrimagnetism, as demonstrated in the Re compounds.^{103,104} The idea that this principle could be extended to Mo and W magnetic oxides raised some doubt. The compounds with the formula A_2CrMoO_6 (where $\text{A} = \text{Ba}^{2+}$, Ca^{2+} or Sr^{2+}) were found to have different T_C , with the compositions containing larger A-site cations having the higher T_C . It was also found that the Ca^{2+} ion favours orthorhombic distortion, which in turn changes the O-B-O bond angle from 180° which is favoured for magnetic interaction.^{105,106}

Even though research continued into double perovskite systems and their properties, it wasn't until 1998 when Kobayashi published the discovery of the half-metallic ferromagnetic (HMFM) properties of $\text{Sr}_2\text{FeMoO}_6$, that a renewed interest was triggered.^{63,101} Due to these properties in SFMO and in other double perovskite systems, these materials are seen as a real alternative to the manganese perovskites. They also have the added advantage of a much wider temperature range, between 110 K ($\text{Ba}_2\text{MnReO}_6$) to 725 K ($\text{Sr}_2\text{CrRuO}_6$),¹⁰⁷ which makes them desirable for practical applications in magnetoresistive materials which can be used in magnetic storage devices.¹⁰⁸

A lot of research is currently ongoing with a view to developing double perovskites for a number of different applications, many of which are within the spintronics area for solid state storage devices.⁴⁷ These include (but are not limited to) thermoelectrics ($\text{Sr}_2\text{MnMoO}_6$ with La doping),¹⁰⁹ giant magnetoresistance ($\text{Mn}_2\text{FeReO}_6$)¹¹⁰ and tunnelling magnetoresistance (A_2FeWO_6 where $A = \text{Ca}^{2+}$ or Sr^{2+}).¹¹¹

This research will examine the behaviour of a series of complex double perovskites in order to observe magnetic and electric behaviour within the systems. $\text{Sr}_2\text{FeMo}_{1-x}\text{W}_x\text{O}_6$ and $\text{Sr}_2\text{CrMo}_{1-x}\text{W}_x\text{O}_6$ have been chosen due to their well characterised structure and properties. It is hoped that the compounds will show differences when coupling in the E- and H-fields using MWTA and show interaction with induced magnetic currents using the novel IHTA instrument. Further investigations will include doping $\text{Sr}_2\text{FeMoO}_6$ with La^{3+} on the A-site, discussed below.

1.6.2 Electron Doping of perovskites

The doping of perovskite systems has been the centre of much research, starting in the mid-20th century.^{112,113} Since the discovery that different valence Mn ions (+3/+4) can change the electrical and magnetic properties of these systems⁶⁸, ions of different valences have been substituted onto the A- and B-sites to find more desirable properties.

1.6.2.1 Ln Doping of ABX_3 perovskite systems

The lattice parameters and atom positions are critical to the electronic and magnetic properties of the perovskite system and lanthanides have been a popular choice of dopant to increase and optimise the desired properties. Lead titanate (PbTiO_3) is a useful piezoelectric material due to its high intrinsic polarisation and relatively high T_c of between 568 K and 708 K, depending on the stoichiometry ($\text{Pb}_{1-x}\text{TiO}_{3-x}$).¹¹⁴ The tetragonality in this system prevents the processing of high density ceramic materials, and because a lot of studies have investigated Ln^{3+} doped barium titanate (BaTiO_3)¹¹⁵, it was thought that doping

the PbTiO_3 with a Ln^{3+} ion could reduce the lattice parameters while still retaining the piezoelectricity at optimal levels.^{75,116}

1.6.2.2 Ln doping of AB_2X_6 double perovskite systems

The introduction of a rare earth metal (Ln) into a double perovskite system has been the focus of a lot of recent research. Kobayashi's findings⁶³ have stimulated research into increasing the T_c of these materials. A higher T_c allows these materials to have more practical uses in higher temperature devices. Holes are introduced in charge doped manganites by substituting a trivalent lanthanide for a divalent cation, as in $\text{La}_{1-x}\text{Ca}_x\text{MnO}_3$.¹⁰⁹ The research discussed in this thesis observed the properties and behaviour of $\text{Sr}_{2-x}\text{La}_x\text{FeMoO}_6$ (where $x = 0.05, 0.10, 0.15$ and 0.2). As outlined above, research has shown that T_c can be increased by substituting La^{3+} onto the A-site, and other research examining the changes in properties for this series has discovered that doping $\text{Sr}_2\text{FeMoO}_6$ with La^{3+} enhances the magnetoresistive (MR) properties⁴¹ and T_c .⁶¹ of this compound. Narsinga-Rao *et al.*⁴¹ found that where $x > 0.4$, the increase in MR began to reduce again. The final part of the research discussed in this thesis focuses on the properties of this series, and due to the findings of previous research, reduced amounts of La were used. This is discussed further in Chapter 4.

1.7 Objectives

The objective of this study is the use of MWTA and IHTA for novel thermal analysis of functional ceramic materials. The research will utilise different materials (oxides, perovskites and double perovskites with substitutions of the A- and B-site cations) to further develop the thermal analysis equipment. The investigation will be accomplished using novel instrumentation (MWTA and IHTA) developed at the University of Huddersfield.²⁴ Previous work by Rozanski, Gillie and Parkes - unpublished results – suggest that ferroelectric and antiferroelectric transitions can be tracked qualitatively when materials are heated in the electric field maximum, therefore the possibility of whether the same is apparent with magnetic ordering events in the magnetic field component of the microwave field was investigated.

The novel instrumentation techniques include microwave thermal analysis and induction heating thermal analysis. The method development and adaptation of these instruments is presented in Chapter 3.

To examine the use of MWTA and IHTA for magnetic and electrical properties, simple metal oxides were initially investigated. Solid solutions were synthesised to observe the

differences in coupling with the instrument and the properties of the corresponding metal oxides. This work is presented in Chapter 4.

More simple perovskites were then analysed on the instruments, PbTiO_3 , PbZrO_3 and BaTiO_3 , to observe their behaviour in separated fields. This work, along with a comparison with their corresponding metal oxides is presented in Chapters 4 and 5.

The initial double perovskite system to be investigated is the $\text{Sr}_2\text{FeMo}_{1-x}\text{W}_x\text{O}_6$ series. This solid solution series has been thoroughly characterised since its HM-FM property was discovered in the late nineties.⁶³ The electrical and magnetic properties are well known so this series is ideal to use initially with the induction and microwave thermal analysis techniques. This work is presented in Section 5.10.

The effect of substituting the $\text{Fe}^{2+/3+}$ on the B-site with Cr^{3+} to give the $\text{Sr}_2\text{CrMo}_{1-x}\text{W}_x\text{O}_6$ series has been investigated using IHTA and MWTA. Investigation of the T_C and changes in magnetic and electrical properties of this series have been examined. This solid series has been documented previously as having a high T_C at room temperature,^{101,105,107,117} which is why further investigation with the novel instrumentation was deemed necessary as it was hoped that the phase change would be observable with the induction heater. This work is presented in Sections 5.11.2 and 5.12.2

Substitutions on the A-site have also been investigated in this study. Using Ln^{3+} ions (where $\text{Ln} = \text{La}$), as a substitution for Sr^{2+} ions in the solid solution series $\text{Sr}_{2-x}\text{La}_x\text{FeMoO}_6$. In this series, where $x=0, 0.05, 0.1, 0.15, 0.2$, it is hoped the La^{3+} ions will be forced to substitute on the A-site due to their large ionic radius, as previous research suggests, and that these changes will be evident in the thermograms from the MWTA and the IHTA. This series has been analysed using the IHTA and MWTA, and the work is presented in Sections 5.11.3 and 5.12.3

All the series have been characterised using powder X-ray diffraction (P-XRD). These instrumental techniques will be discussed in Chapter 2.

Chapter 2

2.0 Experimental

2.1 Sample Synthesis

Metal oxides and perovskites were purchased from Fischer Scientific and Sigma-Aldrich chemical suppliers. Solid solution series and the complex perovskite systems were synthesised *via* the standard ceramic route. Stoichiometric amounts of dried starting materials were ground together with a pestle and mortar, with acetone as a homogenising medium. The subsequent mixtures were heated in furnace using an alumina crucible until a single phase was formed.

2.1.1 Ni_x-Mg_xO solid solution

Nickel nitrate (Ni(NO₃)₂·6H₂O) and magnesium carbonate basic (MgCO₃·Mg(OH)₂·3H₂O) were weighed according to the required ratio (Where x = 1.0, 0.25, 0.5, 0.75 and 0.0). Enough deionised water was added to make a green paste. The paste was heated in an alumina crucible for approximately one hour at 110°C to remove water. The dried mixture was re-ground and calcined at 800°C overnight, which resulted in a grey solid.¹¹⁸ This was ground to a fine powder and analysed with powder XRD (fig. 2.1 below).

2.1.2 Sr₂FeMo_{1-x}W_xO₆

The following samples were synthesised using strontium carbonate, Iron (II) oxide, tungsten oxide, and ammonium molybdate tetrahydrate *via* grinding with acetone. Initial synthesis was prepared *via* the route outlined by Kobayashi,⁶³ but further heating was required with some samples which was increased gradually to remove impurities.

- Sr₂FeMoO₆ – synthesised *via* the following heating patterns. Grinding of sample was repeated between each heating phase.
 - 300 °C in air for 2 hours.
 - 800 °C for 24 hours in air.
 - 1075 °C for 6 hours (× 2) 5% H₂/N₂ atmosphere
- Sr₂FeMo_{0.75}W_{0.25}O₆ - synthesised *via* the following heating patterns. Grinding of sample was repeated between each heating phase.
 - 300 °C in air for 2 hours.
 - 800 °C for 24 hours in air.
 - 1100 °C for 6 hours (× 2) H₂/N₂ atmosphere
 - 1175 °C fo 6 hours 5% H₂/N₂ atmosphere

- $\text{Sr}_2\text{FeMo}_{0.25}\text{W}_{0.75}\text{O}_6$ - synthesised *via* the following heating patterns. Grinding of sample was repeated between each heating phase.
 - 300 °C in air for 2 hours.
 - 800 °C for 24 hours in air.
 - 1100 °C for 6 hours ($\times 2$) 5% H_2/N_2 atmosphere
 - 1175 °C for 6 hours 5% H_2/N_2 atmosphere
- $\text{Sr}_2\text{FeMo}_{0.5}\text{W}_{0.5}\text{O}_6$ - synthesised *via* the following heating patterns. Grinding of sample was repeated between each heating phase.
 - 300 °C in air for 2 hours.
 - 800 °C for 24 hours in air.
 - 1200 °C for 6 hours ($\times 2$) 5% H_2/N_2 atmosphere
- Sr_2FeWO_6 - synthesised *via* the following heating patterns. Grinding of sample was repeated between each heating phase.
 - 300 °C in air for 2 hours.
 - 800 °C for 24 hours in air.
 - 1200 °C for 6 hours ($\times 2$) 5% H_2/N_2 atmosphere

It was found after numerous heating and grinding phases for each sample that these heating patterns gave the least impurities in the final compositions.

2.1.3 $\text{Sr}_{2-x}\text{La}_x\text{FeMoO}_6$

The following samples were synthesised using strontium carbonate, lanthanum (III) oxide, Iron (II) oxide, and ammonium molybdate tetrahydrate *via* grinding with acetone.⁴¹

- $\text{Sr}_{1.95}\text{La}_{0.05}\text{FeMoO}_6$ – synthesised *via* the following heating patterns. Grinding of sample was repeated between each heating phase.
 - 900 °C for 3 hours in air.
 - 1100 °C for 12 hours in 5 % H_2/N_2 reducing atmosphere.
 - 1150 °C for 12 hours in 5 % H_2/N_2 reducing atmosphere.
 - 1200 °C for 12 hours in 5 % H_2/N_2 reducing atmosphere.
- $\text{Sr}_{1.9}\text{La}_{0.1}\text{FeMoO}_6$ – synthesised *via* the following heating patterns. Grinding of sample was repeated between each heating phase.
 - 900 °C for 3 hours in air.
 - 1100 °C for 12 hours in 5 % H_2/N_2 reducing atmosphere.
 - 1150 °C for 12 hours in 5 % H_2/N_2 reducing atmosphere.
 - 1200 °C for 12 hours in 5 % H_2/N_2 reducing atmosphere.

- $\text{Sr}_{1.85}\text{La}_{0.15}\text{FeMoO}_6$ – synthesised *via* the following heating patterns. Grinding of sample was repeated between each heating phase.
 - 900 °C for 3 hours in air.
 - 1100 °C for 12 hours in 5 % H_2/N_2 reducing atmosphere.
 - 1150 °C for 12 hours in 5 % H_2/N_2 reducing atmosphere.
 - 1150 °C for 12 hours in 5 % H_2/N_2 reducing atmosphere.
- $\text{Sr}_{1.80}\text{La}_{0.02}\text{FeMoO}_6$ – synthesised *via* the following heating patterns. Grinding of sample was repeated between each heating phase.
 - 900 °C for 3 hours in air.
 - 1150 °C for 12 hours in 5 % H_2/N_2 reducing atmosphere.
 - 1150 °C for 12 hours in 5 % H_2/N_2 reducing atmosphere.

2.1.4 $\text{Sr}_2\text{CrMo}_{1-x}\text{W}_x\text{O}_6$

The following series was synthesised by a final year student to investigate the impact of substituting the Fe ion on the B site for a different transition metal.⁸⁴ The synthesis of this series is outlined below:

- $\text{Sr}_2\text{CrMoO}_6$ - synthesised *via* the following heating patterns. Grinding of sample was repeated between each heating phase.
 - 350 °C for 1 hour in air.
 - 1400 °C for 12 hours in 5 % H_2/N_2 reducing atmosphere
- $\text{Sr}_2\text{CrMo}_{0.9}\text{W}_{0.1}\text{O}_6$ - synthesised *via* the following heating patterns. Grinding of sample was repeated between each heating phase.
 - 350 °C for 1 hour in air.
 - 800 °C for 12 hours in air
 - 1400 °C for 12 hours in 5 % H_2/N_2 reducing atmosphere
- $\text{Sr}_2\text{CrMo}_{0.7}\text{W}_{0.3}\text{O}_6$ - synthesised *via* the following heating patterns. Grinding of sample was repeated between each heating phase.
 - 350 °C for 1 hour in air.
 - 800 °C for 12 hours in air
 - 1400 °C for 12 hours in 5 % H_2/N_2 reducing atmosphere
- $\text{Sr}_2\text{CrMo}_{0.5}\text{W}_{0.5}\text{O}_6$ - synthesised *via* the following heating patterns. Grinding of sample was repeated between each heating phase.
 - 350 °C for 1 hour in air.
 - 1400 °C for 12 hours in 5 % H_2/N_2 reducing atmosphere (× 2)
 - 1400 °C for 6 hours in 5 % H_2/N_2 reducing atmosphere
 - 1400 °C for 12 hours in 5 % H_2/N_2 reducing atmosphere (× 3)
 - Ground using a ball mill for 10 minutes at 300 rpm.

- 1400 °C for 24 hours in 5 % H₂/N₂ reducing atmosphere
- 1400 °C for 12 hours in 10 % H₂/N₂ reducing atmosphere (× 2)
- Sr₂CrMo_{0.3}W_{0.7}O₆ - synthesised *via* the following heating patterns. Grinding of sample was repeated between each heating phase.
 - 350 °C for 1 hour in air.
 - 1400 °C for 12 hours in 5 % H₂/N₂ reducing atmosphere (× 2)
 - 1400 °C for 6 hours in 5 % H₂/N₂ reducing atmosphere
 - 1400 °C for 12 hours in 5 % H₂/N₂ reducing atmosphere (× 3)
 - Ground using a ball mill for 10 minutes at 300 rpm.
 - 1400 °C for 24 hours in 5 % H₂/N₂ reducing atmosphere
 - 1400 °C for 12 hours in 10 % H₂/N₂ reducing atmosphere
- Sr₂CrMo_{0.1}W_{0.9}O₆ - synthesised *via* the following heating patterns. Grinding of sample was repeated between each heating phase.
 - 350 °C for 1 hour in air.
 - 1400 °C for 12 hours in 5 % H₂/N₂ reducing atmosphere (× 2)
 - 1400 °C for 6 hours in 5 % H₂/N₂ reducing atmosphere
 - 1400 °C for 12 hours in 5 % H₂/N₂ reducing atmosphere (× 3)
 - Ground using a ball mill for 10 minutes at 300 rpm.
 - 1400 °C for 24 hours in 5 % H₂/N₂ reducing atmosphere
 - 1400 °C for 12 hours in 10 % H₂/N₂ reducing atmosphere

2.2 Characterisation of synthesised compounds

2.2.1 Ni_x-Mg_xO solid series

Ni_x-Mg_xO was ground to a fine, grey powder and analysed with powder XRD (fig. 2.1 below).

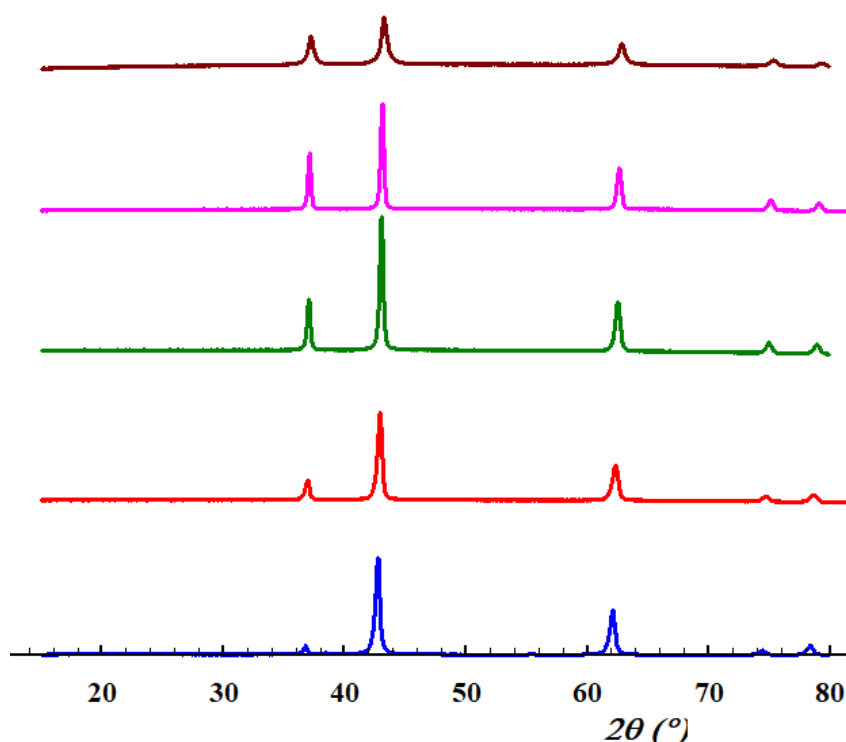


Fig. 2.1 XRD patterns for the Ni_x-Mg_xO solid series 15 – 80 2θ
Blue – Dried MgO. Red – Ni_{0.25}Mg_{0.75}. Green- Ni_{0.5}Mg_{0.5}. Pink - Ni_{0.75}Mg_{0.25}. Brown – dried NiO

NiO and MgO were studied with relation to Vegard's Law, which is an approximate empirical formula which holds that there is a linear relationship between the lattice parameters of an alloy and its constituent elements.¹¹⁹ This behaviour is known in literature already but aided in characterisation of the compounds. In other words, adding one of the oxides to another in a series of solid solutions should yield different sized lattices depending on the amount of oxide added. This relationship was confirmed between the NiO and MgO, as increasing amounts of MgO were added to NiO, the lattice parameters increased linearly due to the larger cation being introduced into the system. This was done using Chekcell software¹²⁰ and lattice parameters are shown in fig 2.2 and table 2.1.

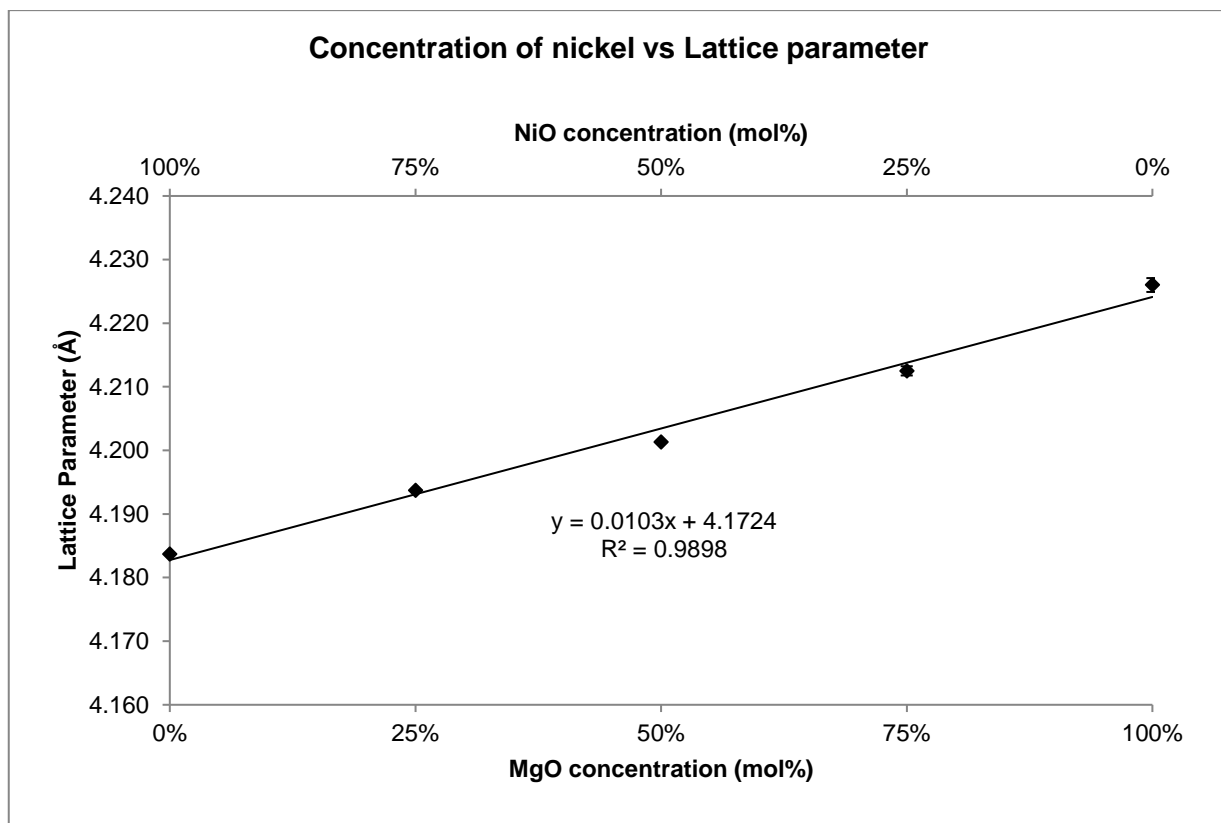


Table 2.1 Lattice parameter values from Chekcell, used to check if rock salt series follows Vegard's law.

Rock salt composition	a = b = c (Å)	$\alpha = \beta = \gamma$ (°)
NiO	4.1837 (1)	90
NiO _{0.75} -MgO _{0.25}	4.1937 (5)	90
NiO _{0.5} -MgO _{0.5}	4.2013 (2)	90
NiO _{0.25} -MgO _{0.75}	4.2125 (7)	90
MgO	4.2260 (1)	90

Fig 2.2. Linear relationship between NiO and MgO in solid solution

2.2.2 $\text{Sr}_2\text{FeMo}_{1-x}\text{W}_x\text{O}_6$

The double perovskite series was synthesised as discussed in section 2.1.2. The resulting powders were analysed using powder XRD (fig. 2.3), initially for 2 hours, the data were then refined using Rietveld analysis in GSAS.¹²¹ These patterns were then substituted into the refinement. A second phase also had to be inserted into the refinement as there was an impurity observed in both the Mo (SrMoO_4) and W (SrWO_4) variations of the compound.

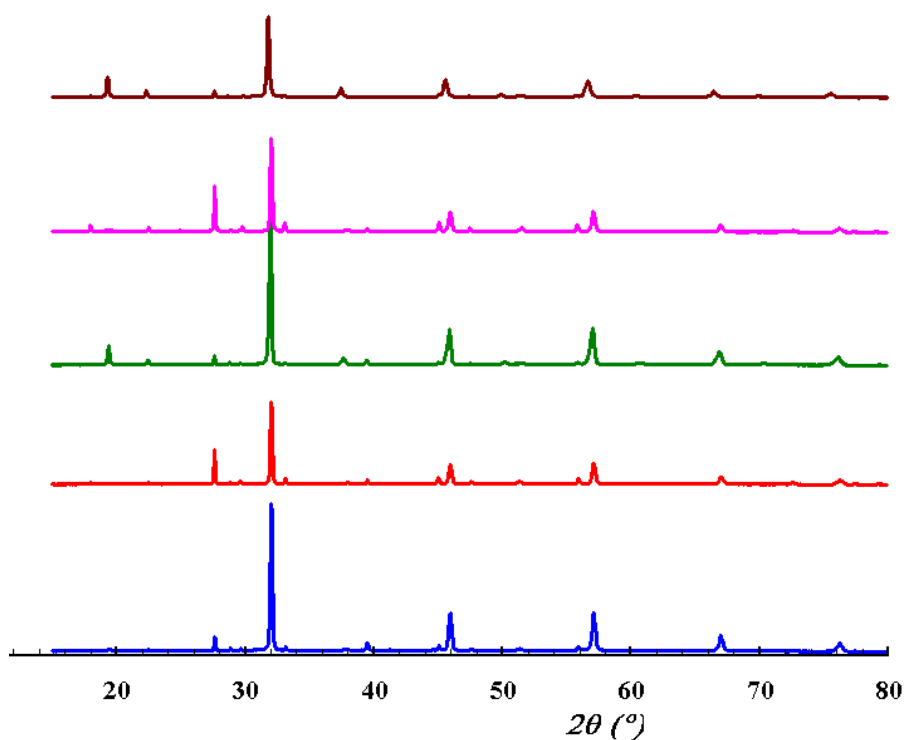


Fig 2.3. XRD patterns for the $\text{Sr}_2\text{FeMo}_{1-x}\text{W}_x\text{O}_6$ series 15 – 80 2θ
Blue – $\text{Sr}_2\text{FeMoO}_6$. Red – $\text{Sr}_2\text{FeMo}_{0.75}\text{W}_{0.25}\text{O}_6$. Green- $\text{Sr}_2\text{FeMo}_{0.5}\text{W}_{0.5}\text{O}_6$. Pink - $\text{Sr}_2\text{FeMo}_{0.25}\text{W}_{0.75}\text{O}_6$. Brown – Sr_2FeWO_6

Refined XRD patterns (using GSAS) are shown in figs 2.4 – 2.6. Red tick marks correspond to the impurity phases and black tick marks are the peaks corresponding to the double perovskite that has been synthesised. The purple pattern indicates the difference between the measured and calculated patterns.

LT013 Sr₂FeMoO₆ 1hr
 Lambda 1.5406 A, L-S cycle 4353

Hist 1

Obsd. and Diff. Profiles

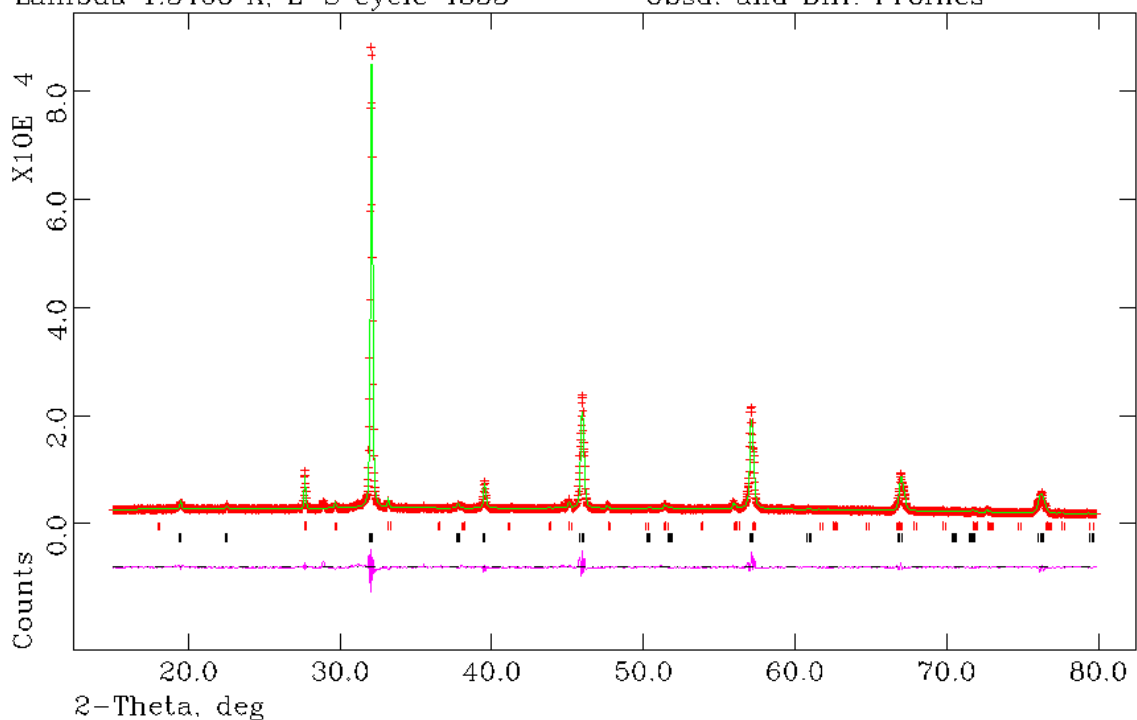


Fig 2.4. Refinement plot for Sr₂FeMoO₆. Starting model for refinement from ICSD database collection code 150701 – green pattern. Refined synthesised pattern – red crosses. Impurity phase – red tick marks. Synthesised double perovskite pattern – black tick marks. Purple pattern indicates difference between measured and calculated patterns.

LT013_Sr2FeW06_1hr
 Lambda 1.5406 A, L-S cycle 1337

Hist 1

Obsd. and Diff. Profiles

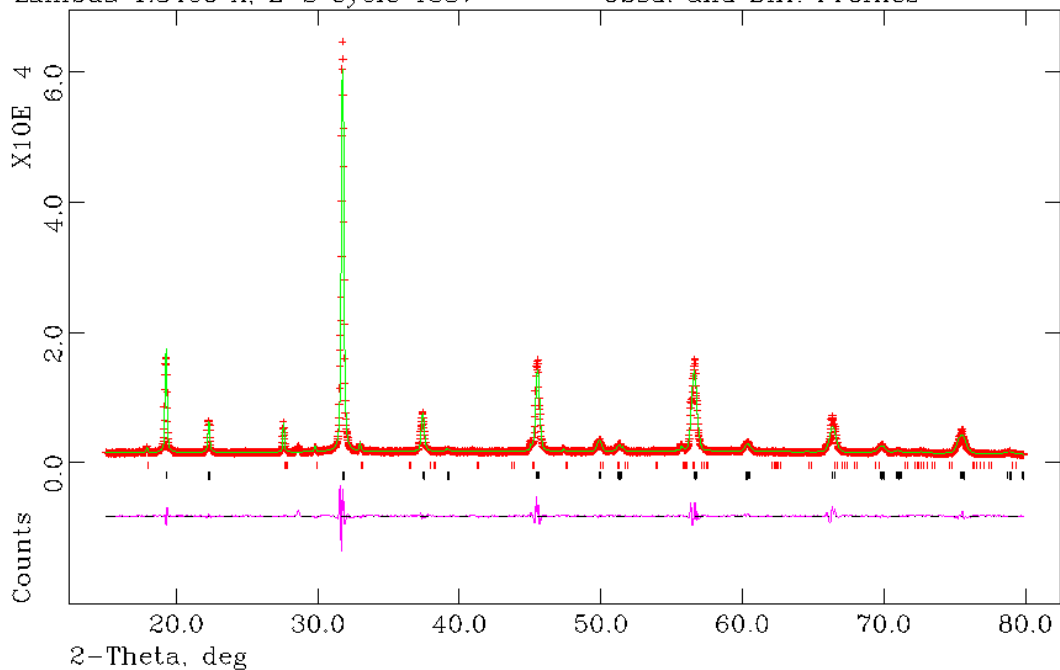


Fig 2.5 Refinement plot for Sr₂FeWO₆ Starting model for refinement from ICSD database collection code 153430 – green pattern. Refined synthesised pattern – red crosses. Impurity phase – red tick marks. Synthesised double perovskite pattern – black tick marks. Purple pattern indicates difference between measured and calculated patterns.

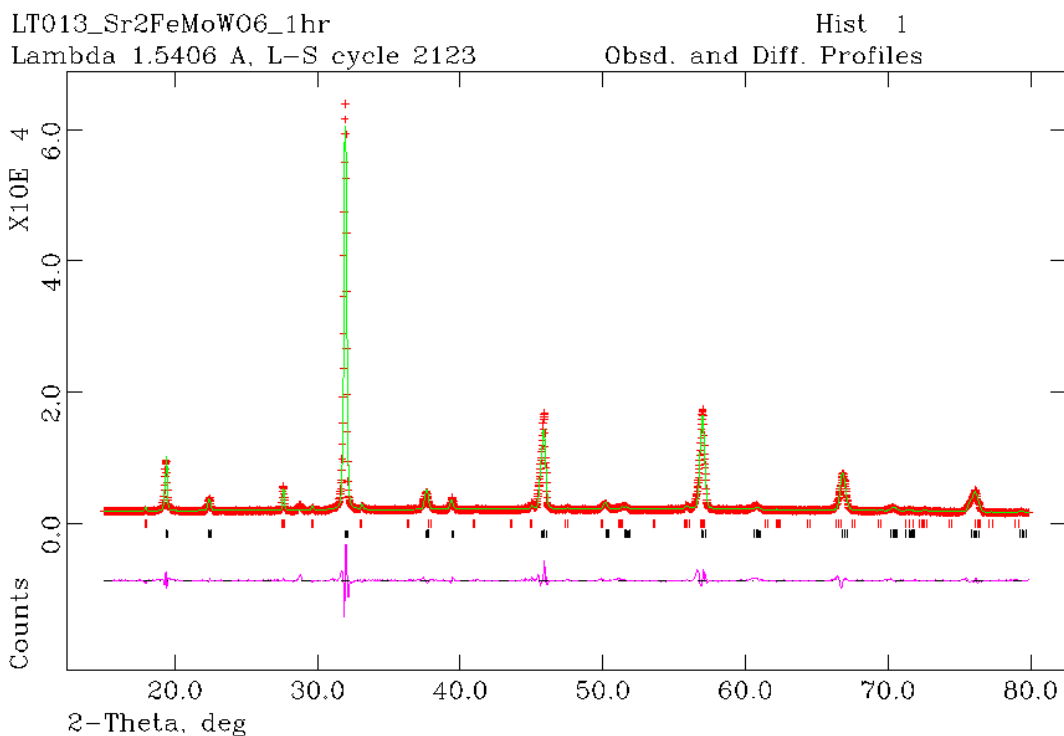


Fig 2.6 Refinement plot for $\text{Sr}_2\text{FeMo}_{0.5}\text{W}_{0.5}\text{O}_6$ Starting model for refinement from ICSD database collection code 153428 – green pattern. Refined synthesised pattern – red crosses. Impurity phase – red tick marks. Synthesised double perovskite pattern – black tick marks. Purple pattern indicates difference between measured and calculated patterns.

Due to instrumentation issues later in the research project, it was difficult to collect and refine some of the data. While initial classification was possible using the XRD, the refined data shown above was gained on a different instrument and due to time constraints, it was not possible to refine the whole sample set.

2.2.3 $\text{Sr}_{2-x}\text{La}_x\text{FeMoO}_6$

In fig. 2.7 overleaf, the XRD patterns for the $\text{Sr}_2\text{LaFeMoO}_6$ compositions are shown. Again due to time constraints, full refinement was not possible, and it was difficult to make a comparison as there were very few literature resources containing a comparable XRD pattern with the compositions investigated here. The patterns overleaf, paired with the research with the MWTA and IHTA instrumentation suggest that the compositions are close to what was expected, although any impurities, as suggested with all other samples investigated, may also influence the results gained.

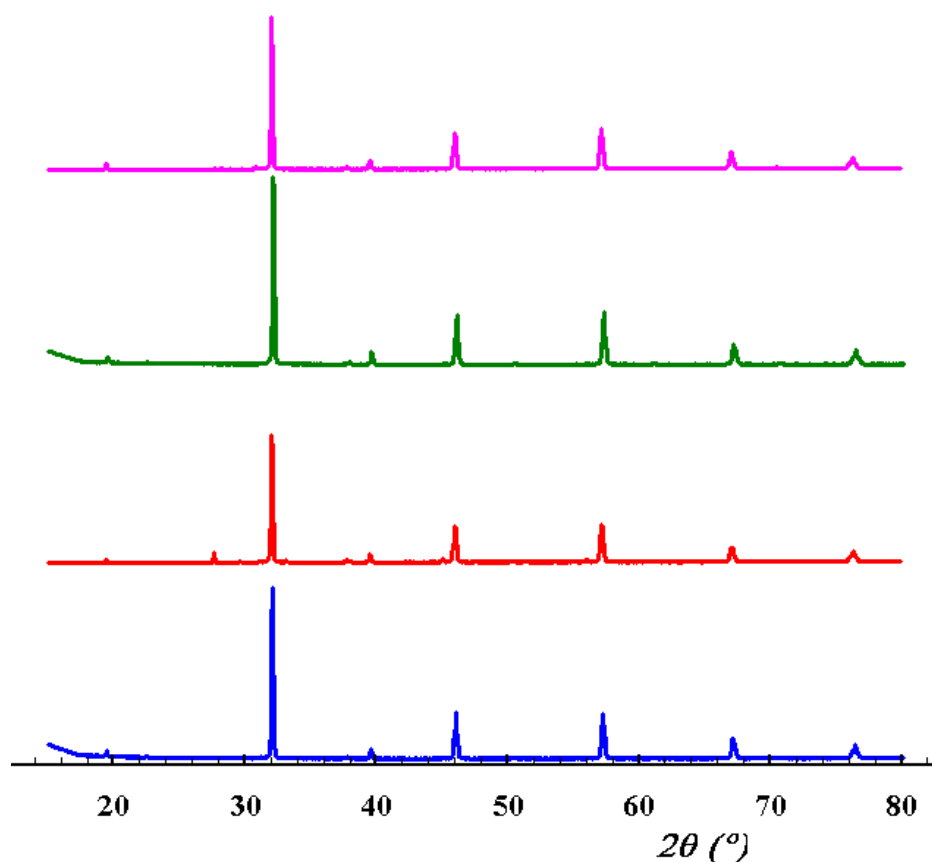


Fig 2.7. XRD patterns $\text{Sr}_{2-x}\text{La}_x\text{FeMoO}_6$ series 15 – 80 2θ
Blue – $\text{Sr}_{1.95}\text{La}_{0.05}\text{FeMoO}_6$. Red – $\text{Sr}_{1.9}\text{La}_{0.1}\text{FeMoO}_6$. Green- $\text{Sr}_{1.85}\text{La}_{0.15}\text{FeMoO}_6$.
Pink - $\text{Sr}_{1.8}\text{La}_{0.2}\text{FeMoO}_6$.

2.2.4 $\text{Sr}_2\text{CrMo}_{1-x}\text{W}_x\text{O}_6$

Fig 2.8 shows four of the $\text{Sr}_2\text{CrMo}_{1-x}\text{W}_x\text{O}_6$ series. More samples were synthesised but the other files were corrupted so it was impossible to open them for characterisation with the other samples so they have been removed from any further analysis. All the samples were analysed with the IHTA and the MWTA but it is impossible at this stage to know whether the desired composition or the impurities are responsible for any results.

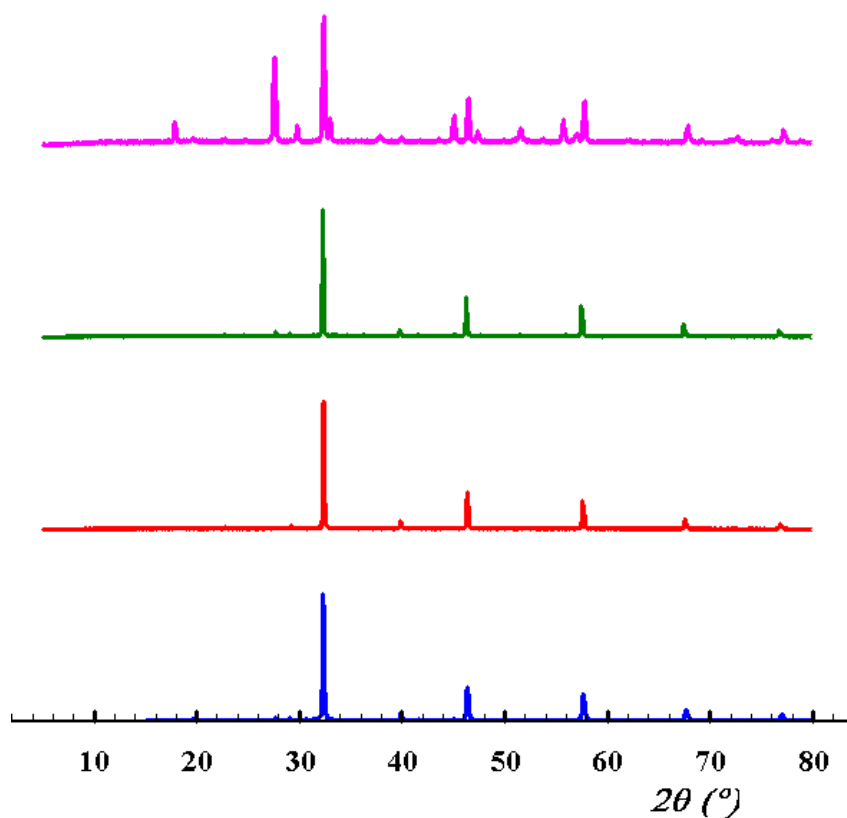


Fig 2.8. XRD patterns $\text{Sr}_2\text{CrMo}_{1-x}\text{W}_x\text{O}_6$ series 15 – 80 2θ
Blue – $\text{Sr}_2\text{CrMoO}_6$. Red – $\text{Sr}_2\text{CrMo}_{0.9}\text{W}_{0.1}\text{Mg}_{0.25}\text{O}_6$. Green- $\text{Sr}_2\text{CrMo}_{0.7}\text{W}_{0.3}\text{O}_6$.
Pink - Sr_2CrWO_6

Chapter 3

3.0 Thermal methods of analysis

3.1 Thermogravimetric Analysis (TGA)

Thermogravimetric analysis (TGA) is a thermal analysis technique where a substance is subject to a controlled temperature programme and the change in mass of the substance is measured as a function of temperature. A loss in mass is only observed if a volatile component is lost.¹²²

In a typical TGA instrument set up, the sample is placed in an inert crucible which is attached to a sensitive balance and a furnace is positioned around the sample. Heat is then transferred to the sample by conduction. This has its limitations and can cause temperature gradients within the sample, reducing the resolution of the data.^{25,122}

3.2 Differential Thermal Analysis (DTA)

The most widely used methods of thermal analysis techniques are differential thermal analysis (DTA) and differential scanning calorimetry (DSC). Information about a sample is obtained by heating the sample alongside an inert reference sample and thermal changes can be observed. W.C Roberts-Austen was one of the first to introduce the concept of modern DTA in 1899.¹²³ His instrument included the reference sample to enable the user to gain a larger value of temperature difference (ΔT). This DTA technique suffered from poor repeatability until Norton¹²⁴ used the peak area instead of peak height to make quantitative measurement. The next advance was in 1955 by Boersma.¹²⁵ His design of a new sample holder separated the reference and sample temperature by heating on a piece of thermally conductive material, enabling the differential temperature to be measured.

DSC is discussed in further detail in Section 3.3, but the practical distinction between DTA and DSC has to do with the nature of the signal obtained from the equipment. With DTA, the signal is proportional to T established between the sample and reference. With DSC, the signal is proportional to difference in thermal power between the sample and the reference.¹²²

3.3. Differential Scanning Calorimetry (DSC)

Differential scanning calorimetry (DSC) is fast, simple and widely available so it is one of the most used methods of thermal analysis. In DSC, a sample and a reference are placed in holders in the instrument. The interior furnace can ramp the temperature at a specified rate (e.g. $10^{\circ}\text{C min}^{-1}$) or can hold the DSC at a specific temperature. The difference in the heat flow between the sample and the reference is measured by the instrument. DSC differs from differential thermal analysis (DTA) in that DSC is calorimetric method, where the energy difference is measured, whereas with DTA, it is the difference in temperature which is measured. The temperature programs for both methods are similar, whereas DSC is considered to be a quantitative method, DTA is a qualitative method.¹⁶ Fig. 3.1 shows a simplified set up of a heat-flux DSC and a power compensated DSC.

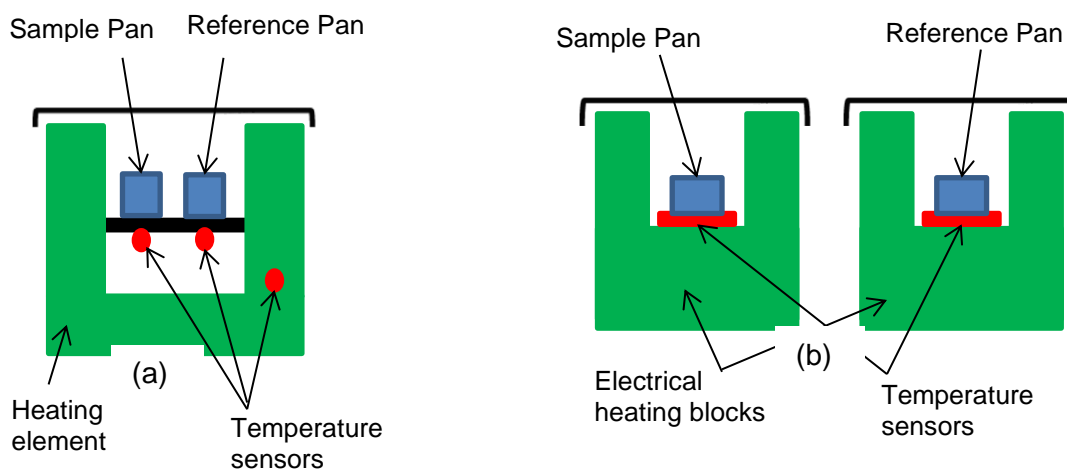


Fig. 3.1 DSC instrumentation (a) Heat-flux DSC (HF-DSC) and (b) Power compensated DSC (PC-DSC).

There are different types of DSC, power compensated DSC (PC-DSC), heat-flux DSC (HF-DSC) and modulated DSC (MDSC). Each one gives a plot of heat flow or power against temperature, called a thermogram.¹⁷

With PC-DSC, the temperatures of the sample and reference are kept equal while both temperatures are increased or decreased linearly. Two independent heating units are employed and these heating units are quite small to give a rapid heating, cooling and equilibration rates. It does have lower sensitivity than HF-DSC but has a faster response time, which makes it ideal for kinetic studies where fast equilibration and new temperature settings are needed.¹⁶

In HF-DSC, the sample and reference are heated by a single heating unit, and the difference in heat-flow into the sample and reference is measured, while the sample temperature is changed at a constant rate. The differential is monitored by chromel-constantin thermocouples and the differential heat flow is directly proportional to the difference in the output of the two thermocouple junctions. Fig 3.2 is a typical DSC thermogram showing the different types of phase transitions and how they appear within the pattern.

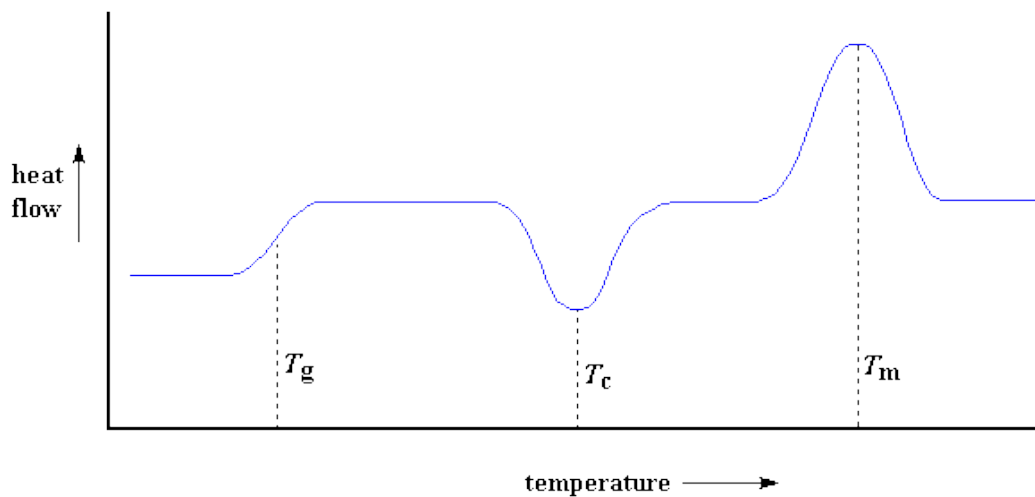


Fig 3.2 Typical DSC thermogram where: T_g = Glass transition temperature, T_c = crystallisation temperature (exothermic event) and T_m = melting temperature (endothermic event).

MDSC has the same set up as HF-DSC. Using Fourier transform methods, the overall signal is split into two parts, a reversing heat-flow signal, which is associated with the heat capacity component of the thermogram, and a non-reversing heat flow signal, which is related to kinetic processes. Different transitions appear in either one or both of the signals.

3.4. Microwave Thermal Analysis (MWTA)

An MWTA instrument was designed, constructed and developed at the University of Huddersfield to allow the analysis of dielectric materials and changes to their properties when held in an electromagnetic field. The initial developments were performed by Dr. G.M.B. Parkes^{14,23,24,126} and Dr. I. Hamilton.²⁵ The schematic of the original MWTA instrument is shown previously in fig. 1.7.

Current research has been focussed on looking at the effect of the separate components of the EM field on dielectric materials – the electric field (E-field) and the magnetic field (H-field). The adaptations are discussed in Section 3.2.4.

3.4.1 Microwave heating

Since the use of microwaves for heating was discovered during the mid-20th century, several various uses have been found due to the induction of heating compared to a conventional furnace or cooker. Initially microwave heating was confined to industrial applications such as drying but more recently has been found to speed up processes such as ceramic sintering and polymer curing. Gedye *et al.*¹²⁷ have also utilised microwaves for organic synthesis and since these investigations, microwave synthesis has become of interest to synthetic chemists.

Although these developments have vastly increased the use of microwaves in both industrial and research areas, it's use as a thermal analysis technique had not been a broad area of research apart from the work by Karmazsin *et al.*^{21,22} This work led to the research undertaken by Parkes *et al.*^{11,14,23,24,126} and later the developments discussed within the current research.

3.4.2 Microwave heating theory

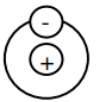
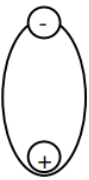
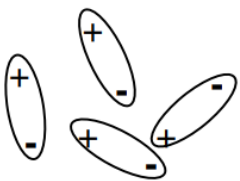
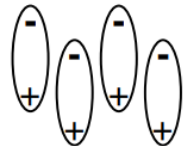
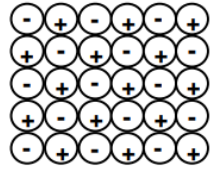
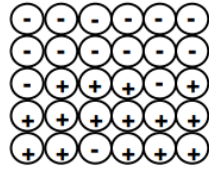
As mentioned in Section 1.1.5, in an electromagnetic wave, the electrical (E-) field and magnetic (H-) field are at 90° to one another with both of these components in phase (fig. 1.5).

Most research has focussed on observing how materials interact with the E-field of the electromagnetic field. Dielectric materials (a material in which polarisation can occur in an applied electrical field) were researched by Hamilton, and they differ from conductive materials in that their charges are bound by atomic or molecular forces. Charges in conductive materials are able to move macroscopic distances. These types of materials interact with microwaves in different ways and this is dependent on a number of factors within the material itself: Polarisation, permittivity, permeability and the electrical properties of the material.

3.4.2.1 Polarisation

When an applied electric field is introduced to a dielectric material, the induced charges will tend to realign. Three different types of polarisation are shown in table 3.1 below.

Table. 3.1 Types of polarisation including diagrams²⁵

Mechanism	No applied field	Applied field
Electronic polarisation		
Dipolar polarisation		
Interfacial polarisation (Maxwell-Wagner polarisation)		

Electronic polarisation causes the electrons to move from their position near the nuclei to an area where they can better track the electrical field. If a permanent dipole is present, the dipole again realigns itself which results in the dipolar polarisation. Interfacial polarisation causes the charges to accumulate in the interfaces of materials which in turn causes an induced dipole within the material.

3.4.2.2 Permittivity, permeability and electrical properties of materials

Permittivity is related to how efficiently the electromagnetic energy is converted into heat. A dielectric loss factor, calculated using the dielectric loss and the conductive loss, is required for a ratio against the permittivity. This ratio is equal to \tan which is a good indicator of the efficiency of material to turn the electromagnetic waves into heat. The greater the phase angle, the greater the losses from the material.²⁵ The electrical properties of a material have a large effect on the extent to which it heats in a microwave and while Hamilton's research²⁵ focussed primarily on the heating resulting from the electrical component of the wave, this research moved towards the significance of the magnetic component of the wave and the

permeability of the materials. Permeability of a material is the degree of magnetisation in response to an applied magnetic field. Materials with permeability equal to one are non-magnetic – the permeability is negligible.

Looking at the difference in temperature between the separate fields will give a better understanding of ability of materials to be heated by the microwaves. This will also lead on to the heating of particular materials when they are put into the IHTA instrument, as it is predicted, due to induction theory³⁰, that only the samples that heat well in the H-field of the microwave will heat in the induction heater.

3.5. Induction heating

3.5.1. Introduction

In 1831, English physicist Michael Faraday discovered the basis for induction heating after experimenting in his laboratory with two coils of wire wrapped around an iron core.^{26,27} Faraday concluded that a changing magnetic field can produce an electric current. Faraday's law of induction states that '*the electromotive force (emf) induced in a circuit is directly proportional to the time rate of change of magnetic flux through the circuit.*' The initial research following the findings of Faraday focussed on the development of equipment to generate a high frequency alternating current²⁷ for changing the level of voltage making electric transmission more efficient.²⁶ This process resulted in heat generated by the magnetic core of the induction equipment, and while attempts were made to reduce this heating, the exact opposite was explored for melting metal. De Ferranti¹²⁸, Colby¹²⁹ and Kjellin¹³⁰ developed induction furnaces (patents) that used non-conducting crucibles where electrical currents were induced directly into the metal charge.²⁷ Following the use of induction heating to melt metals, other applications were researched including hardening of steels.²⁷ During the mid-20th century, induction heating came under a broad term of 'radio frequency heating'.

3.5.2 Theory of Induction heating

Induction heating is an effective method as the heat is generated internally within a sample and the sample is not contaminated as there is no physical contact.¹³¹ The rate of heating is dependent on the frequency of the induced current, the intensity of the induced current and the specific heat capacity of the material. The magnetic permeability of the material is also of importance due to magnetic hysteresis. Magnetic hysteresis only occurs in magnetic materials. The magnetic flux field causes the magnetic dipoles within the material to oscillate as the magnetic poles change their orientation each cycle – much like the dipole interaction within the E-field of the microwave heating instrument.

Eddy currents are produced on the surface of the sample and therefore the depth at which heating will occur within the sample is dependent on the frequency and temperature.³⁰ The information surrounding induction heating relates to solid metal samples, therefore it is unknown whether the skin depth would have an effect on a ground sample.

There are many advantages to induction heating, the following being the most commonly recognised; Fast heating, efficient, controllable heating, improved industrial processes and cleanness and safety. Controlled heating is of importance within this research as the power

applied by the IH instrument can be accurately controlled through the design of the coil and the power convertor. It has been stated that specific features can be implemented such as localised heating, heating profiles and predefined temperatures.¹³²

Interest in the potential of induction heating for different applications has recently gained attention as it provides a contactless, efficient heating of conductive materials.¹³² It is becoming a favoured heating method of industrial, domestic and medical applications. Gomez-Polo *et al.*¹³³ investigated the use of IH for the synthesis of nanoparticle systems ($\text{Fe}_3\text{O}_4\text{-TiO}_2$) and have found that the procedure is much quick without fundamentally changing the magnetic response of the Fe_3O_4 nanoparticles and their further research is to investigate other metal oxide based precursors.

Chapter 4

4.0 Instrumentation

4.1 Non-thermal methods of characterisation

4.1.1 X-ray

X-ray is a term that encompasses all techniques for characterisation of materials using X-ray excitation. This includes powder X-ray diffraction (powder XRD).

If some form of excitation causes an electron to be lost from an inner shell of an atom, this electron is replaced by an electron from an outer shell. An X-ray photon is emitted as a difference in energy and the photon has a characteristic wavelength for the element.

4.1.2 X-ray Powder Diffraction (XRPD)

Three basic elements make up an X-ray diffractometer; an X-ray tube, a sample holder and an X-ray detector (fig. 4.1¹³⁴). The X-rays are generated in an X-ray tube, where a filament is heated to produce electrons. When the electrons have enough energy to dislodge an inner shell electron of the target material, characteristic patterns are produced. They consist of several components, the most common being K_{α} and K_{β} radiations. K_{α} consists of $K_{\alpha 1}$ and $K_{\alpha 2}$, but $K_{\alpha 1}$ has a slightly shorter wavelength and twice the intensity of $K_{\alpha 2}$. The wavelengths are characteristic of the target material (Cu, Fe, Mo and Cr). Copper is the most common target material, with $\text{Cu}K_{\alpha}$ radiation = 1.5418 Å. When the geometry of the incident X-rays satisfy the Bragg Equation (see equation 5) constructive interference of X-ray beams occur and a 'Bragg Reflection' will be picked up by a detector scanning at this angle. The detector opposite the source reads the intensity at 2θ away from the source. (fig. 4.2).¹³⁵ Positions of reflections give information about the inter-layer spacing of atoms in the structure. Peak intensities give information about how much X-ray scattering is contributing to that reflection, indicating where certain atoms lie, or how much of a specific phase is present. As a highly ordered system is required for diffraction to occur, only crystalline systems will diffract, whereas a generic shape of the background can indicate the presence of amorphous materials.

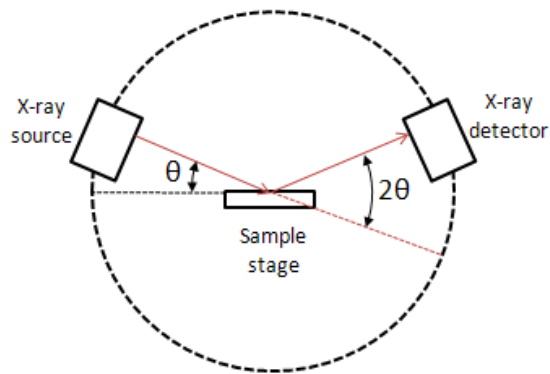


Fig. 4.1 Set up of an X-ray diffraction instrument¹³⁴

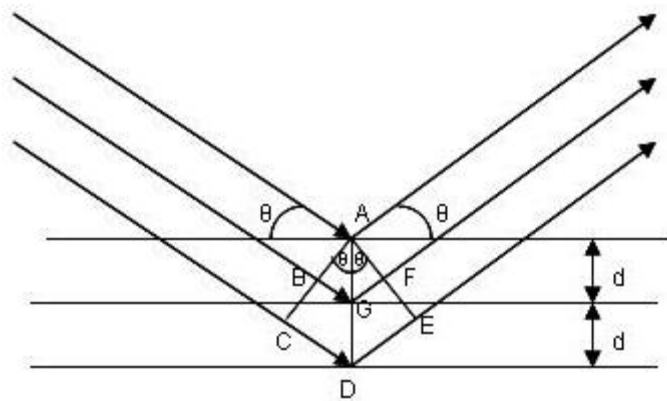


Fig. 4.2 Incident X-ray strikes a set of planes (with an interplanar distance (d), at an angle of 2θ)

Sir W.H Bragg and his son, Sir W.L. Bragg, discovered a geometric relationship between the distance of planes within a crystal and the angle of reflection to the X-rays that are diffracted off the crystal. The distances and the angle of reflection have to be in phase in order to signal, and only angles that satisfy the equation will register. Equation 5 is known as Bragg's Law:

$$\sin\theta = \frac{n\lambda}{2d}$$

Equation 5

Where:

- d is the spacing between diffracting planes
- θ is the incident angle
- n is any integer
- λ is the wavelength of the beam

4.2 Microwave (MW)

An MWTA instrument was designed, constructed and developed at the University of Huddersfield to allow the analysis of dielectric materials and changes to their properties when held in an electromagnetic field. The initial developments were performed by Dr. G.M.B. Parkes^{14,23,24,126} and Dr. I. Hamilton.²⁵ The schematic of the original MWTA instrument was shown earlier in fig. 1.7

Current research has been focussed on looking at the effect of the separate components of the EM field on dielectric materials – the electric field (E-field) and the magnetic field (H-field). The adaptations are discussed in Section 4.2.2.

4.2.1 MWTA basic cells

During the initial development of the MWTA instrument, the sample holders mainly consisted of an alumina cell coated with a susceptor material which assisted in the heating of the samples. Other cell designs consisted of a glass bulb which varied in size, allowing for different sample sizes to be investigated. The main disadvantage to this type of cell was that the material had to couple well with the electromagnetic field for heating to occur. Hamilton's research focussed on developing a sample cell that would allow the use of smaller sample sizes and allow more advanced analysis.

A number of cells developed by Hamilton are available to view in the doctoral thesis.²⁵

4.2.2 New MWTA cells for E- and H- analysis

In fig. 4.3 there is an aerial view of the new microwave sample section developed by Dr. G Ashton and Dr. G. Parkes. The thermocouple inlet corresponds to the inlet shown in figure 1.7, but in the adapted section, the inlet houses a glass tube packed with ceramic beads and quartz wool (see figure 4.8). The sample to be analysed is poured into the tube, between two fixed points to allow a fixed volume for each sample. This tube can then be moved a specified distance within the sample chamber, to allow the material to be housed where the maximum of the H-field is prevalent.

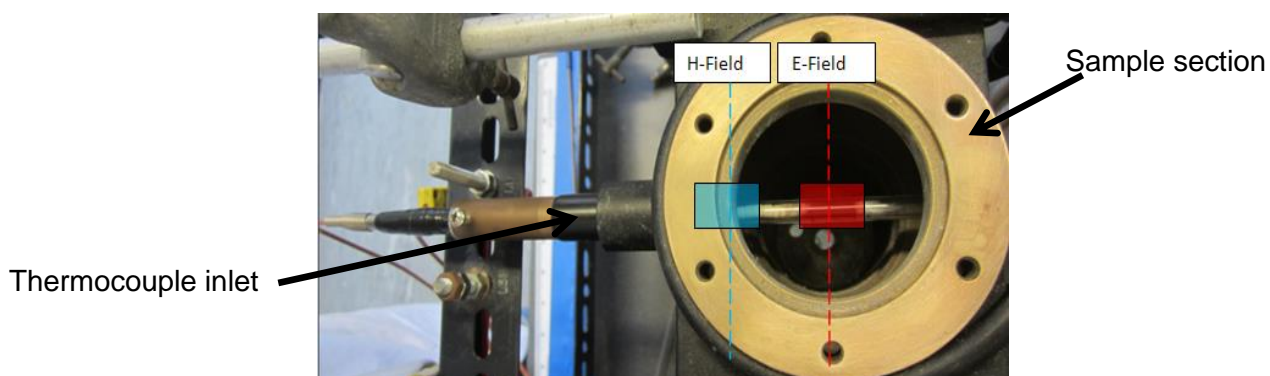


Fig. 4.3 Aerial view of the two sample locations within the electromagnetic wave.

Simplified diagrams of a sample in the different fields are shown in figures 4.4 (a) and (b).

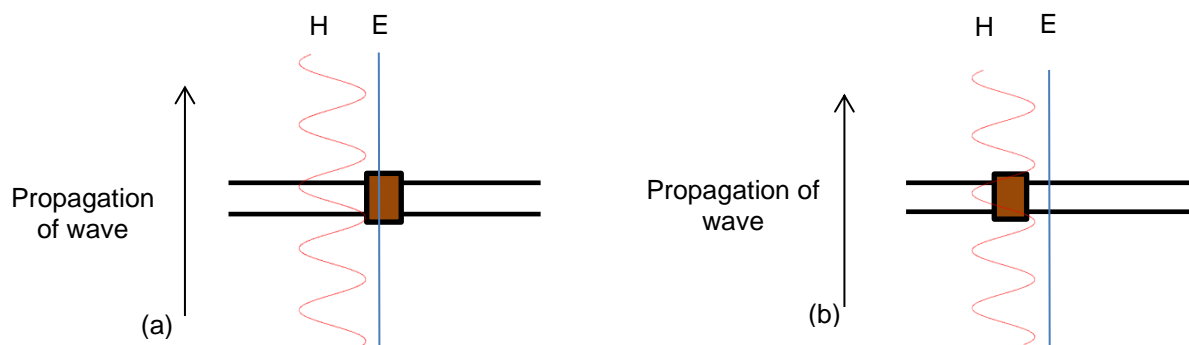


Fig. 4.4 (a) Sample shown in brown within the E-field of the electromagnetic wave and (b) within the H-field of the electromagnetic wave.

Fig. 4.5 (a) and (b), below, show the E- and H-field interacting with the sample. The sample here is placed in the adapted sample holder and it can clearly be seen how the fields interact with the sample within the microwave cavity.

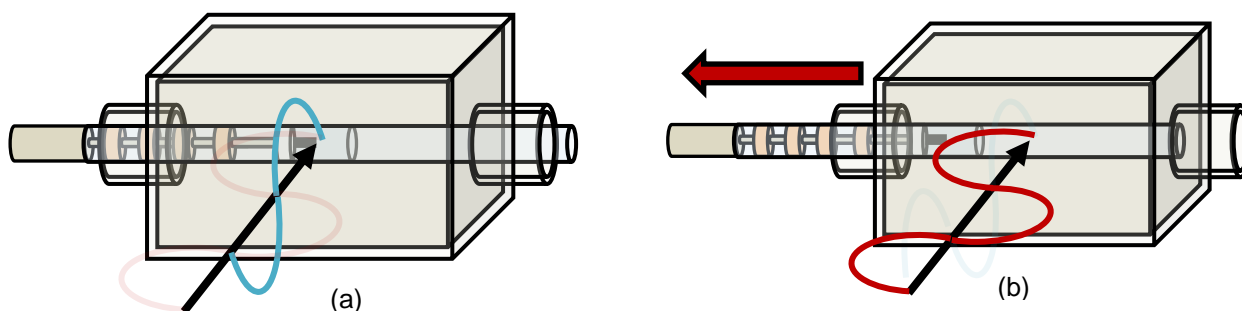


Fig. 4.5 (a) Sample located to the centre of the wave guide, Maximum electric field (E – Field)
 (b) Remove the sample a fixed distance into the Maximum of the Magnetic field (H-Field)

Figure 4.6 overleaf shows a schematic of the adapted sample holder for use in the microwave. The holder was made up of a thin glass tube containing a thermocouple which was fed through several ceramic beads. The sample was then loaded into the tube from above with a small lid to hold the sample in position. One issue with this sample holder is that it was not possible to weigh the sample. A volume marker was etched onto the holder and the samples were analysed via volume as opposed to weight.

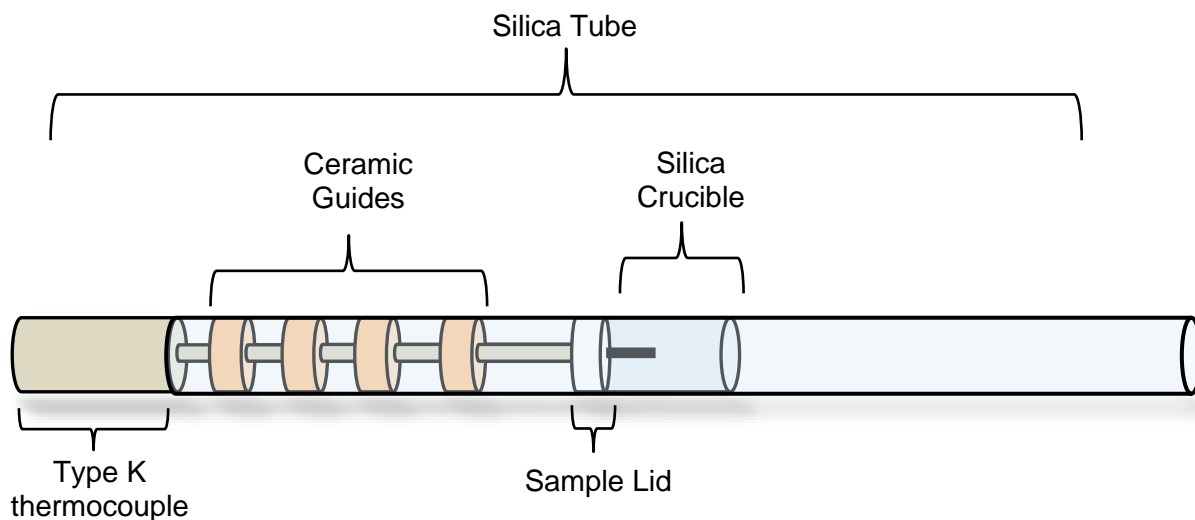


Fig. 4.6 Schematic of the sample holder allowing the sample to move location within the microwave.

4.3 Explanation of microwave thermogram

The following section examines the different ways in which microwave data can be presented. The relevance of the different representations allows interpretation of the results depending of different factors such as power, time and temperature. There is also the presentation of comparison data, which can be complicated when presented visually. In order to overcome this, temperatures or power input (depending on the experiment aim), is presented in an additional table.

Several experiments were completed by Dr. G Parkes in order to find the best way to represent the data. The microwave is capable of running two different types of experiments; linear heating and linear power.

With linear heating, a heating rate, or multiple heating ramps, is set and power is adjusted to keep this heating rate constant. An isothermal hold can also be utilised as it allows for a stable power trace. If an 'event' occurs, the power will adjust itself accordingly to compensate, e.g. a melting point will cause an increase in power in order to fully melt the sample.

Figure 4.7, shown overleaf, shows linear heating with three different temperature ramps (A, B and C). The ramps were set at $10\text{ }^{\circ}\text{C min}^{-1}$ and then an isothermal hold for 10 minutes. In this case, A has a longer heating ramp than B and C as the sample was heating from a lower temperature, less than $30\text{ }^{\circ}\text{C}$. The power can be seen adjusting to the set temperatures, with a small spike before each isothermal hold. The power holds relatively

steady when the sample temperature is isothermal. Table 4.1 gives a brief description of the temperature ramps seen in fig. 4.7.

Table 4.1. Power ramps and temperatures in MWTA thermogram.

	Temperature increase	Description
A	0-100°C	First temperature ramp from room temperature to 100°C then isothermal for 10 minutes
B	100-150°C	Second temperature ramp up to 150°C then isothermal for 10 mins
C	150-200°C	Third temperature ramp to 200°C then isothermal for 10 mins

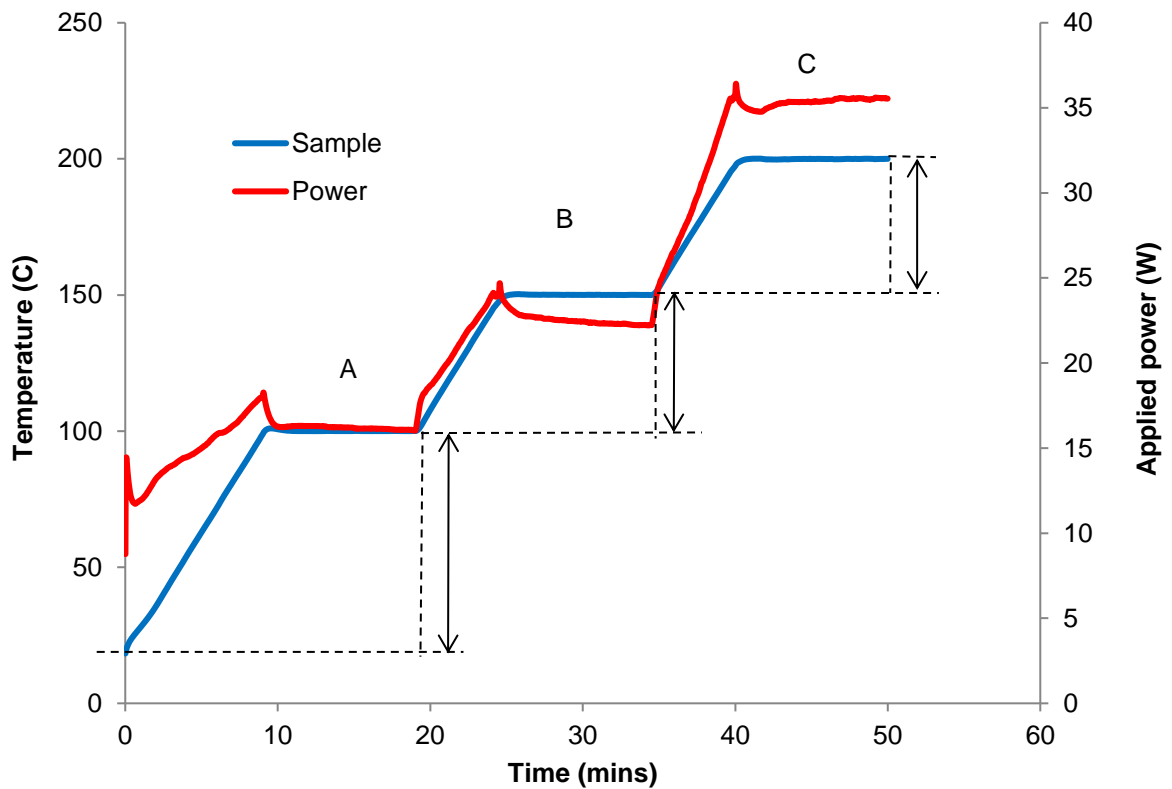


Fig 4.7 MWTA linear heating diagram

It can be observed in figure 4.7 that the power trace and sample temperature initialise at different points on the scale. Where temperature and power are plotted together, this is to be expected as the power always begins at zero, whereas the start temperature is dependent on room temperature. Where samples have been analysed on the microwave, and the room temperature differs, initial temperature readings have been normalised.

Linear power involves a constant input of power, or multiple power inputs, with isothermal holds until the set power is reached. This allows the temperature the freedom to adjust as a function of power. Fig. 4.8, below, shows the linear power heating of a sample. The applied power is set at three ramps with an isothermal hold after each point is met. The three ramps are set at 10 % (30 W), 15 %, (45 W) and 20 % (60 W). Table 4.2 gives a brief description of the three abbreviations displayed in fig. 4.8. This sample behaves well; its temperature increasing each time the power is increased. The one flaw with this type of heating is that there is an increased chance of thermal runaway, an example of which is shown in fig. 4.9 overleaf.

. Table 4.2 Description of abbreviations shown in fig 4.10.

Abbreviation	Description
ΔT_{30}	Temperature difference from 0 – 30 W applied power
ΔT_{45}	Temperature difference from 30 – 45 W applied power
ΔT_{60}	Temperature difference from 45 – 60 W applied power

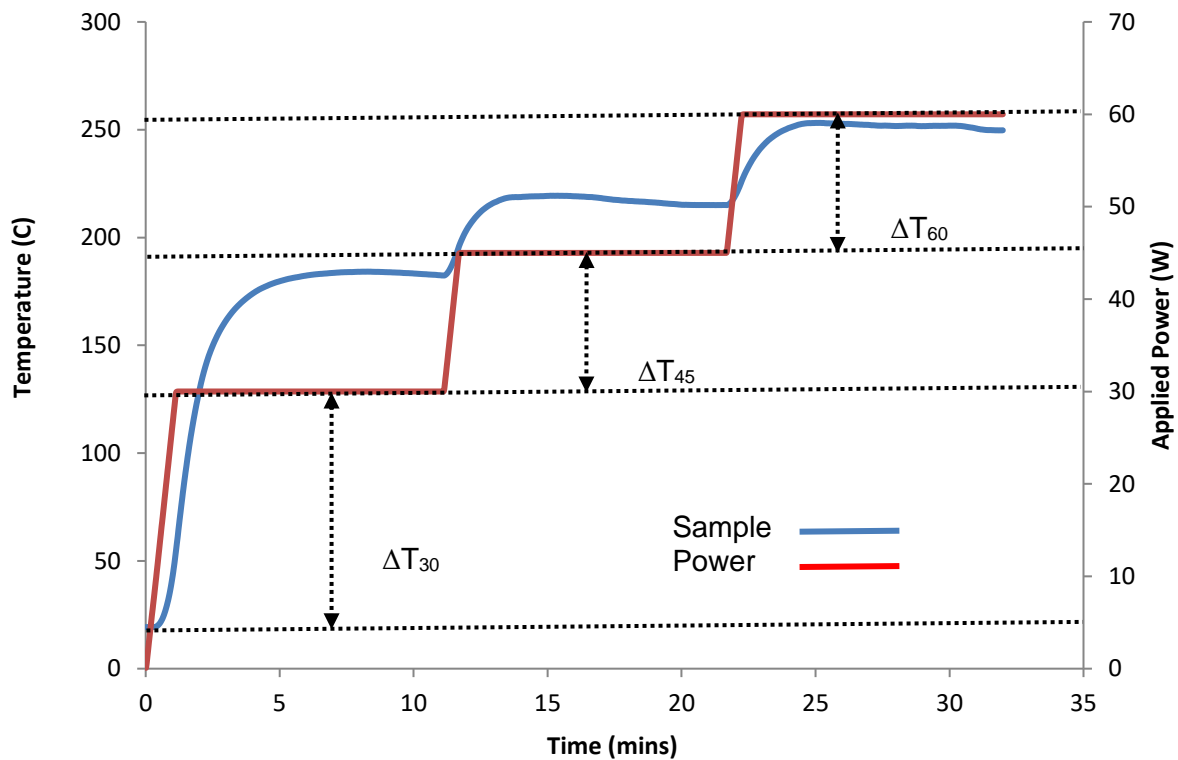


Fig 4.8 MWTA Linear power diagram

As can be seen in fig. 4.9, the power reaches 45 W and only gets partially through the isothermal hold before the temperature of the sample reaches the safety cut off value (250 °C). The sample temperature increases exponentially at approximately 98 °C.

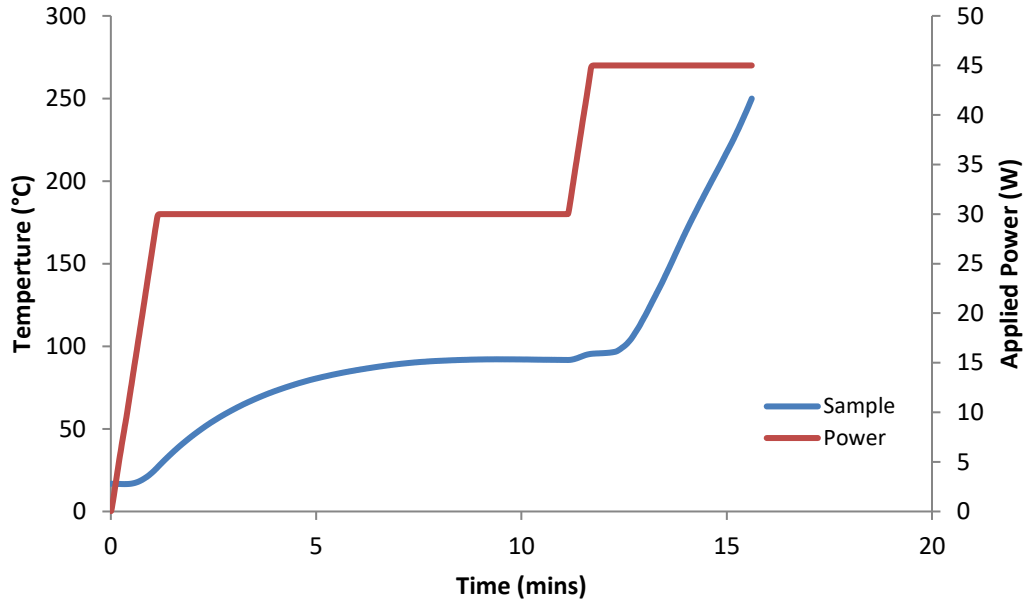


Fig 4.9 Linear power sample – thermal runaway

The data presented in this thesis will usually be shown in comparison to other data sets. The sample data analysis below shows the typical presentation which will be used throughout this section, allowing a simplified discussion of the materials' behaviour when held in the E-field and the H-field of the microwave.

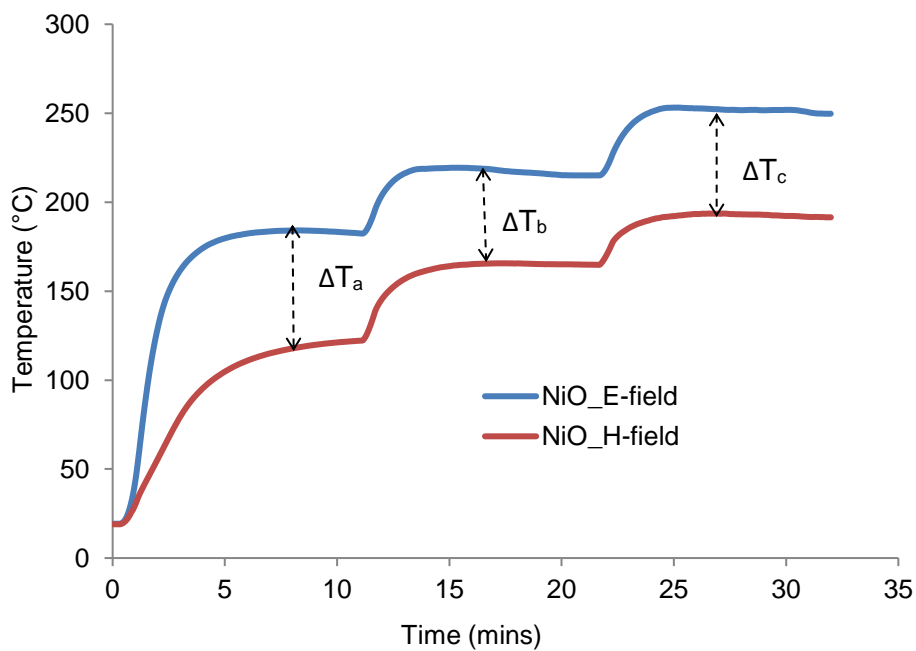


Fig 4.10 Sample comparison (NiO) using linear power programme

See table 4.3 (below) for explanation of ΔT_a , ΔT_b and ΔT_c . A subscript number shows temperature difference between more than two samples when compared together (see fig 4.10).

Table 4.3 Description of abbreviations used in fig. 4.10

Abbreviation	Description
ΔT_a	The difference in temperature of one sample, run in both the H-field and E-field at 30 W.
ΔT_b	The difference in temperature of one sample, run in both the H-field and E-field at 45 W.
ΔT_c	The difference in temperature of one sample, run in both the H-field and E-field at 60 W.

Fig. 4.11 below explains how data will be presented when samples are compared against one another. The abbreviations and brief description are detailed in table 5.4.

Table 4.4 Description of abbreviations in fig.4.11.

Abbreviation	Description
ΔT_{a1}	Temperature difference between NiO and MgO
ΔT_{a2}	Temperature difference between NiO and ZnO
ΔT_{a3}	Temperature difference between NiO and MnO

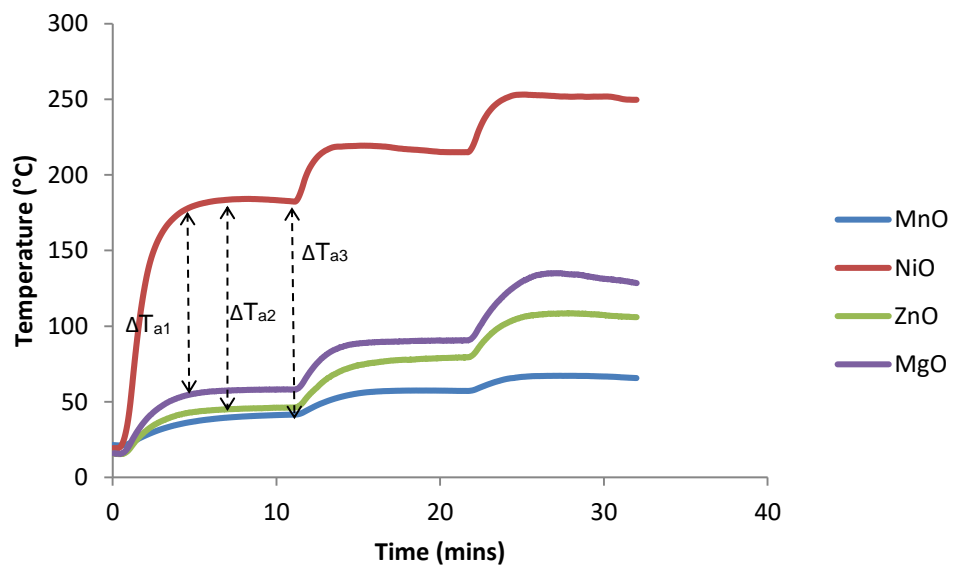


Fig 4.11 Temperature differences between more than two samples.

Looking at the difference in temperature between the separate fields will give a better understanding of ability of materials to be heated by the microwaves. This will also lead on to the heating of particular materials when they are put into the IHTA instrument, as it is predicted, due to induction theory³⁰, that only the samples that heat well in the H-field of the microwave will heat in the induction heater.

4.3.1 MWTA method development

To determine whether the samples were moving an appropriate distance within the sample cavity, a number of standard samples were analysed with the new adapted system. The samples chosen were well characterised with the E-field of the microwave and it was determined that these would be ideal standards to ascertain whether the coupling taking place was different as the new holder was shifted. In Fig. 4.12 below, Fe_2O_3 and Fe_3O_4 were analysed. The experiment was completed using linear power input to prevent any thermal runaway of the sample.

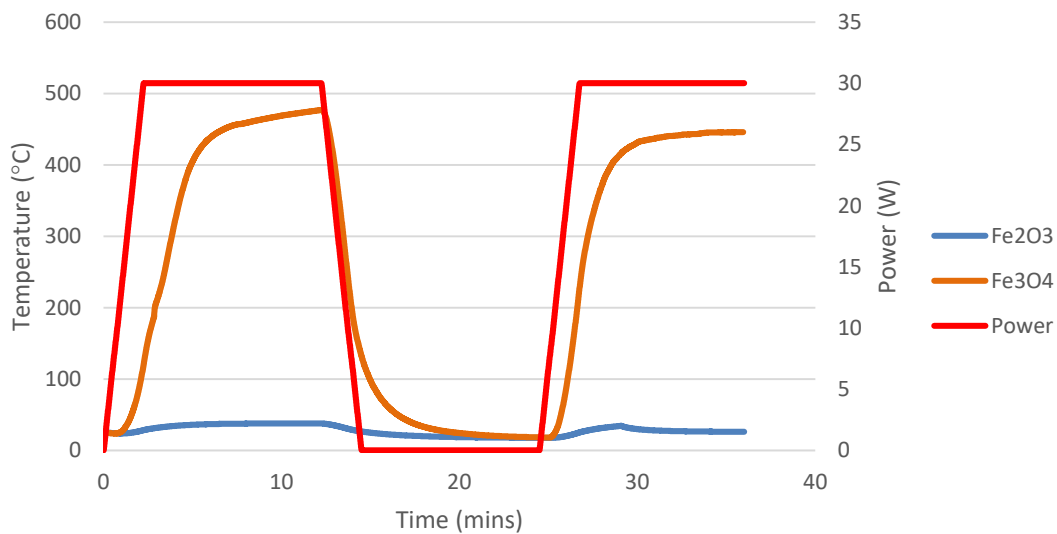


Fig. 4.12 Analysis of Fe_2O_3 and Fe_3O_4 within the E- and H-fields of the MWTA instrument,

It can be seen that Fe_3O_4 couples as expected within the E-field and the same results were determined during other testing. As the power reduces to zero, this enabled the sample holder to be shifted within the cavity in preparation for the H-field test. The Fe_3O_4 again couples well with the H-field of the microwave field which was expected due to the known magnetic susceptibility of Fe_3O_4 . In both the E-field and the H-field there was no couple of Fe_2O_3 with the electromagnetic field.

As an extension to the Fe samples, Magtrieve (CrO_2), was also used to test the development of the new MW sample holder. This is discussed in more detail in Chapter 5.

4.3.2 Limitations

It must be noted, that this method of thermal analysis is not without its limitations. Due to the design of the sample cell (section 3.2.3), experimental uncertainties were unavoidable. The sample was placed into the sample cell as a volume, between two marked points, therefore differences in the amount of sample would depend on its density and also particle size. The cell was moved within the cavity between the E- and H-fields using a marked point on the cell. Any difference in the placement of the cell could cause results to differ, and human error may be a factor within some results. Emphasis is required on the fact that the samples have some thickness, therefore when the sample is placed in the E-field position there will still be some H-field heating, and *vice-versa*. Finally, the purity of the samples is not 100 %, and these impurities may make a big difference to how susceptible the materials are to the microwave fields.

4.4. Induction heater (IH)

4.4.1. Introduction

The design and operational modes for the induction heater developed at the University of Huddersfield are discussed in more detail below, including workings of the instrument, software development and development of the sample chamber. The induction heater can be used in a number of different modes and a variety of events may be detected including Curie point and phase transitions. For some systems, the instrument may also provide quantitative as well as qualitative information. Some examples given below include heating of common iron oxides, Magnetite (Fe_3O_4) and Haematite (Fe_2O_3), the melting of tin (Sn) and the Curie point of Chromium Oxide (CrO_2).

4.4.2 Induction heater for thermal analysis.

A novel induction heating instrument for thermal analysis has been developed at the University of Huddersfield. It utilises a 6-turn water-cooled copper coil with current alternating at 125 kHz. The sample is situated in an insulated silica tube within the coil. Power control and temperature measurement (*via* a shielded thermocouple) is achieved using software developed at Huddersfield (figs. 4.13 and 4.14).

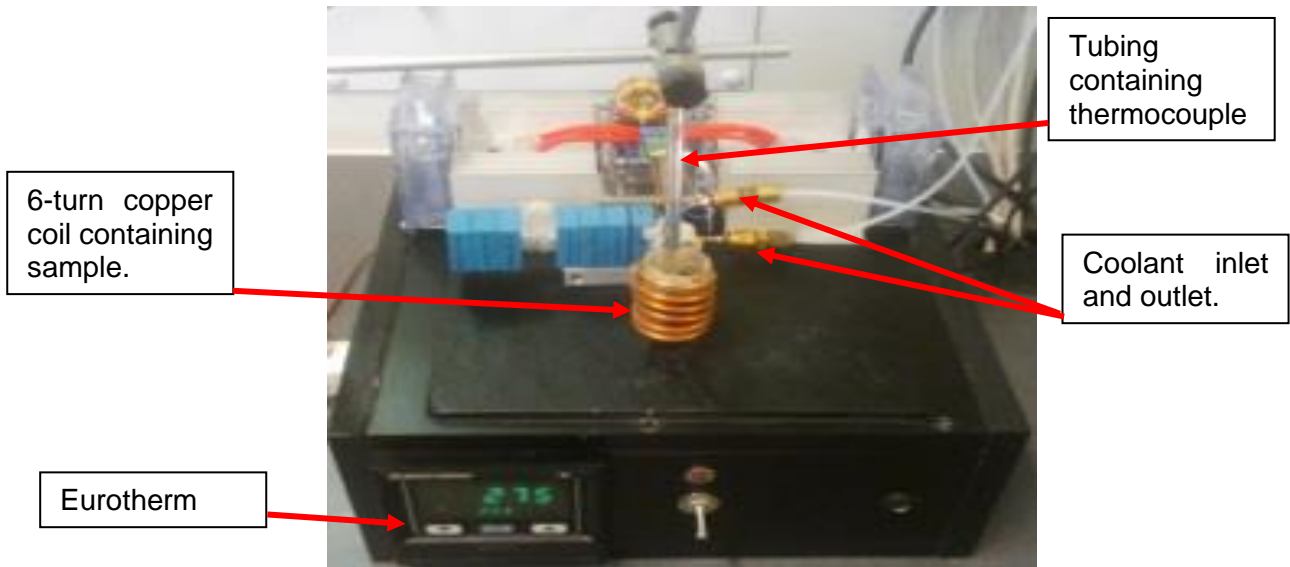
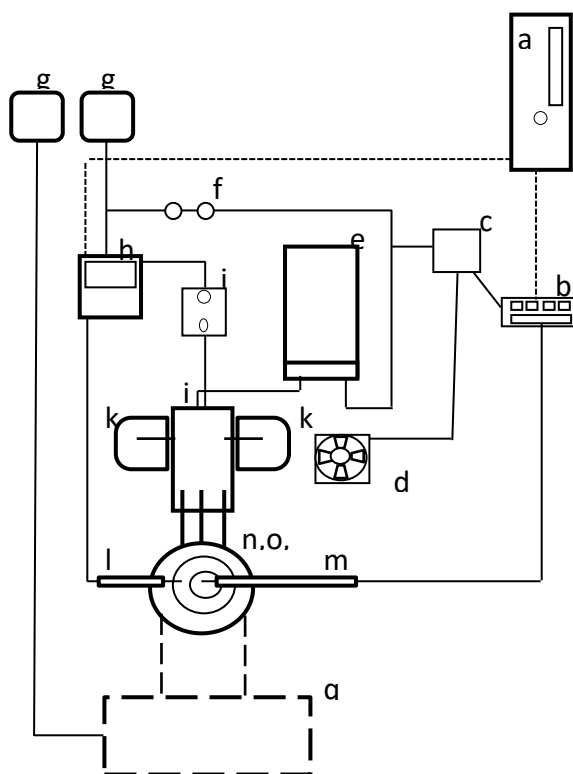


Fig. 4.13 Induction heater for use as a thermal analysis instrument developed at Huddersfield.



Hardware

- a) Computer
- b) Weeder
- c) 12V power supply
- d) Cooling Fans
- e) 24V A power supply
- f) Switch
- g) Mains inlets
- h) Eurotherm E818p temperature controller
- i) Solid state relay
- j) Modified Power resonator module (RMCybernetics)
- k) Heat sinks
- l) Reference type K thermocouple
- m) Sample type K thermocouple
- n) Induction coil (Outer ring) ,
- o) Reference material (middle ring)
- p) sample (inner ring)
- q) Cooling reservoir for induction coil.

Fig. 4.14 Induction heater (IH) schematic developed at Huddersfield

4.4.3 IHTA Sample holder development

Several sample holders were developed in order to meet the need of the user and the type of experiment to be run. These sample holders consist of the standard cell, the differential thermal analysis (DTA) cell and the atmosphere controlled (AC) cell.

The standard IH cell is the simplest and consists of the sample surrounded by an insulating jacket, placed in the centre of the induction coil (fig. 4.15). There are several of these cells to allow for changes in sample size. A more detailed description of this cell is available on page 75.

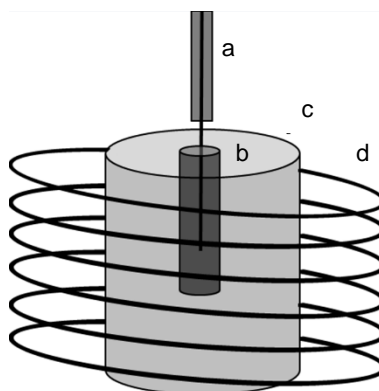


Fig. 4.15 Standard IH cell - a) Sample thermocouple, b) Sample Cell, c) Insulating jacket, d) Induction Coil

The IH-DTA cell is similar in appearance to the standard cell. The sample is placed inside a magnetic susceptor bed (reference material is a solid suspension of Fe_3O_4 in sodium silicate) which is then placed in an insulating jacket. This cell allows for a differential temperature measurement to be taken (fig. 4.16). The size of the sample can vary from 10 mg to several grams. This type of cell was also investigated being made with Fe, as this acted as a susceptor material and the cell itself could provide some of the heat to the sample. This was seen previously²⁵ in the cell development for the MWTA instrumentation where the alumina crucibles were coated with a susceptor material to aid heating of the sample.

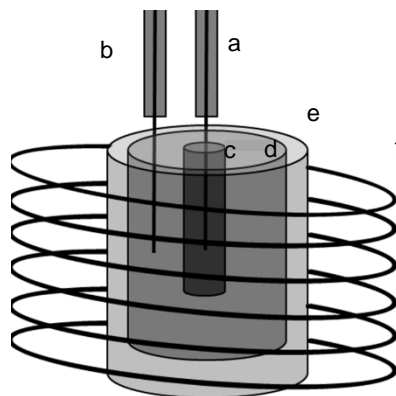


Fig. 4.16 DTA-IH cell - a) Sample thermocouple, b) Reference thermocouple, c) Sample Cell, d) Reference material, e) Insulating Jacket, f) Induction coil

The AC-cell is shown in fig. 4.17. This cell allows for the atmosphere surrounding a sample to be controlled by loading the sample into a silica glass tube and using a Cajon Swagelok to seal the sample in an airtight atmosphere. Samples can be investigated within the induction coil in inert or reactive atmospherical conditions. Sample size for this cell is between 1 – 3 mg.

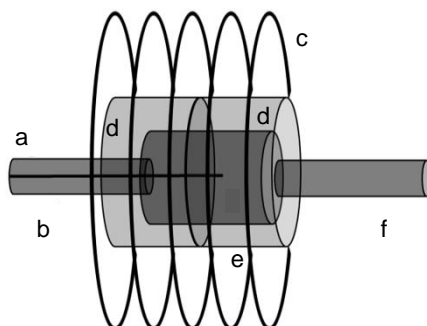


Fig. 4.17 AC-IH cell - a) Gas inlet, b) Sample thermocouple, c) Induction coil, d) Removable insulating jacket, e) Inner sample cell, f) Gas Outlet

The samples investigated within this thesis mostly used the standard IH cell. A more detailed diagram is shown in fig. 4.18 below.

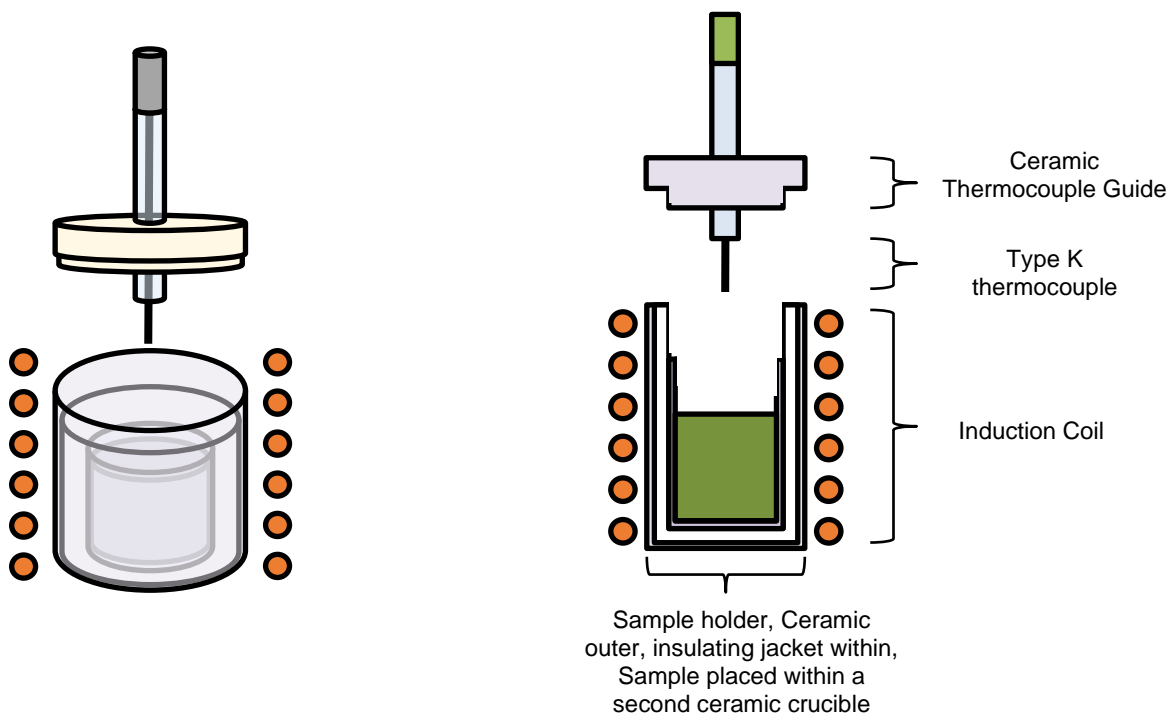


Fig. 4.18 Induction heater (IH) cell.

Further development of the standard IH cell by Dr. G Parkes allowed for better data collection of the sample interaction within the magnetic field. The ceramic thermocouple guide meant that the thermocouple was always within the centre of the sample whereas previously this couldn't be guaranteed which lead to ambiguity in results. The cell and thermocouple guide were alumina which means that the only source of heat is directly from the sample.

4.4.4 IHTA Method development

Various experimental methods have been developed for use with the IHTA instrument. The simplest method is allowing the IHTA instrument to run on full power and allow the sample to reach its maximum temperature. However, in order to prevent damage to the instrument, a maximum power of 75% has been set, as constant use at 100% could destroy the transistors. The transistors are the limiting factor of the instrument and more efficient transistors would be needed to allow the instrument to run for longer. The transistors are monitored regularly to ascertain whether they need replacing. The thermograms shown throughout this section are given as an example to show the various methods investigated for use with the induction heater. Further discussion surrounding the results of these investigations will be discussed in Chapter 5.

The two main experimental methods are a linear heating and a stepwise setpoint, the former being the most easy to use. A heating rate, target temperature and dwell time are selected. Up to 8 heating and cooling rates can be achieved in any one experiment. Fig. 4.19 shows the linear heating of elemental iron. The parameters of the experiment were: 5 °C min⁻¹ to 300 °C, 10min isothermal hold. -5 °C min⁻¹ to 150 °C, 10min isothermal hold. And finally, -10 °C min⁻¹ to 30°C.

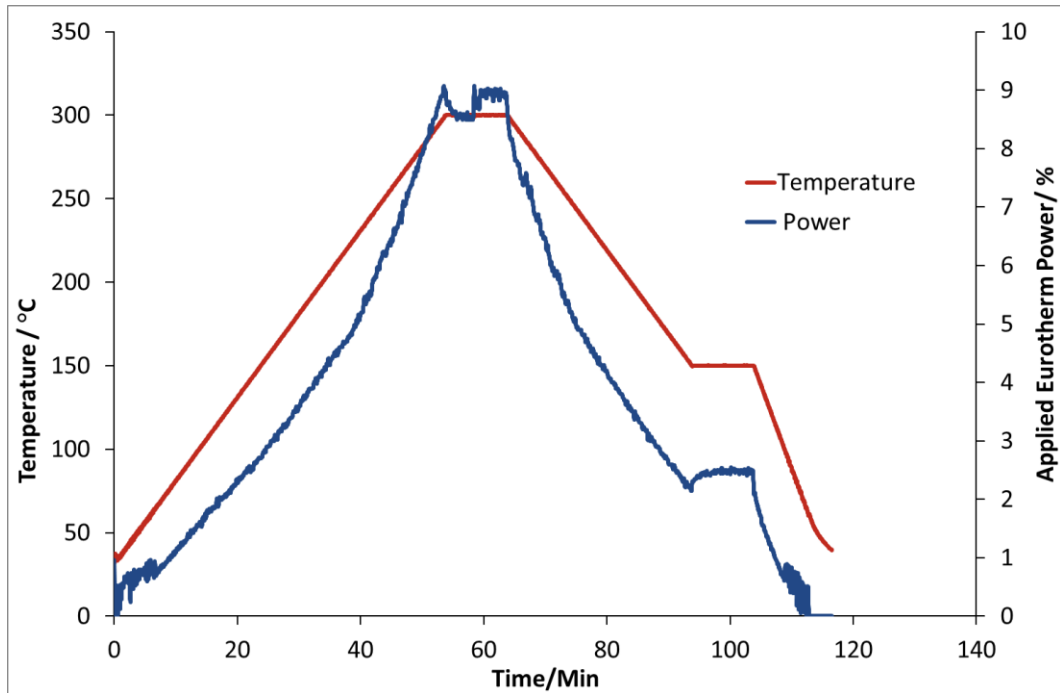


Fig. 4.19 Linear heating/cooling of elemental iron in the IHTA instrument

In these types of experiments the instrument continuously adjusts the power as required to achieve the desired heating rate. The thermogram clearly shows that the instrument only required 9% of the total power to hold the sample at 300 °C for 10 minutes. The total length of the experiment is approximately 2 hours. It can also be observed from the thermogram that the instrument has good control when heating to a specified program.

The second experimental mode is a stepwise setpoint. In this mode, a temperature is pre-set and power is applied to the coil in an attempt to reach this temperature. The temperature would be held for an isothermal period, after which more power is applied to reach the next 'step temperature'. This is repeated until the final temperature is reached. Fig. 4.20 shows the heating of elemental tin using the stepwise setpoint experimental method. The heating program utilised in this experiment was as follows: 180 °C to 280 °C, isothermally hold for 4 minutes and then step the temperature by 5 °C.

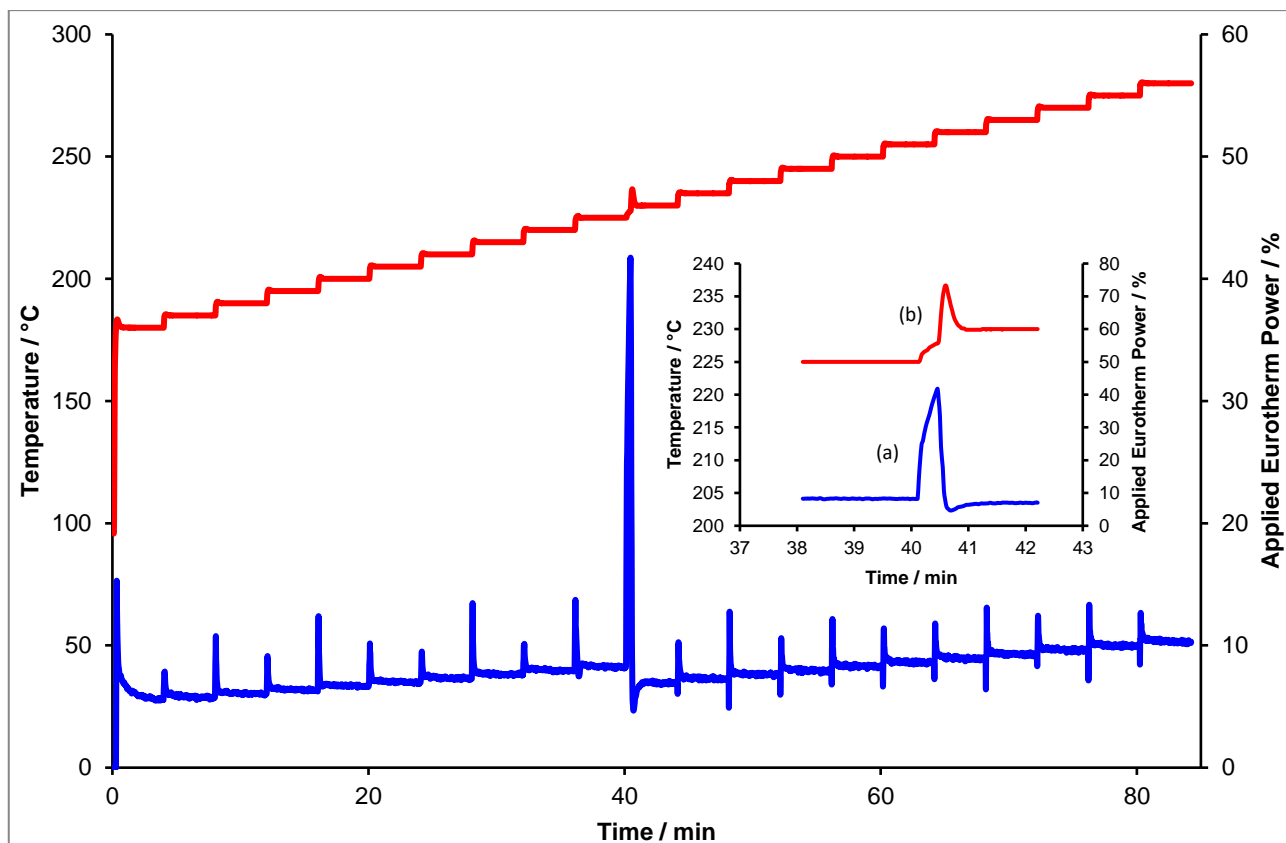


Fig. 4.20 Stepwise setpoint IHTA method of elemental tin. The insert shows magnified portions of fig. 4.20 (a) power spike and (b) stepwise temperature control with temperature spike during phase transition. Red data line – temperature, blue data line – power.

It can be observed that there is a large spike in the power input as the sample reached approximately 230 °C. This is due to the melting enthalpy of tin at 232 °C.¹³⁶

(a) and (b) of the insert show magnified portions of fig. 4.20 to better see the step change in the temperature of the sample and the spike in power as the phase transition occurred.

(a) clearly shows the spike in power compared the smaller power peaks at either side. The same spike in temperature, which coincides with the power spike, can be observed in (b) and the step is not as smooth as the steps on either side. The incremental step changes can also be seen clearly in (b) as the temperature is increased by 5 °C at each step. This shows good control of the instrument when utilising this method of heating.

Fig. 4.24 overleaf shows the average power that is applied in each step. It can be clearly seen that after tin has gone through its phase transition, considerably less power is required to continue heating the sample. It can also be observed that the increase in power for each step increment is linear showing good control of heating with the instrumentation and the software.

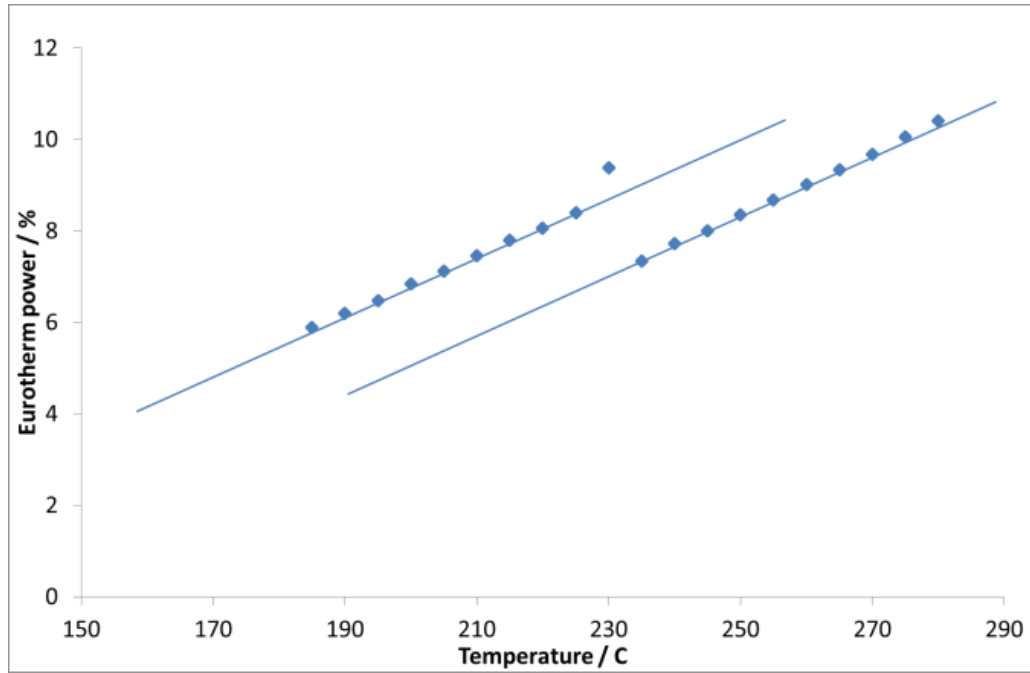


Fig. 4.24 Temperature points show the linearity of the sample in fig. 4.15, including the increase in temperature and power as a phase change takes place.

The samples chosen and discussed within this thesis utilised the linear and stepwise setpoint experiments for determination of magnetic properties.

T_C investigation and quantitative analysis using the IHTA are discussed in Chapter 5.

Chapter 5

5.0 Results and Discussion

5.1 MWTA Introduction

In order to further investigate the use of microwaves for thermal analysis, the current MWTA instrument was adapted to allow materials of interest to be moved from the E-field maximum to the H-field maximum. The materials that have been examined during this method development include metal oxides (sections 5.4 - 5.6), $\text{Ni}_{1-x}\text{Mg}_x\text{O}$ solid solutions (section 5.9), perovskites (section 5.10) and double perovskites (section 5.11). The materials were chosen with increasing complexity to examine how the different fields (H and E) interact with the samples. It is hoped that events, such as T_c and phase changes may be noticeable. In addition, heating profiles for specific compounds can also be examined and that events taking place within the H-field of the microwave will correlate with the induction heating thermal analysis (detailed in Section 5.12). In section 5.4, there is an explanation of how the data from MWTA can be presented.

5.2 Preparation

The preparation, synthesis and characterisation of the compounds is detailed within Chapter 2. The synthesised compounds were produced *via* the standard ceramic synthesis route. Standard metal oxides and simple perovskites were stock samples purchased from Fischer Scientific and Sigma-Aldrich.

5.3 MWTA initial testing

Fig. 5.1 gives an indication of how the MWTA instrument can be used for analysis of both the E- and H-field for the heating of different compounds. It can be clearly seen that there are two distinct areas where the sample holder has been moved from the maximum of the E-field to the maximum of the H-field. The procedure developed by Dr. G. Ashton and Dr. G. Parkes, explained in more detail in Chapter 2, was to hold the instrument at a set power for certain time, after which the sample is cooled and the power reduced to the start point. The holder is then shifted within the MW cavity to allow the sample to be held in the maximum of the H-field and the power is once again ramped to a set point and an isothermal hold incorporated.

The data in fig. 5.1 are for Fe_3O_4 and Fe_2O_3 for testing purposes only but shows a difference in the temperatures reached in the two different fields.

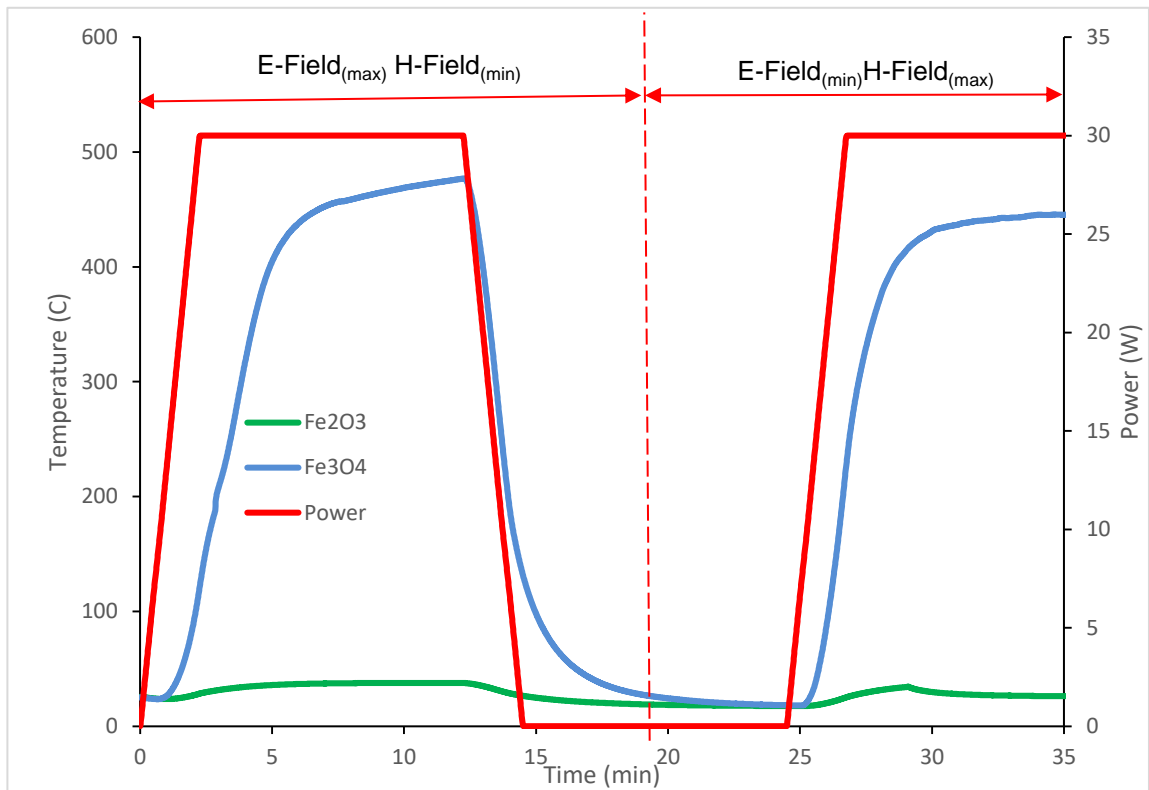


Fig. 5.1 Comparison of Fe_2O_3 and Fe_3O_4 starting in maximum E-field moving out towards minimum E-field at 30W power

As an extension to the Fe samples, Magtrieve (CrO_2), was also used to test the development of the new MW sample holder. As shown in fig. 5.2 overleaf, CrO_2 coupled reasonably well with the EM field in both the E and H field. Fe_3O_4 was added to the CrO_2 in different amounts (66%/33% and 33%/66%) and the mixtures tested in sequence to determine whether the iron would influence the coupling ability of the CrO_2 . The Fe_3O_4 only had a negligible effect on the H-field heating of the CrO_2 but reduced the heating within the E-field. When Fe_3O_4 was added at 66%, the coupling capability of CrO_2 is visibly reduced with the E-field. It was also noted that a smaller percentage of Fe increased the coupling capability of the CrO_2 within the H-field but reduced it within the E-field. The higher percentage decreased with coupling in both fields.

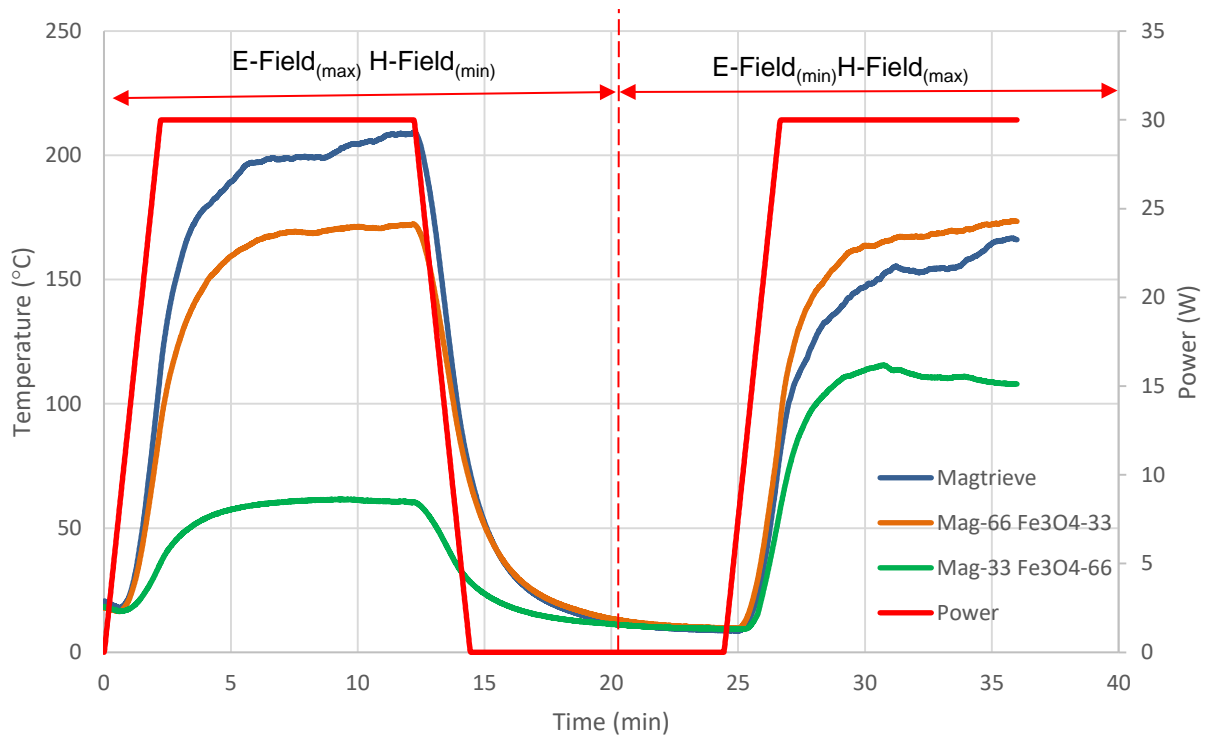


Fig. 5.2 Analysis of CrO_2 and Fe_3O_4 within the E- and H-fields of the MWTA instrument at 30W

It was expected that the addition of Fe_3O_4 to the CrO_2 would increase the coupling capability of the CrO_2 as a susceptor. While this was the case with the smaller amount of Fe_3O_4 and only in the H-field, it reduced coupling in all the other experiments. The internal mechanisms taking place during microwave heating are still not fully understood so it is unclear why they behaved in this way. It is possible that the coupling of both materials affects the coupling of the other due to the electrical field induced within each.

5.4 Metal oxide microwave susceptibility.

Initial experiments using the MWTA instrument with the newly developed sample cell used metal oxides to determine whether the materials coupling susceptibility in the MWTA, changed depending on whether the sample was in the E-field or H-field maximum. It was also required to show that there was a difference between the two parts of an EM field and whether the sample susceptibility was more dependent on one field than the other.

Nineteen different oxides were analysed using the MWTA system. The thermogram resulting from this analysis is shown in figures 5.3 and 5.4 overleaf. Due to the number of results shown on the thermogram, and the fact that this research is focussing on the electrical and magnetic properties of ceramic materials, figures 5.3 and 5.4 depict only the metal oxides that coupled and heated well within both the E- and H-field of the MWTA system.

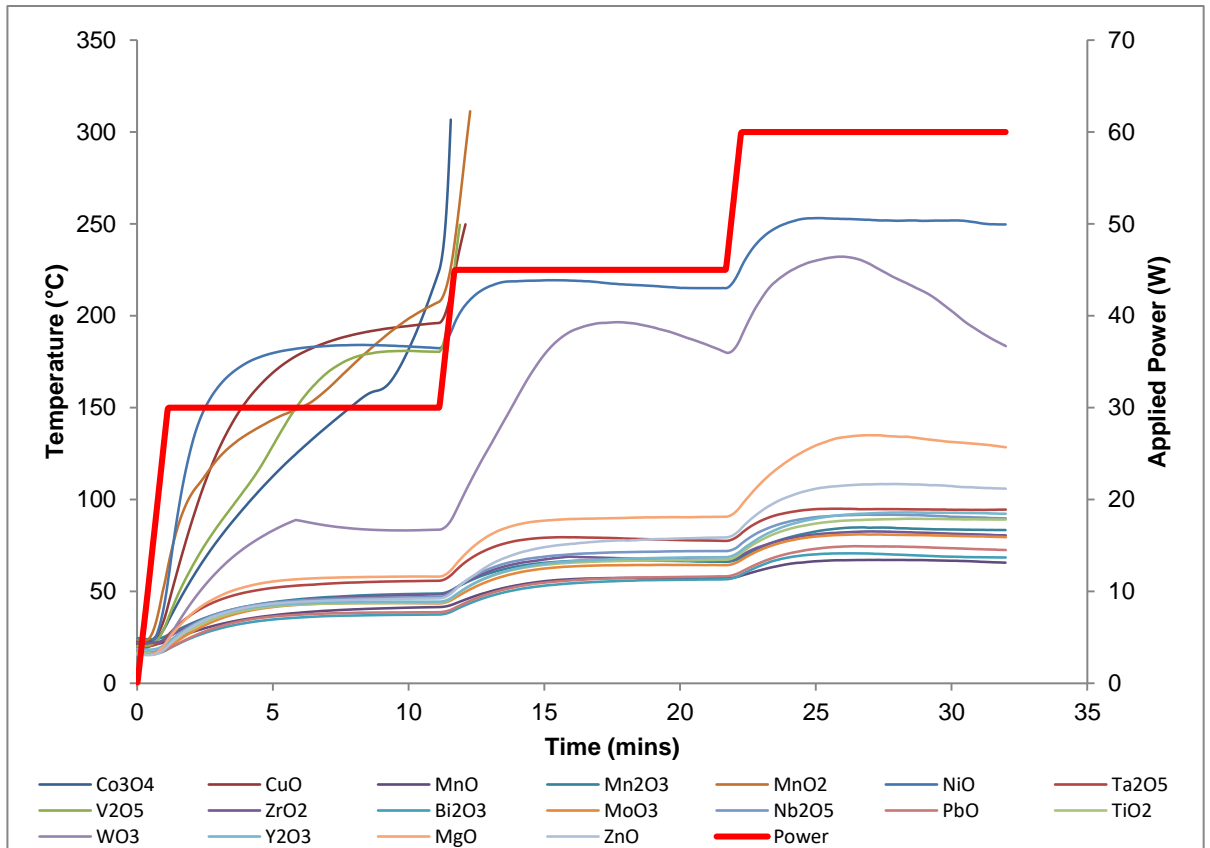


Fig 5.3 Comparison of metal oxides when analysed in the E-field of the MWTA instrument. Three power ramps with a 10 minute isothermal hold at 30W, 45W and 60W.

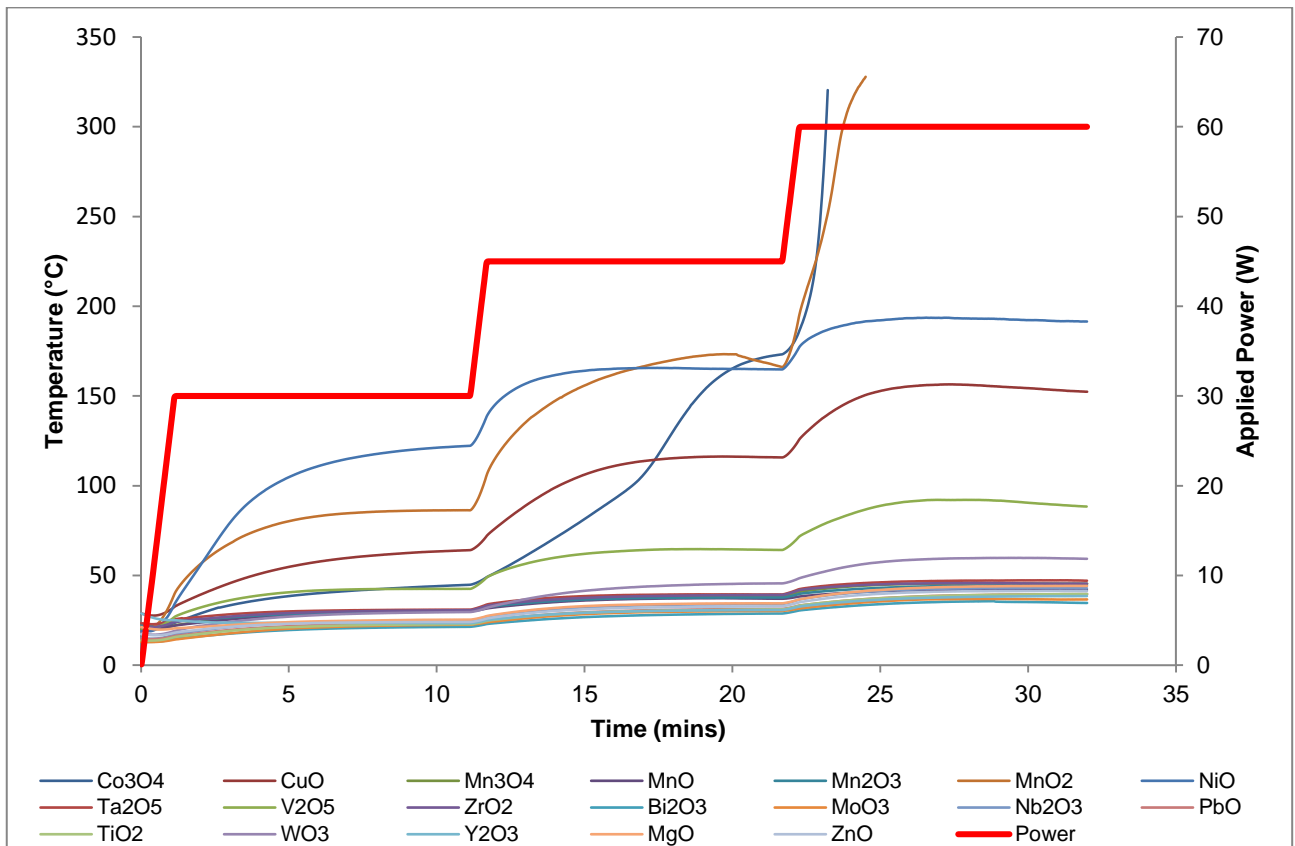


Fig 5.4 Comparison of metal oxides when analysed in the H-field of the MWTA instrument. Three power ramps with a 10 minute isothermal hold at 30W, 45W and 60W..

Fig. 5.5 shows these results depending on the materials susceptibility to the microwave field. Table 5.5 gives all the temperatures reached by the metal oxides in both the E- and H-field, in order of increasing E-field temperature. In the H-field, only Co_3O_4 and MnO_2 reached a temperature where thermal runaway became a problem.

summarises the metal oxide susceptibility in each group.

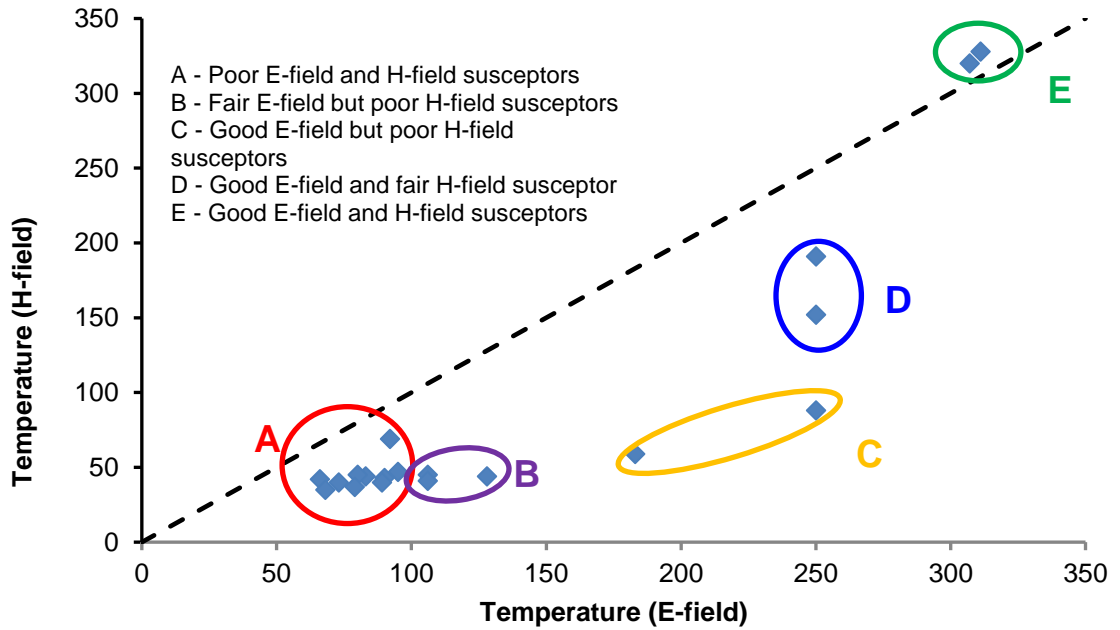


Fig. 5.5 Summary of temperature reached ($^{\circ}\text{C}$) by metal oxides in the E- and H-field

Table 5.6. Maximum temperatures reached by metal oxide samples in both the E-field and H-field, in order of increasing E-field temperature.

Composition	T_{\max} ($^{\circ}\text{C}$) at AP = 60 W ($\pm 5^{\circ}\text{C}$)	
	E-field	H-field
MnO	65	41
Bi_2O_3	68	34
PbO	72	39
MoO ₃	79	36
ZrO_2	80	45
Mn_2O_3	83	44
Nb_2O_5	89	42
TiO_2	89	39
Y_2O_3	92	68
Ta_2O_5	94	47
Mn_3O_4	105	45
ZnO	105	41
MgO	128	44
WO_3	183	59
CuO	249	152
NiO	249	191
V_2O_5	249	88
Co_3O_4	306	320
MnO_2	311	327

It can be seen in fig. 5.5 that Co_3O_4 and MnO_2 heated extremely well, experiencing a thermal runaway as the power increased to 45 W. These samples reached 300 °C and the power had to be manually stopped to protect the integrity of the instrument. Table 5.5 shows an experimental error of ± 5 °C. This is primarily due to two limitations of the instrument. The sample holder had to be moved manually and while every care was taken to ensure the same distance for each experiment, even a difference of 1 mm would make a difference. There is also the added effect of variations within the samples such as sample mass and volume. The sample mass could not be used due to the nature of the sample holder and the volume could change due to density of the different samples.

After these samples, a safety “cut-off” of 250 °C for the temperature was utilised to prevent any damage to the instrument, which is why the CuO and V_2O_5 sample only reached 250 °C before stopping. WO_3 is semiconducting¹³⁷ and expected to heat well in the E-field. However, WO_3 behaved unusually as it heated well, but as the sample was isothermal for 10 minutes, the temperature began to gradually decrease, until the power was increased to the next ramp. It is as yet unclear why the WO_3 behaved in this way, but as tungsten can exist as $\text{WO}_3 \cdot \text{H}_2\text{O}$, there is a possibility there is a dehydration reaction happening.

When the metal oxides were examined in the H-field, the samples that coupled well are the same as the ones that coupled well in the E-field, the exception being WO_3 which agrees with literature¹³⁸ regarding the non-magnetic behaviour of this oxide. This also indicates that the E-field interaction with the samples is also at a minimum. Table 5.6 gives a summary of all the temperatures reached by the oxides shown in fig. 5.5.

Table 5.6 Summary of metal oxide groups shown in fig. 5.5. Letters A to E refer to the groupings.

A – Poor E-field and H-field susceptors.	B Fair E field but poor H-field susceptors.	C Good E field but poor H-field susceptors.	D Good E field and fair H-field susceptors.	E Good E field and H-field susceptors.
MnO	MgO	V_2O_5	NiO	Co_3O_4
Mn_2O_3	Mn_3O_4	WO_3	CuO	MnO_2
Ta_2O_5	ZnO			
Bi_2O_3				
MoO_3				
Nb_2O_5				
PbO				
TiO_2				
Y_2O_3				
ZrO_2				

Initially, from the maximum temperatures reached by the samples, it can be observed the adaptations to the MWTA instrument were successful. The metal oxides have clearly been subjected to E-field and H-field radiation, as the susceptibility changes quite drastically between the two fields. If the sample was still partially retained in the E-field, it was expected that the H-field temperatures would be higher due to the E-field interaction. This interaction cannot be completely ruled out as one of the limitations to this instrumentation.

Conventional band theory predicts that because the d-levels in the transition metal oxides are partially filled, the electrons should be delocalised and therefore these oxides should exhibit metallic behaviour. However, many of these oxides exhibit insulating behaviour, which suggests that the d-electrons are localised. Hamilton²⁵ found that materials most likely to heat in the microwave field (through Ohmic heating) were semiconducting materials and the results shown above support this finding (WO_3 , NiO, CuO, V_2O_5 , Co_3O_4 and MnO_2). Although the majority of metal oxides are insulating, some show an increase in conductivity as a function of temperature increases and some are semiconducting. It is also possible that O^{2-} ion content could cause an increase or decrease in electrical conductivity⁵⁰ which is supported when looking at the Mn oxide results from the microwave. They show very different susceptibility to one another with both the E and H fields.

5.5. Specific Metal Oxides

In order to continue the investigation into the heating of metal oxides within the E and H-fields of the microwave, specific oxides were studied further. Metal oxides with a rocksalt structure were examined due to the simplicity of the structure, and the known characterisation of their properties. It was hoped that the examination of these compounds would aid in the development of MWTA utilising both the E and H-fields.

5.5.1 Nickel Oxide (NiO)

NiO is initially a green powder that is a poor conductor. NiO is known to have insulating properties¹³⁹ but upon heating with oxygen it becomes a black powder and is semiconducting. It retains the same structure (rock salt) but there is a mixture of Ni^{2+} , Ni^{3+} and cation vacancies that are distributed on the octahedral sites.¹⁴⁰

Figure.5.6 shows the results of an MWTA experiment of NiO heated in the E- and H-fields using a power of 60W. A greater extent of heating is observed in the E-field than in the H-field (249 C and 191 C respectively). This indicates that a greater power input would be required for the NiO sample in the H-field to reach the higher temperatures seen in the E-field.

The electrical heating of NiO was expected, as the electrical conductivity can increase due to the vacancies on the octahedral sites.^{140–142} NiO, while initially thought to be a Mott-Hubbard insulator¹⁴³, has since been described as a charge-transfer insulator, where conduction through the solid occurs between the anion and cation.^{139,144,145} The composition of NiO with oxygen vacancies is Ni_{1-x}O, where $0 \leq x < 1$ ¹⁴⁶ but the conductivity of NiO is difficult to control, as it is dependent on the degree of oxidation when heated in an oxygen rich atmosphere.¹⁴⁷

This indicates that a greater power input would be required for the NiO sample in the H-field to reach the higher temperatures seen in the E-field.

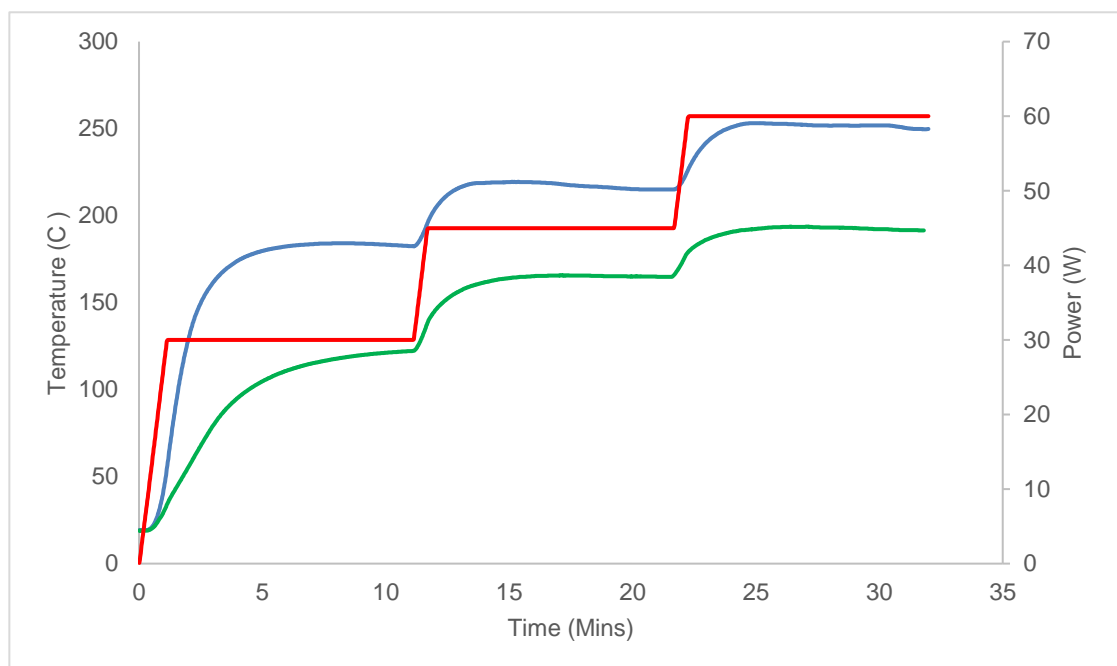


Fig. 5.6 Heating profiles of NiO in the E-field and the H-field. Blue line shows the coupling profile of NiO in the E-field. Green line shows the coupling profile of NiO in the H-field. Red line gives the power profile for the materials showing three ramps at 30W, 45W and 60W. The power levels are set with an isothermal hold for 10 minutes as each power level is reached.

Research by Cheng *et al.*¹⁴⁸ showed that the heating of conducting samples, such as metal and carbide powders (Fe, Cu and WC) can be more efficiently achieved in the E-field, whereas ceramic samples (Al₂O₃, ZnO) with low conductivity had much higher heating rates in the H-field.¹⁴⁸ It is interpreted that Ohmic is the primary source of heating when the NiO sample is in the E-field, due to it being a charge transfer insulator.¹⁴⁹ However, even though this may be the primary heating mechanism, there is also the fact that dielectric losses could also be involved in the heating of the sample due to its insulating properties.¹⁴⁹ The method of heating within the H-field is thought to be eddy current losses and as NiO is antiferromagnetic¹⁴¹ it is assumed magnetic hysteresis losses are not contributing to the heating of the sample.

Figures 5.7 and 5.8 show the results of an MWTA experiment on NiO sample tested using a temperature ramp in the E- and H-fields. There is a clear difference in the power input needed for NiO to reach the set temperatures (7, 12 and 20 W respectively).

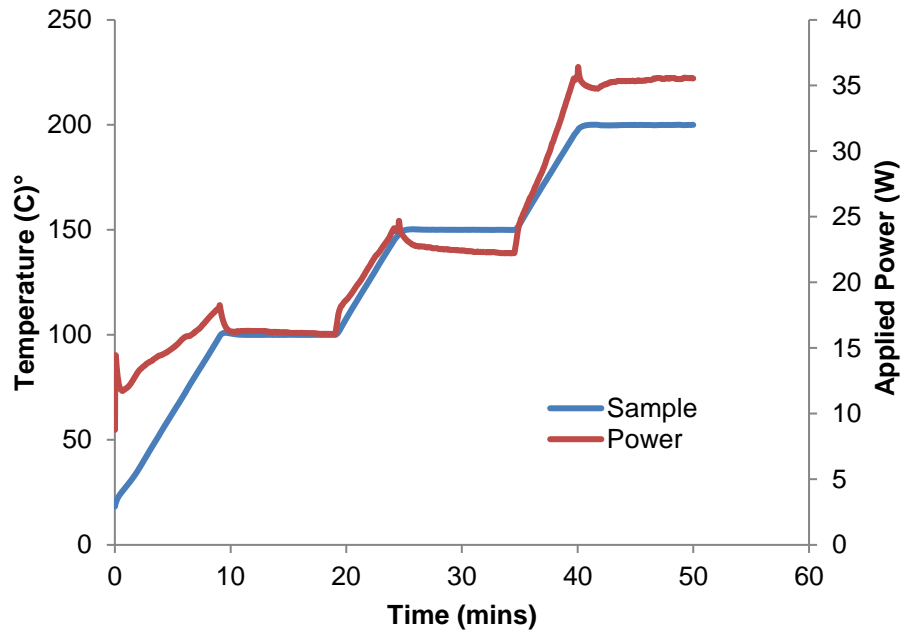


Fig. 5.7 Power and heating profile – NiO in the E-field

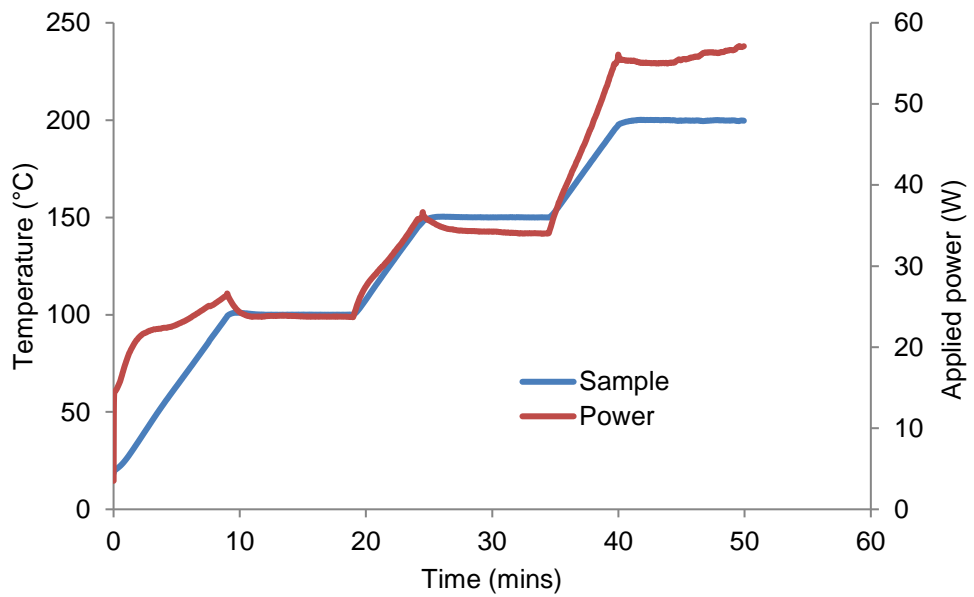


Fig. 5.8 Power and heating profile – NiO in the H-field.

5.5.2 Manganese Oxide (MnO)

MnO is a first row transition metal with a divalent oxidation state. It has a T_N of $-115\text{ }^\circ\text{C}$, above which it is a paramagnetic insulator. Below T_N it is an antiferromagnetic insulator.⁴⁰

Fig 5.9 shows the heating profile of the MnO in the E- and H-field. Although the sample does heat in the E-field, the temperature only reaches $65\text{ }^\circ\text{C}$, and in the H-field, the maximum temperature is $42\text{ }^\circ\text{C}$. This correlates well with the fact that MnO is an insulator¹³⁹ and it was therefore not expected to heat well. While Cheng et al. did not report any findings on MnO, the researchers did investigate the heating of ZnO and FeO within the E and H-fields. These showed good heating to high temperatures in the E-field, but not in the H-field, similar to the behaviour observed in Al_2O_3 by Agrawal *et al.*¹⁵⁰ The research found that the heating of Al_2O_3 was difficult, but improved as the temperature of the sample increased. The fact that MnO reached a temperature of $60\text{ }^\circ\text{C}$ indicates that with higher power levels, this oxide may also get to a high temperature within the E-field. It is unlikely that it will reach higher temperatures within the H-field, if this oxide continues to behave similarly to Al_2O_3 , as for many materials (but not all) increased temperatures increases the extent of microwave coupling. This usually requires a significant temperature change and the results presented here only cover a range of $30\text{ }^\circ\text{C}$ to $40\text{ }^\circ\text{C}$. There is also a temperature dip at the end of the experiment which indicates that a limit may be reached with continued heating.

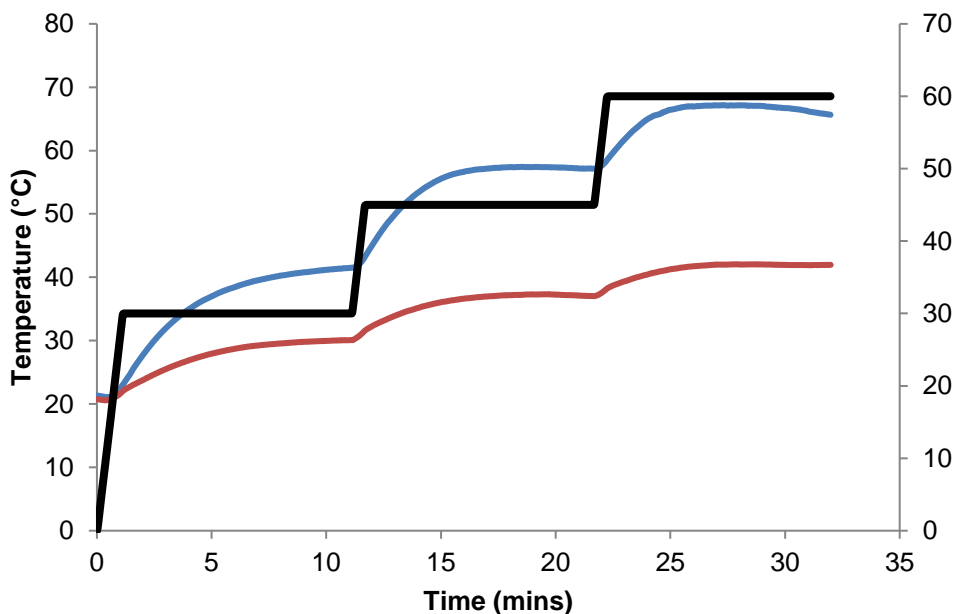


Fig. 5.9 Heating profile – MnO in the E-field (blue) and H-field (red). Time vs. temperature. Power profile (black)

Figs. 5.10 (a) and (b) show each individual heating pattern with the power profile. Although the power input is the same, it is evident that heating occurs much more readily in the E-field.

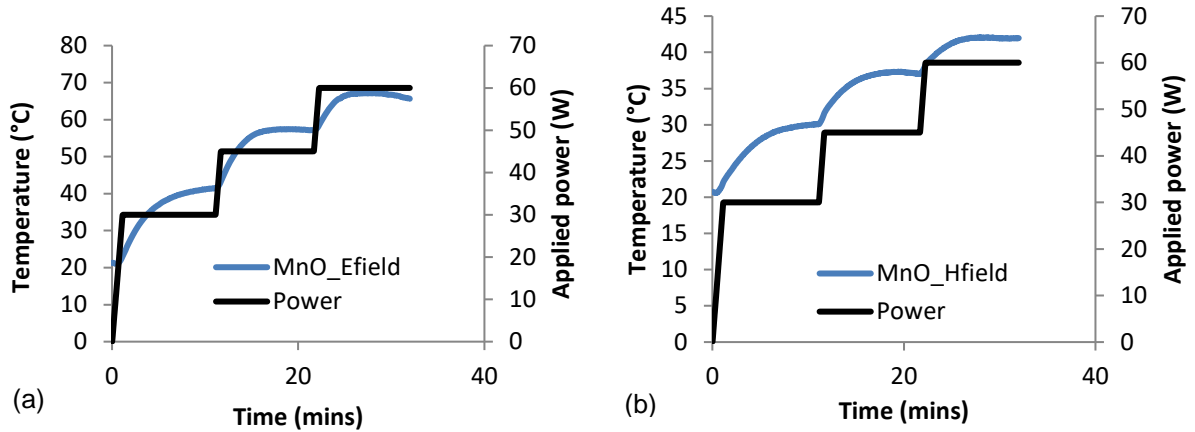


Fig. 5.10 Power profile – MnO in the E-field and H-field. Power vs. temperature

The type of heating taking place within this sample is thought to be Ohmic heating only. The oxide did not heat at all in the H-field, therefore the H-field will have had no impact on heating within this sample. These results prove that the sample is definitively separate in both fields when moved inside the cavity.

5.5.3 Zinc Oxide (ZnO)

ZnO is a semi-conductor material that can exhibit ferromagnetism when doped with transition metal elements.¹⁵¹ While some studies have shown FM behaviour with Mn and Co in doped ZnO samples, different synthesis mechanisms were applied i.e. sol-gel¹⁵² and solid solution¹⁵³ among others. Rao and Deepak have shown that doping with these transition metals shows no FM behaviour, and suggest that where FM behaviour has been observed, there is a possibility that spinel impurity phases were present due to high temperature synthesis.¹⁵³ Unlike NiO, MnO and MgO, ZnO doesn't adopt a rocksalt structure, but rather the würtzite structure as this is more thermodynamically stable.

Fig. 5.11 shows the ZnO sample heated in the E- and H-fields. Like MnO, ZnO heats relatively well in the E-field, reaching a temperature of 105 °C, where as in the H-field the material reached a maximum temperature of 41 °C, the same as MnO.

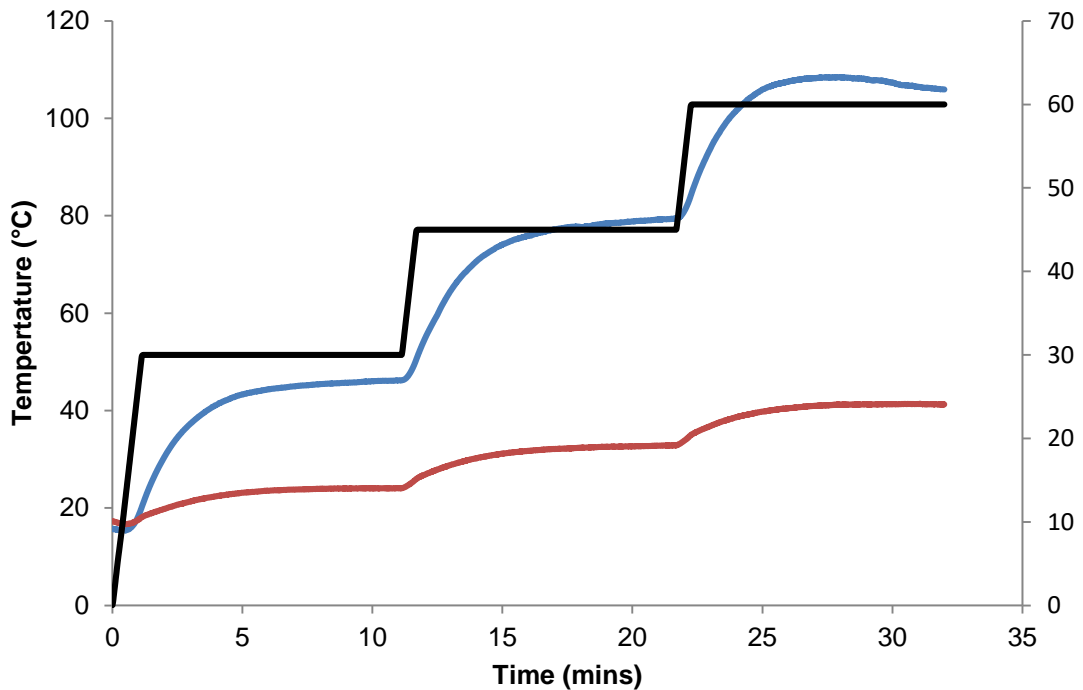


Fig. 5.11 Heating profile – ZnO in the E-field (blue) and H-field (red). Temperature vs time. Power profile (green)

ZnO was studied by Cheng *et al.*¹⁴⁸ and they found the same results as presented here in both the E-field and H-field. This indicates that ZnO may behave in the the same way Al₂O₃, and that only Ohmic heating was taking place within the sample. The difference in the research undertaken by Cheng *et al* and the research presented here is the microwave equipment was able to increase the ZnO to higher temperatures (950 °C) than the equipment at the University of Huddersfield. The research mentioned here by Cheng *et al*¹⁴⁸ does state the power input for the microwave instrumentation, as 1.2kW but it is also stated that they power was adjusted due to the temperature increase being too fast and in some cases arcing occurred at the highest temperatures. 500W is given for a number of their investigations but the power with ZnO is not specified. Samples were also cold-pressed which could also contribute to how well a material interacts with the microwave field. Due to the size and shape (Chapter 2) of the sample holder during this research, it wouldn't have been possible to place pressed powders into the cavity while being able to move the holder into the different field maximum.

5.5.4 Magnesium oxide (MgO)

Although magnesium oxide is not a transition metal monoxide, it has a number of applications, particularly in the field of catalysis¹⁵⁴ and thin films.¹⁵⁵ During this research, MgO has been used to synthesise $\text{Ni}_{1-x}\text{Mg}_x\text{O}$ solid solutions in order to determine the magnetic and electrical properties. The solutions, discussed further in section 5.9 are examined in both the E-field and H-field, and the MgO is analysed for its behaviour as a starting material. MgO adopts the rock salt structure at room temperature.¹⁵⁵

Fig. 5.12 shows the difference in temperature while the MgO sample is in the E-field and H-field. MgO heats much better in the E-field, up to a maximum temperature of 129 °C, and although the sample does not heat effectively in the H-field, a small amount of heating is observed, with the sample reaching a maximum of 44 °C.

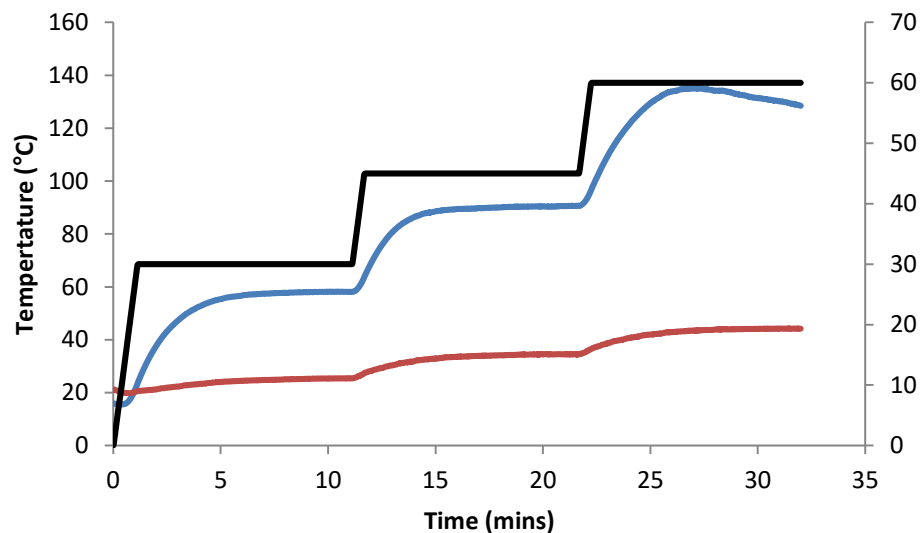


Fig. 5.12 Heating profile – MgO in the E-field (blue) and H-field (red). Time vs. temperature and time. Power profile in green.

Although the same amount of power is put into the system, the differences in the maximum temperatures reached are clearly observed in fig.5.12. MgO is an insulator and has low dielectric losses^{155,156}, which reduces a material's ability to couple with the microwave fields, however, these results suggest that MgO does couple with the E-field in the microwave. The low interaction with the H-field may hinder the coupling of MgO with the E field, as the fields can have an effect on one another, even though the experiments are explicitly designed to separate the two fields. The results show that temperature falls off during the final stage of heating which could indicate the loss of adsorbed moisture.

The heating profile of MgO indicates that although it is not a transition metal oxide, it behaves in the same way as MnO and ZnO when subjected to microwave radiation. This supports previous research by Cheng *et al*¹⁵⁷ who also found that the insulating materials coupled and heated better in the E-field, where Ohmic heating is the primary mechanism.

5.6 Comparison of metal oxides.

Fig. 5.13 shows a comparison of the four oxides mentioned previously, heated in the E-field. There is a clear difference between the samples. This is discussed below and summarised in table 5.7. The explanation for the summary table is shown previously in table 4.4.

Table 5.7 Summary of temperature differences between the metal oxides. a1, b1 and c1 indicate the differences in heating during the first power ramp, a2, b2 and c2 in the second power ramp and a3, b3 and c3 in the third power ramp. The difference is between NiO and the other three oxides.

ΔT ($^{\circ}\text{C}$)										
a1	b1	c1		a2	b2	c2		a3	b3	c3
124	124	121		136	135	143		140	157	184

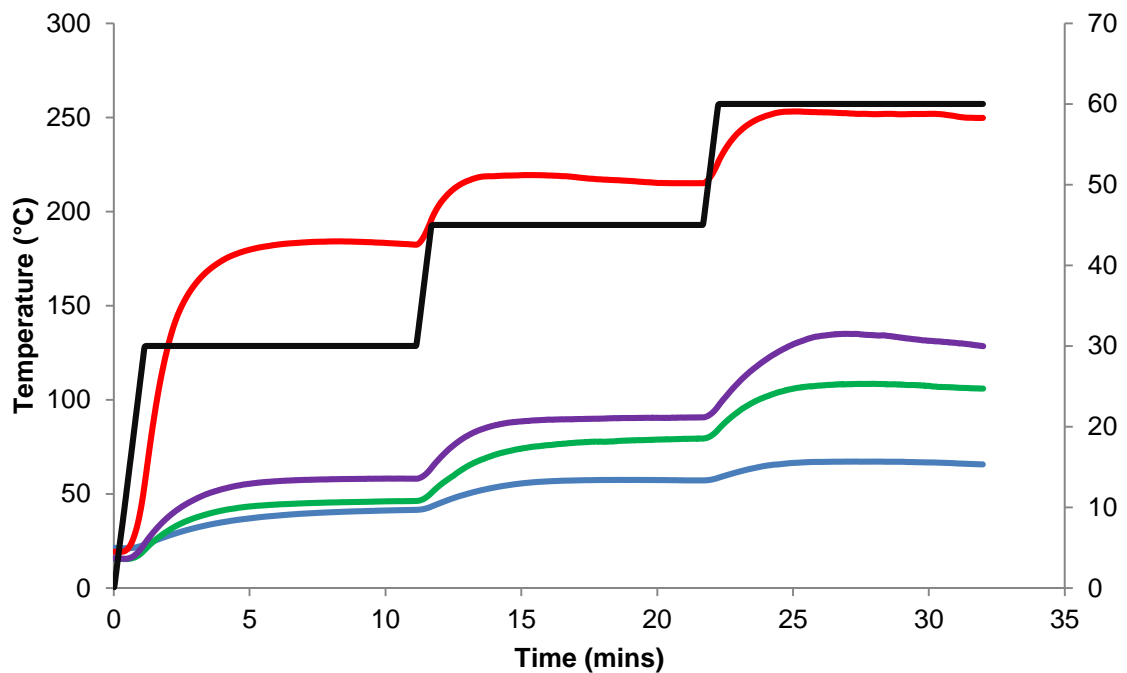


Fig. 5.13 Comparison of metal oxides in MW – E-field heating NiO – red, MgO – purple, ZnO – green and MnO – blue. Power profile - black

The coupling of MnO with the E-field in the microwave reduces as the power is increased, resulting in a larger ΔT during the final hold. The only samples where the ΔT remains the same throughout is the difference between NiO and MgO. Although the temperatures of all four samples climb as the power is increased, ΔT remains the same throughout, indicating that the increase in power does increase the coupling ability of the samples. As mentioned previously, Cheng's work¹⁴⁸ shows that ZnO can get to a much higher temperature, but the equipment would need to be adjusted to allow for these temperatures to be measured. It would be interesting to examine how the more insulating materials compare to NiO under

these conditions. The results correlate well with one another, with temperature increasing gradually as the power level is increased from 30 to 60 W. It also indicates that the coupling ability of the more insulating oxides reduces slightly, as T increases more, particularly between NiO-ZnO and NiO-MnO.

ΔT_{a1} in the H-field results in a much larger difference of 147 °C when compared to the E-field heating, whereas the heating of the other three samples is negligible, with all three only getting to a maximum of 44 °C (MgO), 41 °C (ZnO) and 41 °C (MnO). Previous research has found that conductive samples heat up much better in the magnetic field, while non-conductive samples, such as alumina, heat up better in the electric field (alumina heats better at higher temperatures ~500 °C).¹⁵⁷ This research was studying the effect of microwaves on sintering of powdered metal samples. They found that the powders could be sintered in a much shorter time (30 mins) and that the properties required were sometimes better than the samples sintered *via* conventional heating. They expanded their research to look at the different behaviours in the E- and H-fields of the microwave, but while they used Al₂O₃¹⁵⁷, and later ZnO and series of iron oxides,¹⁴⁸ and found that ZnO behaved similarly to Al₂O₃. The iron oxides, FeO, Fe₂O₃ and Fe₃O₄, also behaved differently to one another. FeO and Fe₂O₃ could only be heated to higher temperatures (>300 C) in the E-field, whereas Fe₃O₄ could be heated to ~500 °C in the H-field and 650 °C in the E-field. These were the only metal oxides that were investigated among a number of metal powders whereas the research presented here explored a much larger range of metal oxides in the separated microwave fields.

These results suggest that MgO, ZnO and MnO have some conducting properties, even though MgO is used as an insulator, as they heat better in the E-field than in the H-field. The temperature reached by these three oxides is quite low and any further interaction with the E-field may reduce the coupling, particularly with MgO as the drop in temperature during the final stage is quite obvious. The MWTA system used in this research was unable to go to temperatures above 300 °C, therefore any further heating at higher temperatures, as discussed by Andriese *et al*¹⁵⁸ and Cheng *et al*^{148,157}, was unable to be examined. It is unclear whether it is dielectric heating or magnetic heating that is taking place within the NiO sample, but because the fields are still within the cavity, the E- and H- fields could be having an effect on the sample, even when it is in the maximum of the opposing field. Fig. 5.14 compares the heating profiles of the four metal oxides when in the H-field.

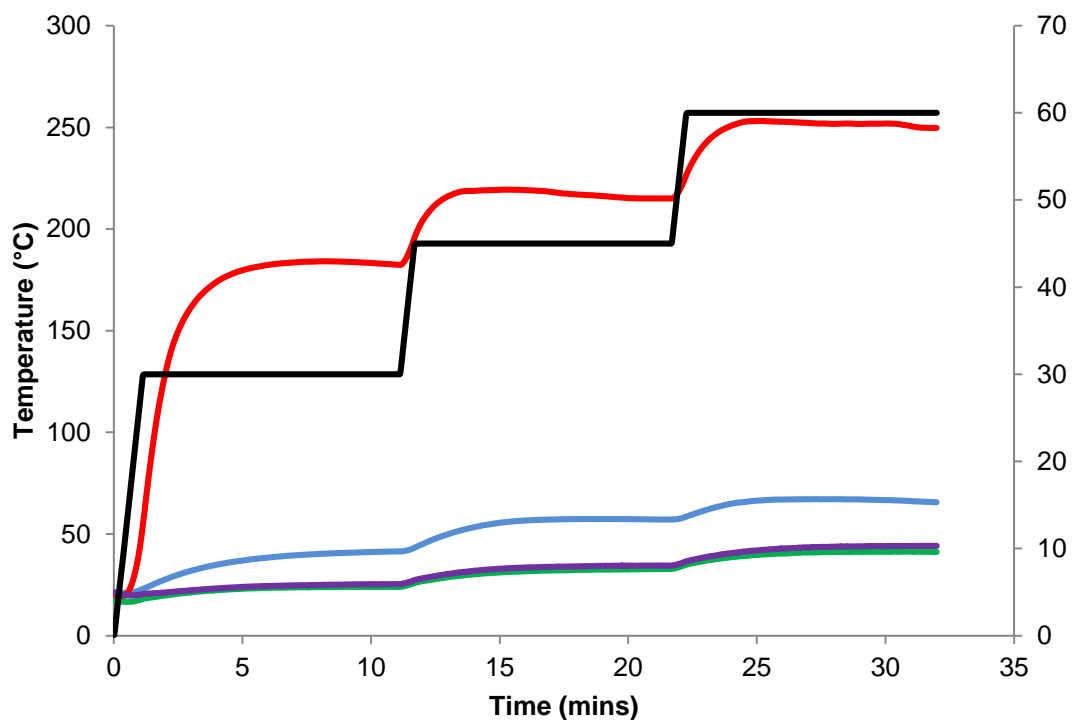


Fig. 5.14 Comparison of metal oxides in MW – H-field heating. NiO – red, MnO – blue, MgO – purple and ZnO – green. Power profile - black

The difference in heating is reduced compared to the heating in the E-field, with MgO and ZnO have near identical maximum temperatures. MnO reaches a slightly higher temperature than it did in the E-field, but NiO is clearly much better at coupling with the microwaves when heated in the H-field. With regard to the three oxides that did not couple well in the H-field, it is thought that this is because of their lack of conductivity and their AFM nature. The heating mechanism in the H-field is primarily due to eddy current losses, and a current needs to be induced within the sample for this type of heating to take place. The secondary heating in the H-field is due to magnetic hysteresis, and the samples need to have some ferro or ferrimagnetic properties for this mechanism to heat the sample.

5.7 Induction Heater

5.7.1 Introduction

This section focuses on the results using the induction heater for thermal analysis. The samples studied here are the metal oxides – some of which coupled well in the H-field of the MWTA, the perovskites (ABO_3) and the double perovskites ($A_2B'B''O_6$ and $A'A''B_2O_6$). There is an explanation in section 5.7.2, outlining the reasons why the data are presented this way. Following on from this, in Sections 5.8 - 5.11, are presentation of the results and a discussion for each analysis. The samples that were analysed using IHTA primarily showed coupling in the H-field of the microwave which resulted in the sample increasing in temperature. However, some samples, while they didn't couple well in the H-field, were still analysed with the IHTA instrument to create a complete set of results. The expectations and final results are discussed within each section.

5.7.2 Explanation of Induction thermogram

The samples analysed using IHTA were samples that had heated well in the H-field of the microwave. It was thought that because the H-field couples with the magnetic components of a sample, the IHTA would also yield positive results due to the induction coil requiring particular components within a sample. As mentioned in Chapter 3, there are three different methods that can be utilised when investigating the effect of the IHTA on a sample.

The data plotted when using the setpoint method, can be difficult to analyse and compare due to the number of data points collected by the instrument, shown in fig. 5.15. Due to the power spikes as each step is increased, the maximum temperatures reached by the sample are hidden. For this reason, the points plotted for the instrument are an average of the power and the temperature of the last minute of each hold as it was assumed the system has reached equilibrium during this period. This is shown in figure 5.16.

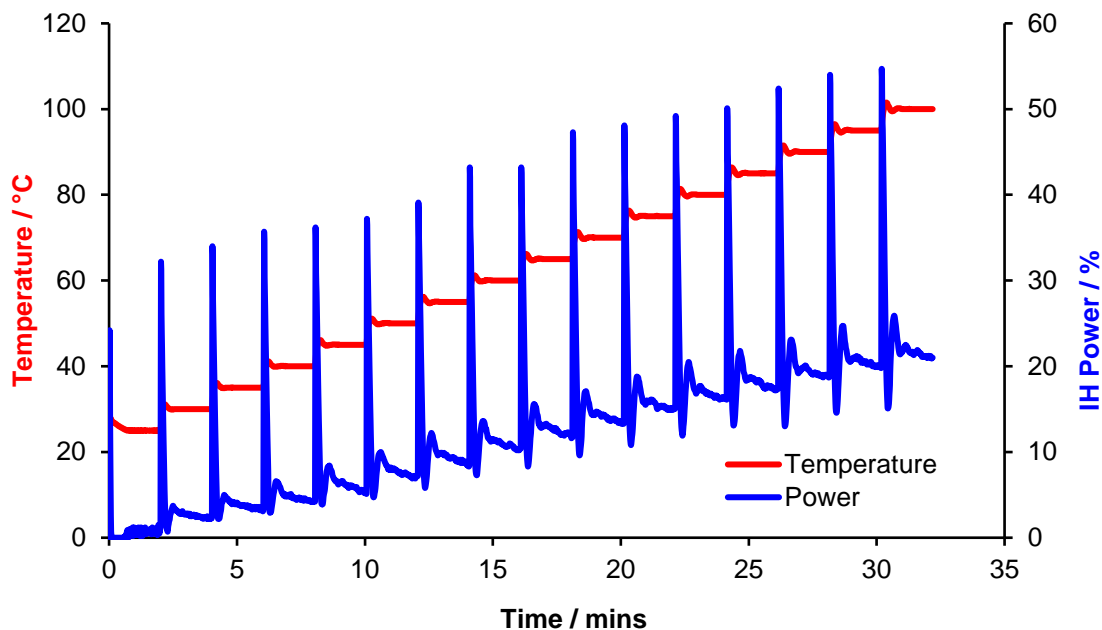


Fig. 5.15. Induction heating of 1g of Fe₃O₄

It can be seen in fig 5.15, that the Fe₃O₄ heats readily as the power is gradually increased. This is to be expected due to the magnetic properties of the Fe₃O₄, which is a common component within metals that are manufactured using the induction heating process. The heating of this compound has been utilised to investigate method development of the induction heater for thermal analysis.

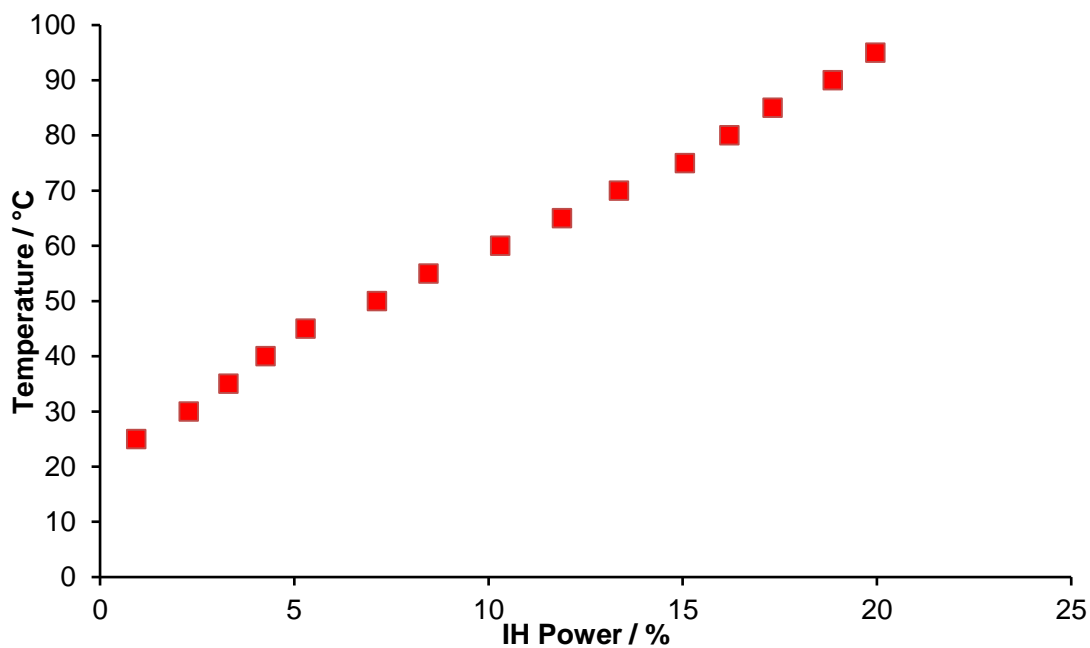


Fig. 5.16. Induction heating of 1g of Fe₃O₄

As can be seen in figure 5.17, the data can now be compared easily to other data sets when they are within the same thermogram, allowing for a simpler observation of the samples. A comparison of the effect of mass on induction heating of Fe_3O_4 is shown in fig. 5.17 below.

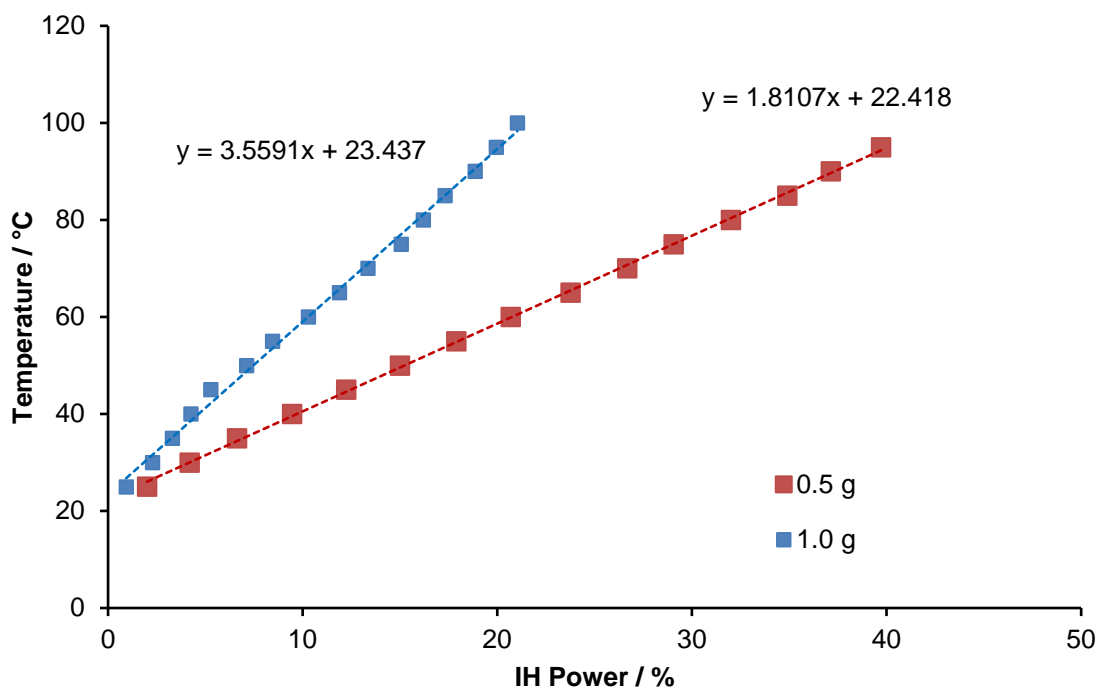


Fig. 5.17 Effect of mass on induction heating of Fe_3O_4

This shows how data can be compared when using different amounts of materials within the induction heater. As fig. 5.17 shows, the larger amount of Fe_3O_4 heats much more readily in the induction heater, requiring a power input of only 21 % to reach 100 °C, whereas the 0.5 g sample required 42 % to reach the same temperature. It has also been observed that the power required halves when the sample amount is doubled. It would be interesting to further examine this theory but due to time constraints it will not be done within this research, but may be completed in future research.

It has also been determined that the IHTA has the ability to detect the curie point (T_C) of compounds. Fig. 5.18 overleaf, it clearly shows the T_C of chromium (IV) oxide (CrO_2). CrO_2 is heated using the IH-DTA utilising a linear program at a rate of $1\text{ }^\circ\text{C min}^{-1}$ and an isothermal hold upon reaching 200 °C. The sample is then cooled at a rate of $-1\text{ }^\circ\text{C min}^{-1}$. The literature value for the T_C of CrO_2 is approximately $120\text{ }^\circ\text{C}^{159}$ and a large step in temperature can be seen at approximately 100 °C in the IHTA thermogram.

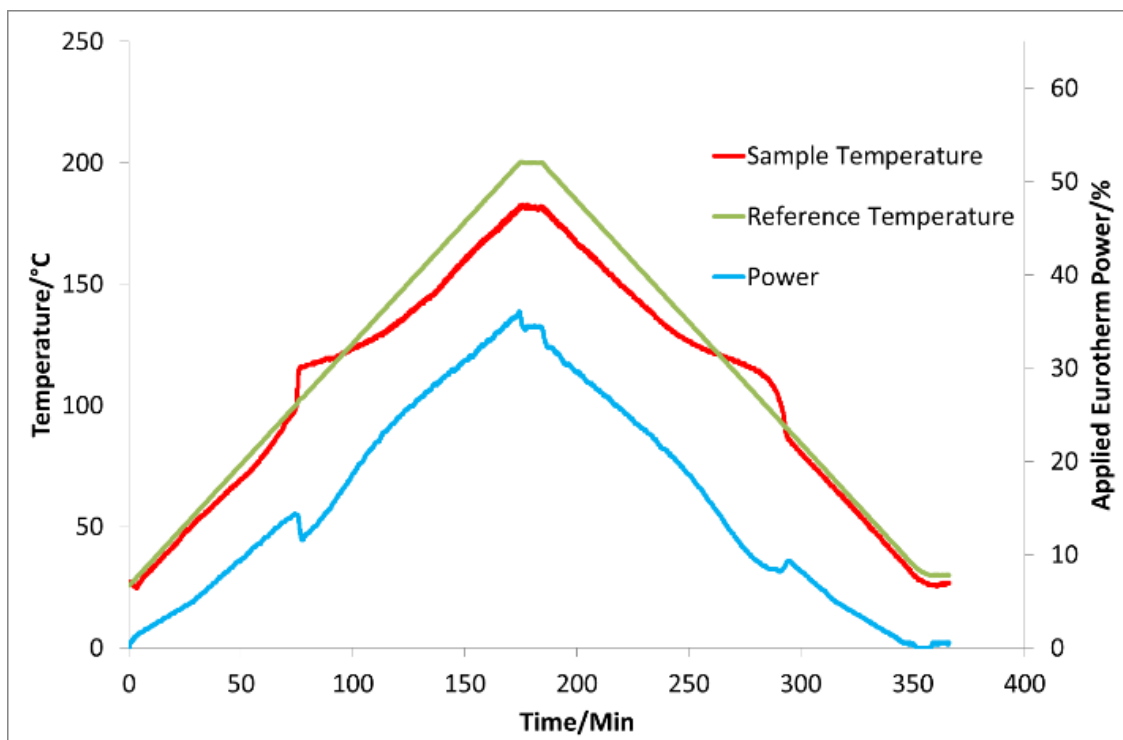
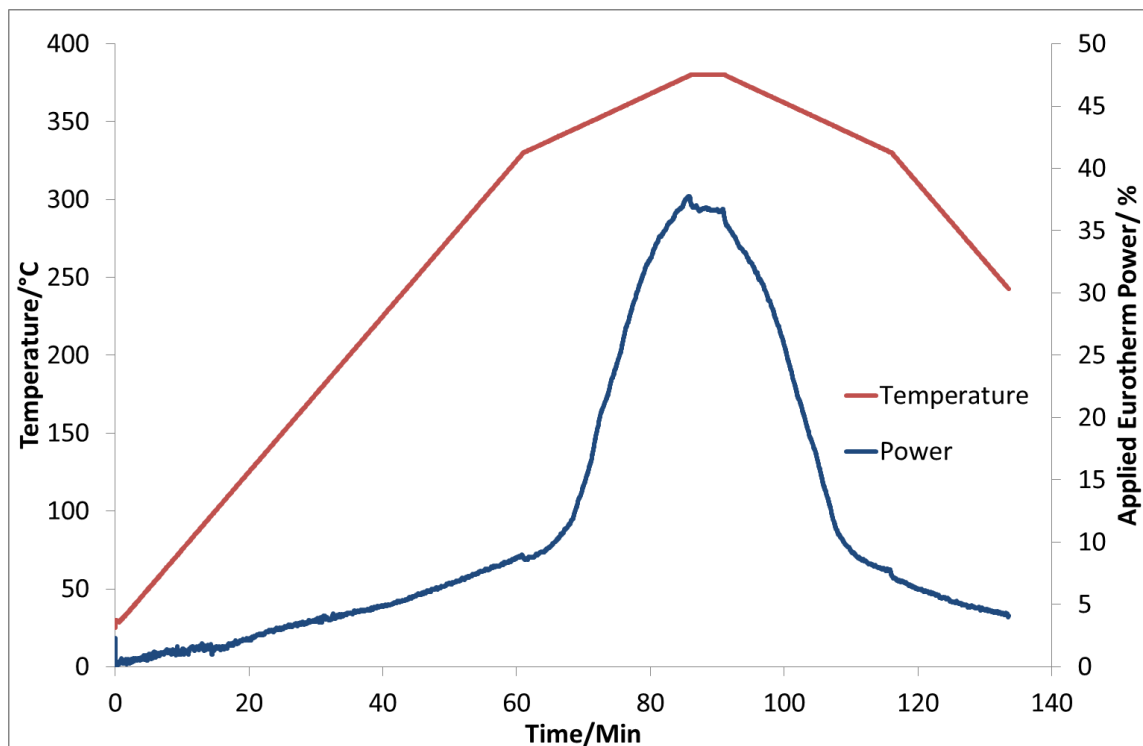


Fig. 5.18 Curie temperature determination for CrO_2

The phase transition is the cause of the downward spike in power, and this process can also be seen to be reversible, as a second upward spike in power is observed in the thermogram, which bears a lot of resemblance to the thermogram observed when using a DSC instrument. It is also interesting to note that it may also be possible to determine if the phase transition is exo- or endothermic using the IHTA instrument, depending on the direction of the peak, although enthalpy effects are likely to be small compared to the effect of changes in magnetic properties.

The T_C of elemental nickel has also been determined using the IHTA instrument. Shown in fig. 5.19, the T_C event is much greater than CrO_2 at approximately 346°C but compared with the literature temperature of elemental nickel at 355°C ¹⁶⁰ it is a bit lower. A large step in power can be observed as Ni goes through its T_C and at the curie point transition a major mode of heating inductively is lost. The initial heating rate of 5°C min^{-1} was reduced to 1°C min^{-1} to give a more accurately measured temperature. A large, broad shoulder was observed in the thermogram as it was thought this was due to the size of the sample, (500 mg), where the surface of the sample would go through the T_C first and the interior following. Non-uniform heating is a general problem in thermal analysis and gets worse as sample mass is increased.

The fact that T_C can be determined using the IHTA instrument is very exciting as this instrument already shows that it has the potential to become a novel technique for characterisation of different materials. The current techniques for measuring Curie points (TGA and DSC) are well known but the instrumentation is expensive and it is hoped the IHTA instrumentation will allow access to more users in the future. It must be noted that more testing on known T_C of materials is required for this to be a definitive result.



The final use determined (at this time) for the IHTA is a quantitative analysis. Fig 5.19 shows the results from several mixtures containing varying amounts of Fe_2O_3 and Fe_3O_4 (wt %). Fe_2O_3 does not couple magnetically which results in poor heating in samples with high percentages of this oxide. Conversely, Fe_3O_4 couples very strongly magnetically and heats to very high temperatures while using a relatively low power input from the instrument.

5.7.3 IHTA standards – Iron oxides

Initial testing with the IHTA instrumentation focussed on the use of iron oxides for method development of both the sample holder and the software developed for the IHTA. These oxides, due to their known electrical and magnetic properties, behaved well and as expected within the IHTA sample cavity.

Fig. 5.15 – 5.19, shown in the previous section, show how different experiments can be run on the IHTA instrument. They also allow the user to observe how differing amounts of a

sample can have an effect on the heating. Fig. 5.20 overleaf indicates that sample composition can also be investigated using the IHTA equipment developed at the University of Huddersfield.

Fig. 5.19 shows a dramatic reduction in the effect of the magnetic field on the heating of the sample depending on the % composition. The power required to increase the temperature for a 100% sample of Fe_2O_3 compared the to 100% sample of Fe_3O_4 is nearly 8 times more. The power and temperatures are shown in table 5.8 below.

Table 5.8 Effective coupling within IHTA instrumentation depending on sample composition of $\text{Fe}_2\text{O}_3/\text{Fe}_3\text{O}_4$

Sample composition	Power %	Max. Temperature ($^{\circ}\text{C}$)
100% Fe_2O_3	75	53
90%/10% $\text{Fe}_2\text{O}_3/\text{Fe}_3\text{O}_4$	75	83
80%/20% $\text{Fe}_2\text{O}_3/\text{Fe}_3\text{O}_4$	75	136
70%/30% $\text{Fe}_2\text{O}_3/\text{Fe}_3\text{O}_4$	58	150
60%/40% $\text{Fe}_2\text{O}_3/\text{Fe}_3\text{O}_4$	37	150
50%/50% $\text{Fe}_2\text{O}_3/\text{Fe}_3\text{O}_4$	23	150
40%/60% $\text{Fe}_2\text{O}_3/\text{Fe}_3\text{O}_4$	19	150
30%/70% $\text{Fe}_2\text{O}_3/\text{Fe}_3\text{O}_4$	18	150
20%/80% $\text{Fe}_2\text{O}_3/\text{Fe}_3\text{O}_4$	13	150
10%/90% $\text{Fe}_2\text{O}_3/\text{Fe}_3\text{O}_4$	12	150
100% Fe_3O_4	9	150

This is also a novel use of the IHTA instrumentation, as the difference between magnetic and non-magnetic materials can clearly be seen in the experiment. While this is still in its infancy, it is extremely promising that this capability can be observed and is achievable for a number of users.

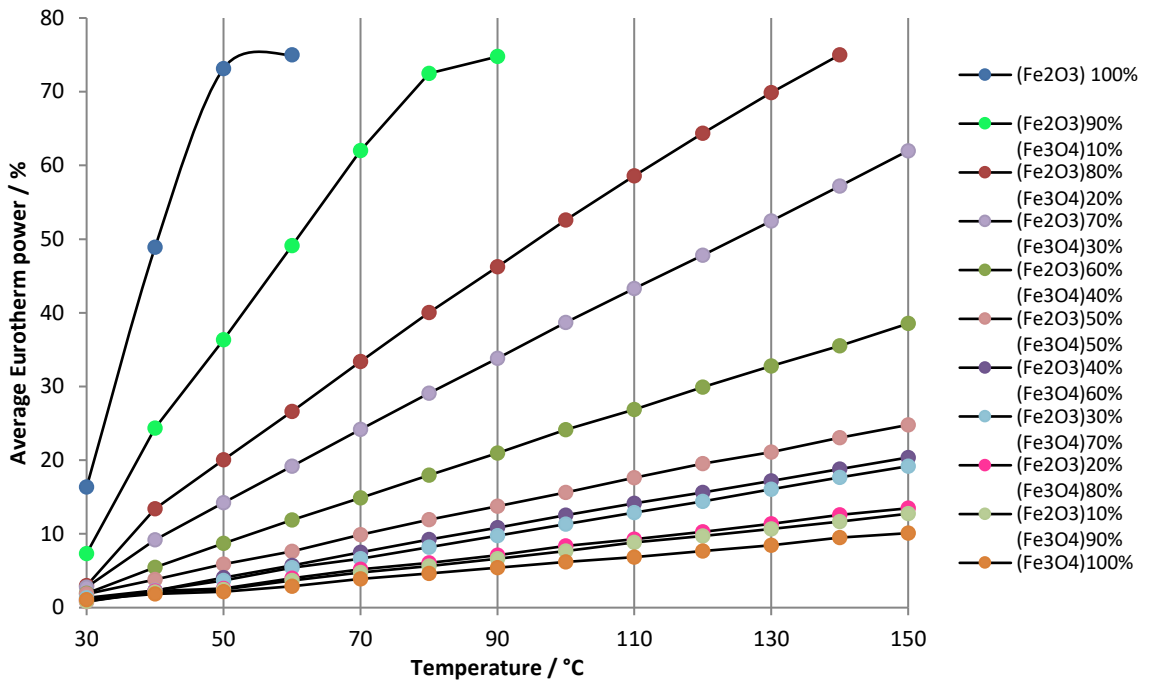


Fig. 5.20 Effective coupling within IHTA instrumentation depending on sample composition of $\text{Fe}_2\text{O}_3/\text{Fe}_3\text{O}_4$ Induction Heating Comparison of mixed iron oxides $(\text{Fe}_2\text{O}_3)_x(\text{Fe}_3\text{O}_4)_{1-x}$ ($x = 1, 0.9, 0.8, \dots, 0.2, 0.1, 0$ / %wt.)

5.8 IHTA of Metal Oxides

The initial samples run on the IHTA instrument after testing, were the metal oxides that had shown a degree of heating within the H-field on the MWTA instrument. A limiting factor with the MWTA is that although the samples are moved out of the $E\text{-field}_{\text{max}}$ and into the $H\text{-field}_{\text{max}}$, it is unknown whether the E-field still has an effect on the heating of a sample that is electrically conducting. Those samples that showed a negligible heating effect in the $H\text{-field}_{\text{max}}$ were excluded from analysis on the IHTA. Table 5.9 below shows the maximum temperatures reached by the metal oxides. These samples were run using the stepwise setpoint method, $5\text{ }^\circ\text{C min}^{-1}$, isothermal hold for 2 minutes up to $60\text{ }^\circ\text{C}$. While the samples were all weighed, due to density differences of the oxides, it wasn't possible to use weight as a variable in this case. For these samples the sample holder was filled half way, and then the mass was measured. This set of experiments were completed to get an initial view of how the metal oxides coupled within the induction heater and to gain an insight into what power would be needed for the samples to reach a set temperature ($60\text{ }^\circ\text{C}$)

Table 5.9 Sample weight, maximum temperature reached and maximum power required to reach maximum temperature.

Material	mass (g)	Maximum temp (°C)	Maximum power (%)
NiO	2.0	60	70
CuO	2.0	58	80
Mn ₂ O ₃	1.3	60	57
MnO ₂	2.0	52	80
ZnO	0.6	60	65
PbO	2.5	60	78
ZrO ₂	1.00	60	51
TiO ₂	0.5	57	80

It is worth noting also that from observing Fe₃O₄ within the IHTA instrument, the mass of sample does have an effect on how successful the sample couples and subsequently heats. This variation in weights constitutes a significant limitation for the IHTA instrumentation as the sample holder was a specific size and the volume of the material to be heated needed to half fill the holder in order to place the thermocouple in the centre of the sample. This is why the masses shown in table 5.9 are very different. In order to gain a set of directly comparable valid results, the same weight needed to be used each time as the Fe₃O₄ results show that there is a direct link between sample mass and heating capability (fig. 5.9).

5.8.1 Nickel Oxide (NiO)

NiO heated readily in the H-field of the microwave, reaching a maximum temperature of 200 °C. Therefore, it was expected that, the NiO would also be susceptible to induction heating.

It can be seen from the table 5.9 that NiO did reach the maximum of 60 °C but the power level required for the sample to reach this was almost at the maximum operating level of 80 %. NiO has low magnetic moment at room temperature¹⁴¹ so this suggests that the induction heater will work better on samples with higher magnetic moment. It also suggests that the E-field of the microwave may be having an effect on the heating of particular samples. Also worth noting, is that the microwave and induction heater are not directly comparable. As discussed in Chapter 3, the microwave uses a frequency of 2.45 GHz, whereas the induction uses a frequency of only 125 kHz. The normal frequency for induction heating is 500 Hz to 10 kHz, but high range frequencies are from 100 kHz to 450 kHz.¹³¹ The issue with high range induction heating is that the depth of current penetration is low, for deeper penetration of a sample low frequency is recommended, usually in the range of 5 – 30 kHz.

The induction heating frequency may have an effect on the heating due to insufficient penetration depth. The difference between the MWTA frequency and MWTA frequency could also have a profound effect on how a material behaves in the induction heater, but it would still be expected to heat due to the magnetism of the sample albeit to a lower temperature than had been seen within the MWTA.

5.8.2 Copper Oxide (CuO)

As with NiO, CuO heated well in the H-field of the microwave, reaching a maximum temperature of 152 °C. However, when placed in the induction heater, the sample only reached a maximum of 58.3 C, and at this point the power level safety parameter tripped the system. CuO is a semiconductor¹⁶¹ and is antiferromagnetic at room temperature,¹⁶² which suggests why the sample coupled well in the MWTA system but did not heat readily in the IHTA system and leans toward the theory that the E-field is still having an effect on the sample when it is placed in the H-field or that the frequency of the IHTA instrument could be changed to allow for better penetration of the sample.

5.8.3 Manganese oxide (Mn₂O₃ and MnO₂)

Mn₂O₃ did not heat as well in the microwave system as did the NiO and CuO, reaching a maximum temperature of 44 °C in the H-field. MnO₂ in comparison, reached 327 °C in the magnetic field of the MWTA instrument and the power was switched off to prevent damage to the system. It is for this reason that both of these manganese compounds were investigated using the induction heater. Mn₂O₃ reached 60 °C as programmed in the set point using only 57 % power. In contrast to this, MnO₂ only reached 52 °C before the power safety level turned the system off at 80 %. Mn₂O₃ has been reported as a semiconductor¹⁶³, and while other samples which are also semiconductors have coupled well in the EM field, these results suggest that semiconducting properties are not paramount to the coupling ability of a material. Mn₂O₃ is thought to be paramagnetic at -193 °C. MnO₂ is a conductor, shown both through previous research¹⁶⁴ and how well it coupled within the microwave system (although it some resistance is necessary for ohmic heating to take place). The lack of heating within the induction heater suggests that MnO₂ has low magnetic susceptibility in comparison to Mn₂O₃.

5.8.4 Lead oxide, zirconium dioxide and titanium dioxide (PbO, ZrO₂ and TiO₂)

Figure 5.21 below shows a comparison thermogram of the 8 oxides that were analysed in the IHTA instrument.

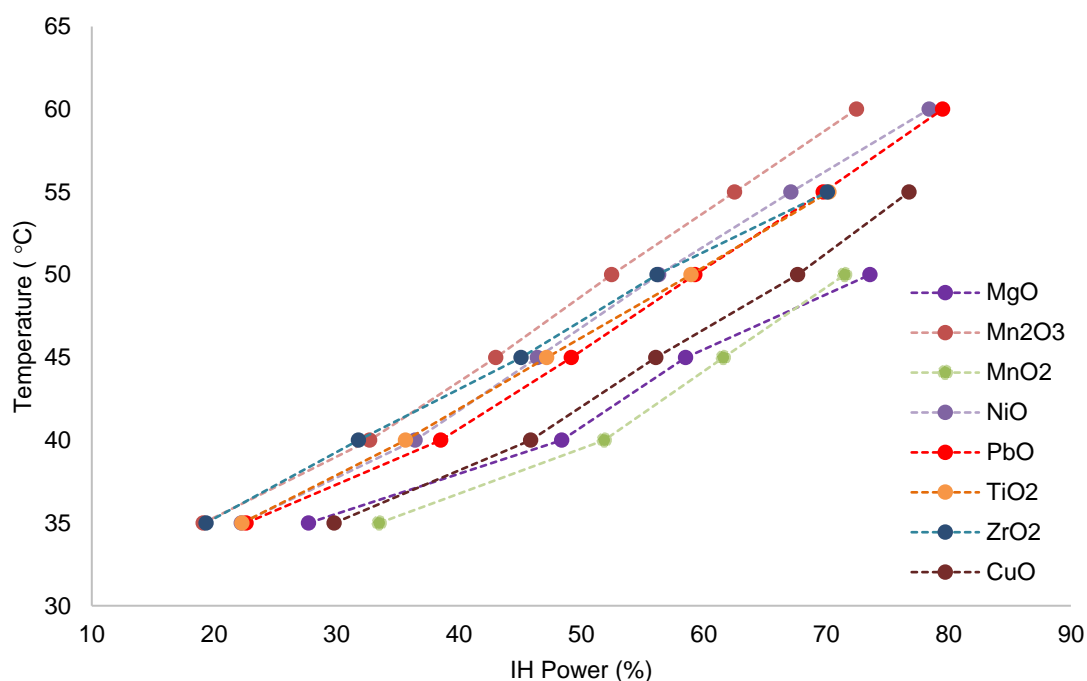


Fig. 5.21. Comparison of oxides analysed on the IHTA instrument (numerical values can be seen in table 5.9 p.90)

As mentioned previously, PbO is diamagnetic and ZrO₂ and TiO₂ are weakly diamagnetic. In the microwave H-field, while a negligible level of heating occurred, it was suggested that this may be caused by the E-field still interacting with the sample. It was decided to analyse these oxides in the IHTA instrument to rule out any interaction of the E-field with the samples, and also to be able to directly compare the corresponding oxides with the perovskites.

The samples of PbO and TiO₂ could be heated to the set temperature of 60 °C, but this required relatively high power of 77 % and 80 % respectively. TiO₂ stopped heating at 58 °C as 80 % power is the set amount before it turns off for safety reasons. ZrO₂ however, heats to the set temperature, only using 50 % of the power. This suggests that ZrO₂ may have some magnetic properties, and supports some studies that have researched the idea that ZrO₂ exhibits magnetic moments at the surface of the oxide.^{46,165} The results for ZrO₂ further support this finding, as the heating that is induced within a material using this method, is restricted to the outside layer of the material¹⁶⁶.

5.9 Ni_{1-x}Mg_xO Rock salt

The rock salt solid solutions that were synthesised (Ni_{1-x}Mg_xO) did not heat very well in the microwave heat field, so they were not expected to heat well when analysed in the IHTA instrument. The results from this series being analysed are shown in fig 5.22 and table 5.10 below.

Table 5.10 Comparison of rock salt solid solutions in IHTA instrument.

Composition	Max Applied power (%)
NiO	68
Ni _{0.75} Mg _{0.25} O	77
Ni _{0.50} Mg _{0.50} O	68
Ni _{0.25} Mg _{0.75} O	61
MgO	80

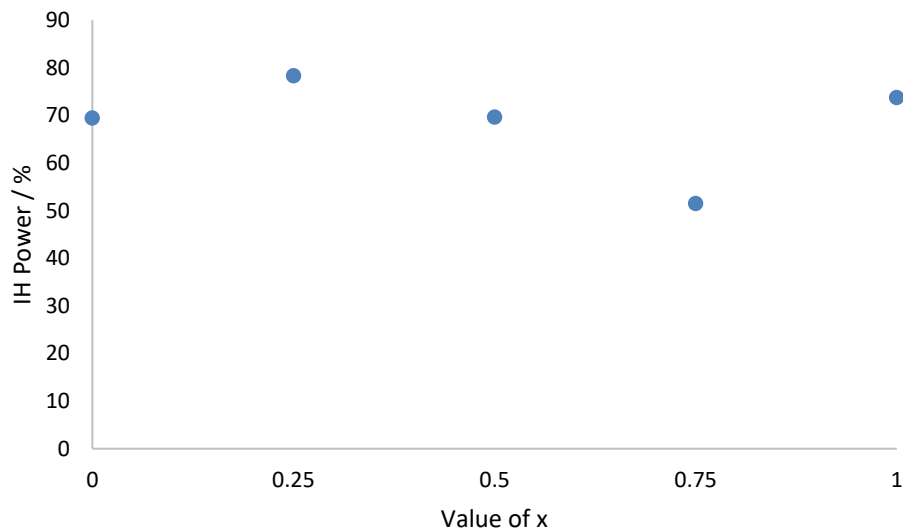


Fig. 5.22. Ni_{1-x}Mg_xO solid solution series. Value of x plotted against power level required to reach 60 °C with IHTA. Numerical values can be seen in Table 5.10.

As can be seen from fig. 5.21 and table 5.10 above, the composition of the rock salt series has an obvious effect on how well the samples heat in the IHTA instrument. Only the MgO did not reach the set temperature, and at 80 % power reached a temperature of 50 °C. This was expected, as discussed in section 5.6. The samples containing nickel, all reached the 60 °C set temperature, but required different percentages of power to reach this temperature. Interestingly, when compared to the H-field of the microwave, the Ni_{0.25}Mg_{0.75}O sample heated the least in the H-field, but required the least power to get to the set temperature in the IHTA, so the analysis is opposing in this case, which was unexpected

as it was thought that the samples would follow the same trend. This pattern will be further examined as the research is continued with more complex materials and within future work (see Chapter 6).

5.10 Perovskites (ABX₃)

5.10.1 MWTA

To help understand the electric and magnetic properties of the double perovskites in the E- and H-fields of the microwave, three different single perovskites were analysed. These three perovskites have well known electric and magnetic properties and have been thoroughly characterised. Fig. 5.23 Shows the three perovskites and their coupling capabilities when in the E-field of the microwave. It is immediately obvious that they are all different, with the PbTiO₃ sample coupling better than the other two samples. PbZrO₃ is antiferroelectric^{167,168} therefore it was not expected to heat well in the E-field of the microwave. PbTiO₃ and BaTiO₃ were expected to show some heating due to their ferroelectric nature.^{169,170} The temperature differences between the samples are shown in table 5.11.

Table 5.11 Temperature differences between the three perovskite samples.

	ΔT (°C)		ΔT (°C)
ΔT_{a1}	15	ΔT_{a2}	32
ΔT_{b1}	30	ΔT_{b2}	54
ΔT_{c1}	31	ΔT_{c2}	66

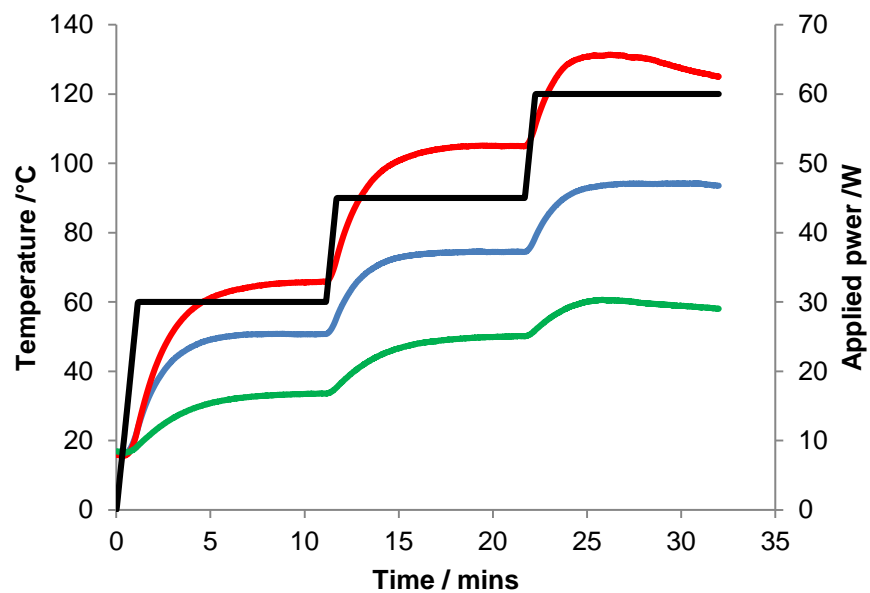


Fig. 5.23 MWTA thermogram of the three different perovskite samples in the E field PbTiO₃ – red, BaTiO₃ – Blue and PbZrO₃ – green. Power profile - black

The figures in table 5.11 show that while the temperature differences initially increase for PbTiO_3 and BaTiO_3 , at ΔT_{c1} the difference in temperature has remained the same as at ΔT_{b1} , indicating that the temperature is increasing at the same rate. Compare this with the temperature differences between PbTiO_3 and PbZrO_3 and the figures show that the difference increases each step. This indicates that the PbTiO_3 sample was increasing in temperature faster with each step, which could show this sample continued coupling well with the MW. The PbZrO_3 , however, seemed to lose coupling strength as the temperature increased.

If these perovskites are compared with their metal oxide counterparts i.e. PbO , ZrO_2 and TiO_2 , it can be seen that, individually, the perovskites behave very differently to the metal oxides. The PbTiO_3 sample reaches a much higher temperature than the PbO and TiO_2 samples (shown in fig. 5.24). This was expected due to the known properties of the oxides and the perovskites.

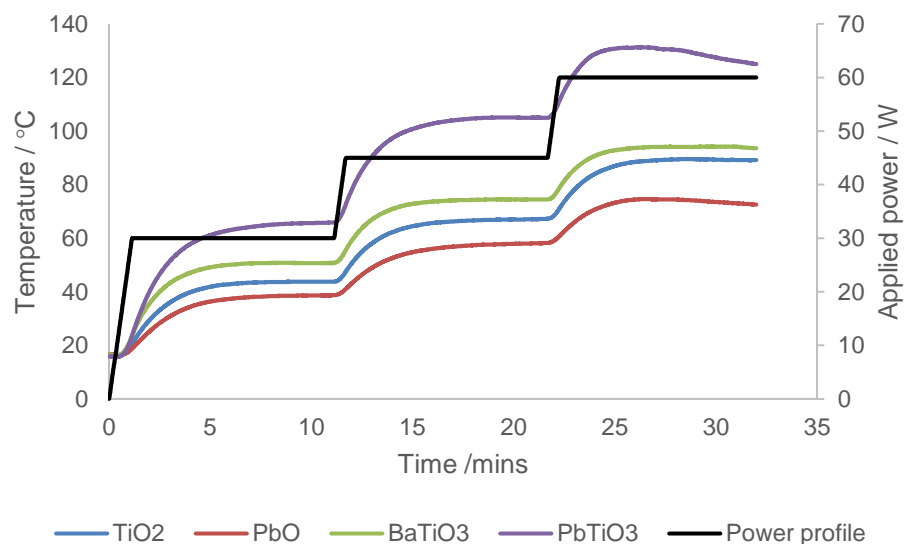


Fig. 5.24 MWTA thermogram of BaTiO_3 and PbTiO_3 with the metal oxides PbO and TiO_2

As mentioned previously, the electrical properties of PbO are not well established, but it is thought to have some conductive properties.¹⁷¹ It did show heating in the E-field which supports this theory. TiO_2 is thought to be a semiconductor,¹⁷² and again, the heating in the E-field, while quite low, does show some coupling with the microwave, supporting these findings. ZrO_2 is an insulating material (large band gap)¹⁷³, which has led to the expectation that this oxide will not couple with the microwaves, and therefore no heating will occur. BaTiO_3 is included in the thermogram with PbTiO_3 for comparison against the TiO_2 metal oxide. Ideally this perovskite would be compared against both TiO_2 and BaO but due to

instability of BaO it was not possible to acquire data on this perovskite within the MWTA and IHTA instruments.

Table 5.12 Maximum temperatures of the three perovskites and comparative metal oxides at each power ramp in the E-field.

	AP at 30 W	AP at 45 W	AP at 60 W
Composition	T ₁ (°C)	T ₂ (°C)	T ₃ (°C)
PbO	38	58	72
TiO ₂	43	67	89
ZrO ₂	48	67	80
BaTiO ₃	50	74	93
PbTiO ₃	65	104	125
PbZrO ₃	33	50	58

With the PbZrO₃ sample, however, the metal oxides reach a higher temperature than the perovskite, shown in fig. 5.25. As mentioned earlier, PbZrO₃ is assumed to be antiferroelectric, and therefore did not couple with the E-field, as expected. ZrO₂, although thought to be insulating, did couple with the microwaves, although the temperature reached was below 100 °C. This could be due to the high dielectric constant (10-23 F m⁻¹)¹⁷⁴ of this material.¹⁷³

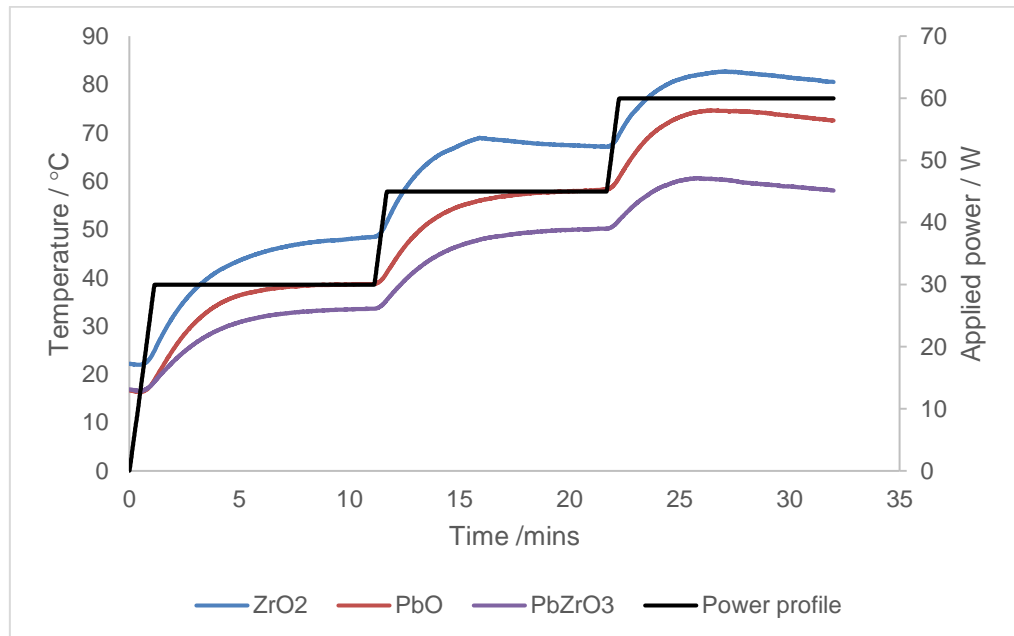


Fig. 5.25 MWTA thermogram of PbZrO₃ and the metal oxides PbO and ZrO₂ in the E-field

Fig. 5.26 below shows the MWTA thermogram for the three perovskite samples in the H field. It was observed that the perovskites coupled relatively well in the H-field (maximum temperatures shown in table 5.13) and that their heating profiles match those observed in the E-field, even though the temperatures were lower. This suggests that none of the perovskites couple better when in the H-field than they do in the E-field. It should also be noted that the PbZrO_3 samples had a slight drop in temperature as the first 30 W power ramp is taking place. This sample was analysed three times on the MWTA instrument to check for an unknown impurity in the sample that may be removed during the analysis, but the same event occurred each time. It is yet unclear why this anomaly is evident only in this sample.

Table 5.13 Maximum temperatures of the three perovskites and comparative metal oxides at each power ramp in the E-field.

	AP at 30 W	AP at 45 W	AP at 60 W
Composition	T_1 (°C)	T_2 (°C)	T_3 (°C)
PbO	23	31	40
TiO ₂	23	31	40
ZrO ₂	31	39	45
BaTiO ₃	27	37	47
PbTiO ₃	31	45	58
PbZrO ₃	23	31	38

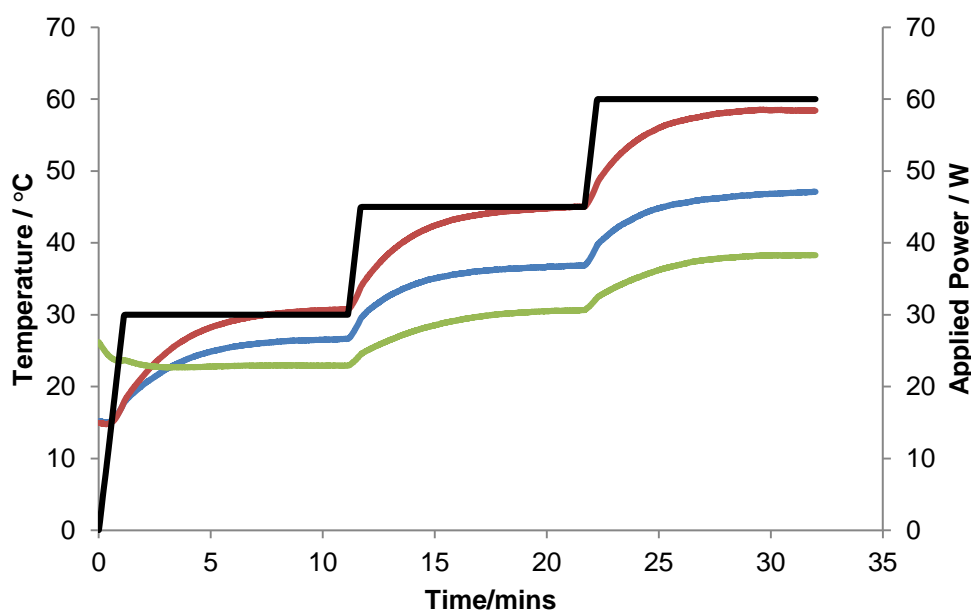


Fig. 5.26 MWTA thermogram the three perovskites in the H-field. PbTiO₃ – Red, BaTiO₃ - Red, PbZrO₃ – green. Power profile - black

Figures 5.27 and 5.28 overleaf depict the individual perovskites compared to their metal oxide counterparts. As with the thermograms in the E-field, BaTiO₃ is included with the PbTiO₃ sample as BaO could not be analysed. The same interactions with the H-field were observed as with the E-field, where the perovskite samples couple better and achieve a higher temperature than the metal oxides, although the temperatures reached were negligible (see tables 5.13 and 5.14) and it has been postulated that the E-field may be having an effect on the heating of these samples. This effect will try and be determined when the samples are analysed in the IHTA system, which will remove the E-field parameter, and only magnetic heating should occur. Table 5.13 gives the maximum temperatures reached by each of the perovskite samples and metal corresponding metal oxides at each power ramp. Table 5.14 compares maximum temperatures (AP = 60 W) reached by each of the perovskites and metal oxides in both the E- and H-field. There is an indication of a linear increase of temperature with each step, although with only three steps it is difficult to draw any major conclusions, it may be possible that higher temperatures could be reached if there was a higher power input.

Although the microwave and induction behaviour should be related to the structure of the material along with the electrical and magnetic properties, it was felt that a comparison with the simpler oxide components would show that any unusual behaviour was not directly related to the oxide and that different behaviours from the more complex materials could be seen with the new instrumentation.

Table 5.14 Maximum temperatures of the three perovskites and corresponding metal oxides in both the E- and H-field.

Composition	T _{max} at AP = 60 W	
	E-field	H-field
PbO	73	40
TiO ₂	89	40
ZrO ₂	80	45
BaTiO ₃	94	47
PbTiO ₃	125	58
PbZrO ₃	58	38

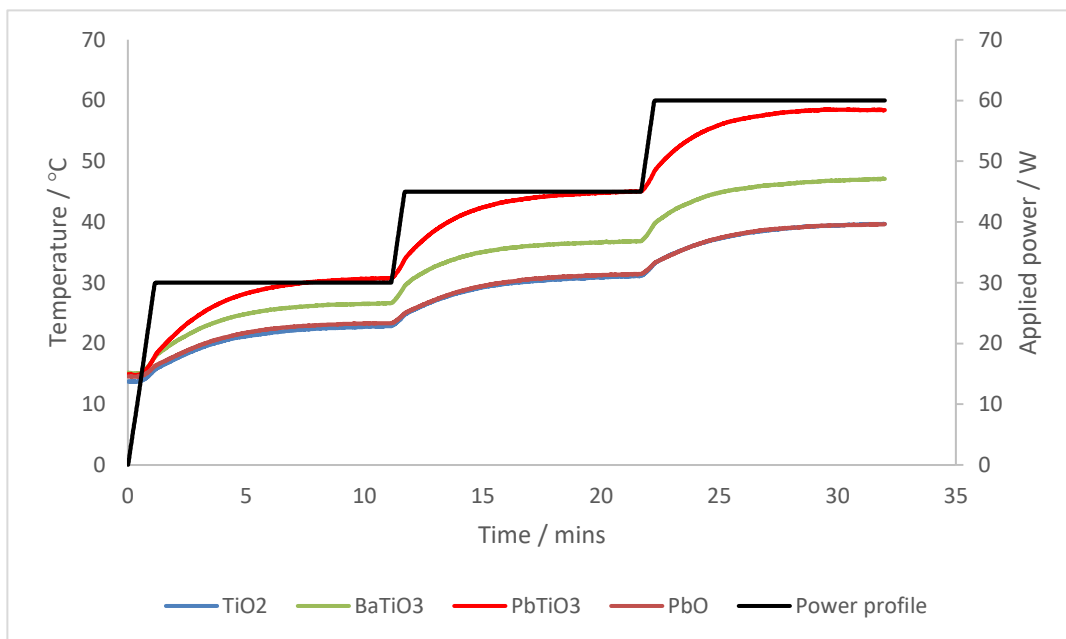


Fig. 5.27 MWTA thermogram BaTiO₃ and PbTiO₃ with PbO and TiO₂ metal oxide counterparts within the H-field

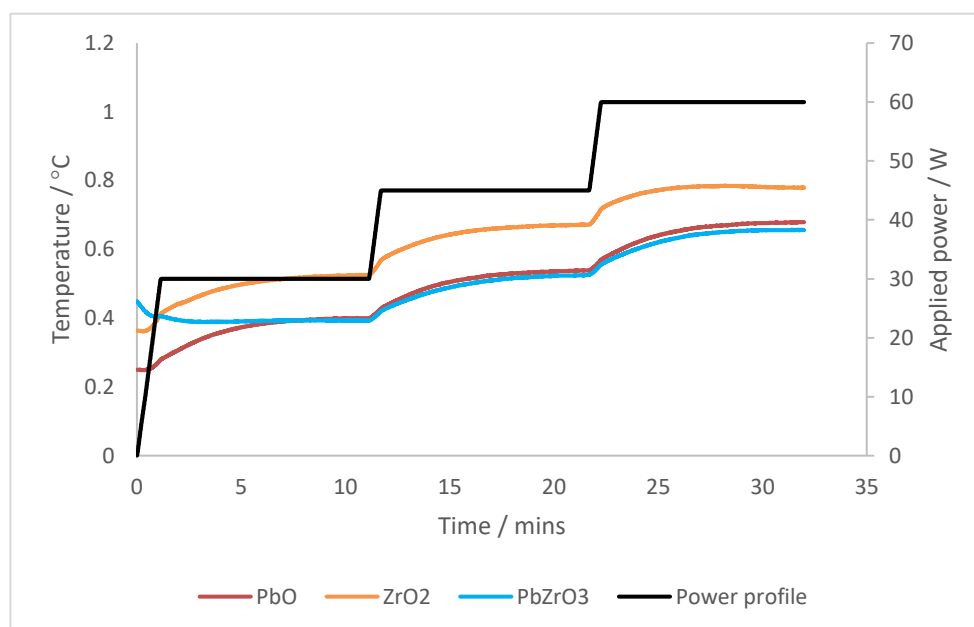
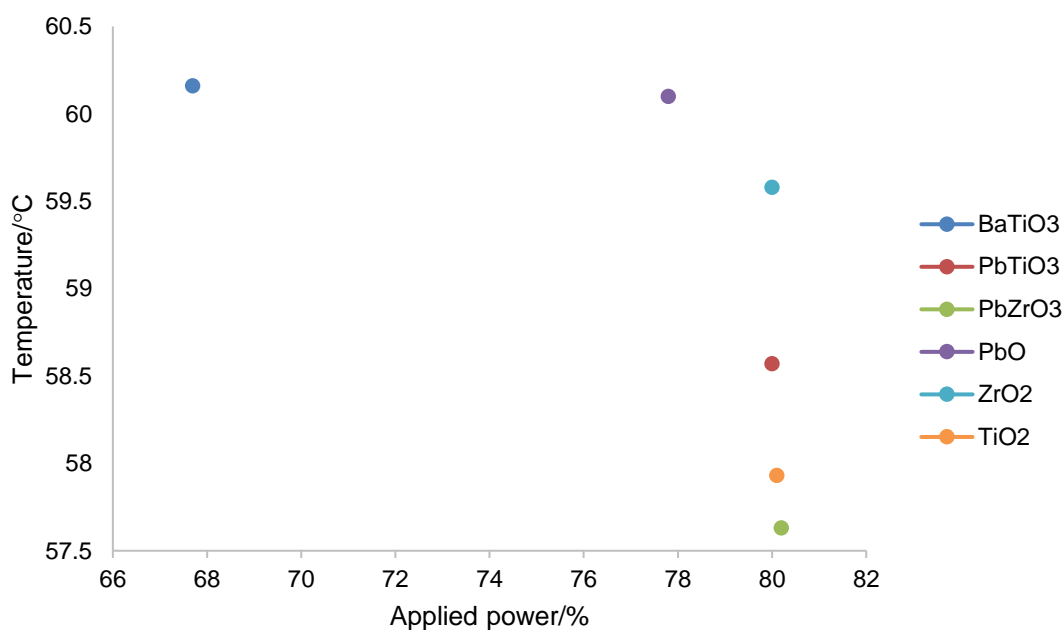


Fig. 5.28 MWTA thermogram PbZrO₃ with PbO and ZrO₂ metal oxide counterparts within the H-field



5.10.2 IHTA Perovskites (ABX₃)

The three perovskite systems, PbTiO₃, PbZrO₃ and BaTiO₃, were analysed on the IHTA instrument as a comparison to the results found in the H-field of the microwave. It is not expected for PbZrO₃ to heat, as the heating observed in the microwave was negligible. PbTiO₃ and BaTiO₃ may heat, as they reached temperatures of 58. °C and 47 °C respectively in the H-field, so similar temperatures were expected to be observed in the IHTA system. These systems were analysed using stepwise setpoint with a set temperature of 60 °C, 5 °C min⁻¹ ramp rate and a 2-minute hold between ramps. The comparison of the perovskites is shown in fig. 5.29 below, and the maximum power input against the temperature is shown in table 5.15.

Table 5.15 Maximum power required to heat the studied perovskites to the set temperature

Material	Maximum power (%)	Maximum temperature (C)
BaTiO ₃	68	60
PbTiO ₃	80	58
PbZrO ₃	80	57
PbO	78	60
ZrO ₂	51	60
TiO ₂	80	57

Fig. 5.29 comparison of three perovskite systems and their corresponding metal oxides.

It can be observed in Table 5.15, two of the perovskites and two of the metal oxides do not heat well in the induction heater. The heating of PbZrO_3 was expected as it heated similarly within the H-field of the microwave instrument. BaTiO_3 was expected to heat better than PbZrO_3 but not as well as PbTiO_3 , as the results showed from the microwave PbTiO_3 coupled better within the H-field. These results from the induction instrument, however, show that BaTiO_3 heats better than the other perovskites, needing much less power to reach the set temperature. This phenomenon could again be attributed to the surface magnetisation of the material, as with the ZrO_2 samples, although further research into these materials is required to acquire more evidence of this type of heating. These results support the idea of utilising induction heating as an analytical tool alongside the MTWA instrumentation as different magnetic behaviours are apparent from each instrument. Discussed previously, the frequency could play a large part in how a material couples, and is a significant aspect when investigating magnetic behaviours as an analytical tool and is worth investigating in the future.

5.11 Double Perovskites (ABB'X₆)

5.11.1 MWTA Sr₂FeMo_{1-x}W_xO₆

As mentioned previously, the double perovskite series Sr₂FeMo_{1-x}W_xO₆ has been well characterised since Kobayashi⁶³ discovered the HM-FM property of Sr₂FeMoO₆. These unique properties meant that this series of materials was selected to be synthesised and analysed with MWTA to determine its behaviour in electric and magnetic fields. It must also be noted that there were impurities within the samples and it is not known what effect these would have on the coupling capabilities of the material. As a future experiment, a comparison with just the impure phase would give a good insight into the behaviour of the double perovskites.

Fig 5.30 gives the seven different compositions synthesised for the material series when heated in the E-field. The series doesn't follow a steady trend where the heating is concerned, with Sr₂FeWO₆ reaching the highest temperature. This could be expected as the WO₃ oxide sample heated particularly well in the E-field, although not in the H-field. However, as the amount of W decreases with in the sample, the heating capabilities of the materials don't get gradually worse. The 60% W also reaches quite a high temperature (116 °C), and the only other composition to get above 100 °C was the Sr₂FeMo_{0.25}W_{0.75}O₆, which managed to reach 103 °C. The other four samples are grouped quite closely together, with the lowest temperature being reached being 77 °C for the Sr₂FeMo_{0.5}W_{0.5}O₆ sample.

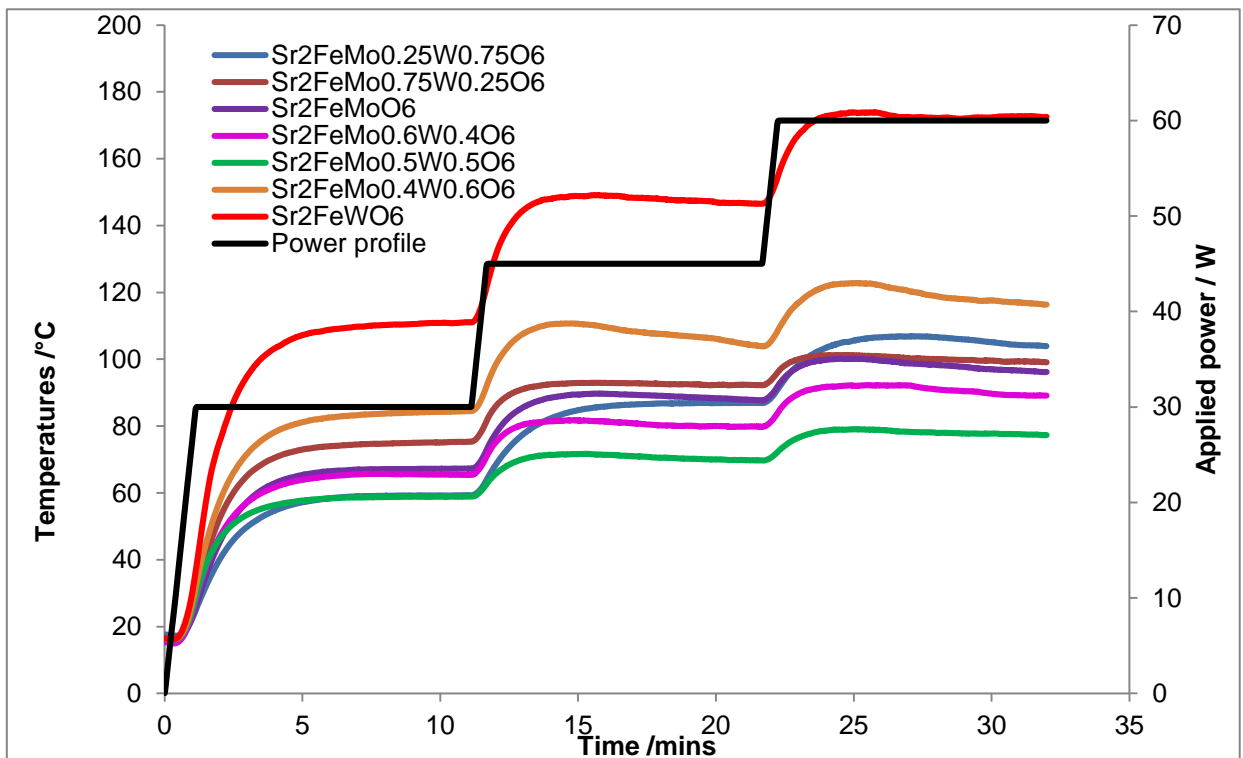


Fig. 5.30 Double perovskite series Sr₂FeMo_{1-x}W_xO₆ results from E-field of microwave.

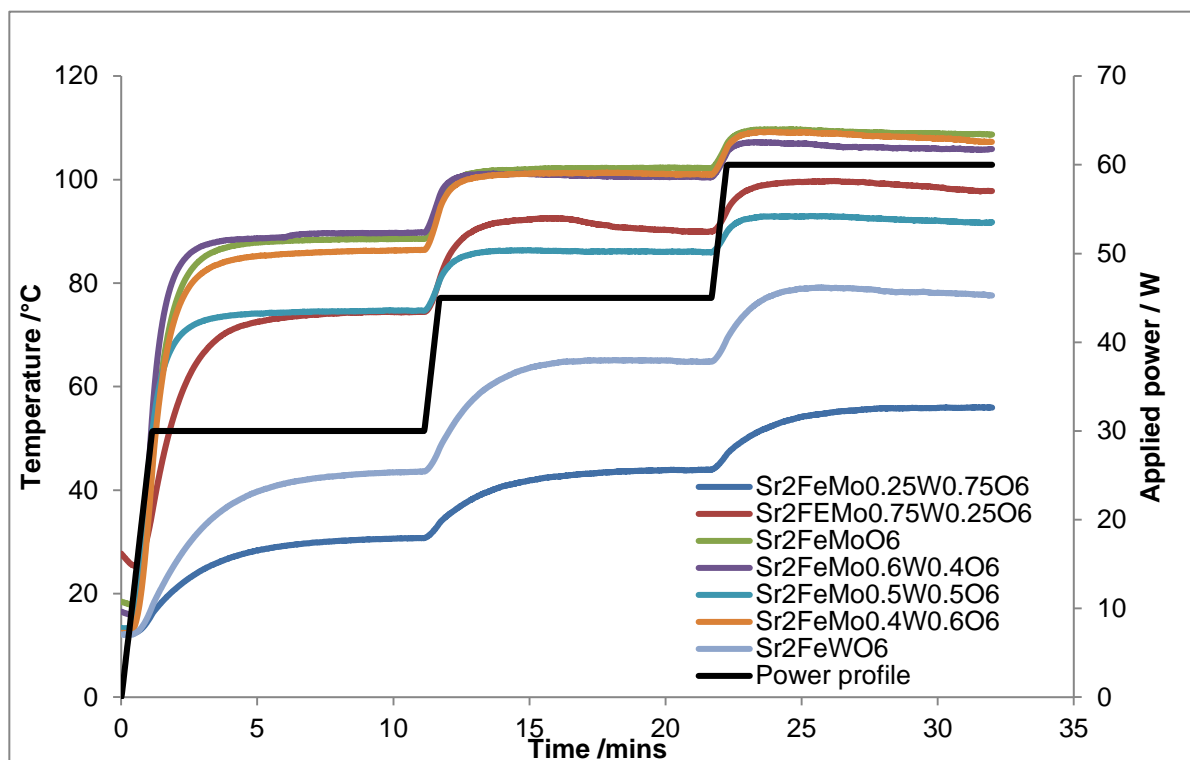
Table 5.16 shows the temperature changes between the steps and it can be noted that the rate of temperature increase is falling, suggesting that a maximum temperature may be reached. Adding extra steps with increased power would be a good way to determine whether this is actually the case, but could not be investigated at this time due to maintaining the integrity of the instrument.

Table 5.16. Temperature difference between the power ramps of the $\text{Sr}_2\text{FeMoO}_6$ series in the E-field of the MWTA instrument.

Composition	Temperature difference °C (T2-T1)	Temperature difference °C (T2-T3)
$\text{Sr}_2\text{FeMoO}_6$	20	8
	19	7
$\text{Sr}_2\text{FeMo}_{0.6}\text{W}_{0.4}\text{O}_6$	14	9
$\text{Sr}_2\text{FeMo}_{0.5}\text{W}_{0.5}\text{O}_6$	11	8
$\text{Sr}_2\text{FeMo}_{0.4}\text{W}_{0.6}\text{O}_6$	19	13
$\text{Sr}_2\text{FeMo}_{0.25}\text{W}_{0.75}\text{O}_6$	28	17
Sr_2FeWO_6	35	26

In contrast to the E-field heating, the H-field heating is very different (Fig 5.31). Sr_2FeWO_6 is known to be antiferromagnetic and therefore was not expected to heat well while in the H-field. In this case, it is the sample at the other end of the series, $\text{Sr}_2\text{FeMoO}_6$ that heats the best, followed extremely closely by the 60:40 compositions. $\text{Sr}_2\text{FeMoO}_6$ heats to a maximum temperature of 108 °C. The two 60:40 samples heat to 106 °C ($\text{Sr}_2\text{FeMo}_{0.6}\text{W}_{0.4}\text{O}_6$) and 107 °C ($\text{Sr}_2\text{FeMo}_{0.4}\text{W}_{0.6}\text{O}_6$). $\text{Sr}_2\text{FeMo}_{0.25}\text{W}_{0.75}\text{O}_6$ reached a temperature of 55 °C, which was the lowest temperature out of all the samples. It was expected that the sample to reach the low temperatures would be the Sr_2FeWO_6 sample, as this is known to be antiferromagnetic¹⁷⁵; however, this reaches a temperature of 77 °C.

Table 5.17, below, shows the same trend as in the E-field, where the rate of heating falls between the power ramps. The only sample that doesn't seem to have a reduction in heating rate is the $\text{Sr}_2\text{FeMo}_{0.25}\text{W}_{0.75}\text{O}_6$ sample. As this doesn't happen in the E-field, it can only be assumed that this is a particular trait when the sample is in the H-field. There is a possibility that the structure is allowing for the sample to couple, and while it has been postulated that some behaviour can be attributed to some dehydration, it is unlikely in this case as the



sample had already been heated within the E-field and no change was observed. It may be that with more power ramps that this sample would then observe similar behaviour to the other three samples and this difference is just an anomaly.

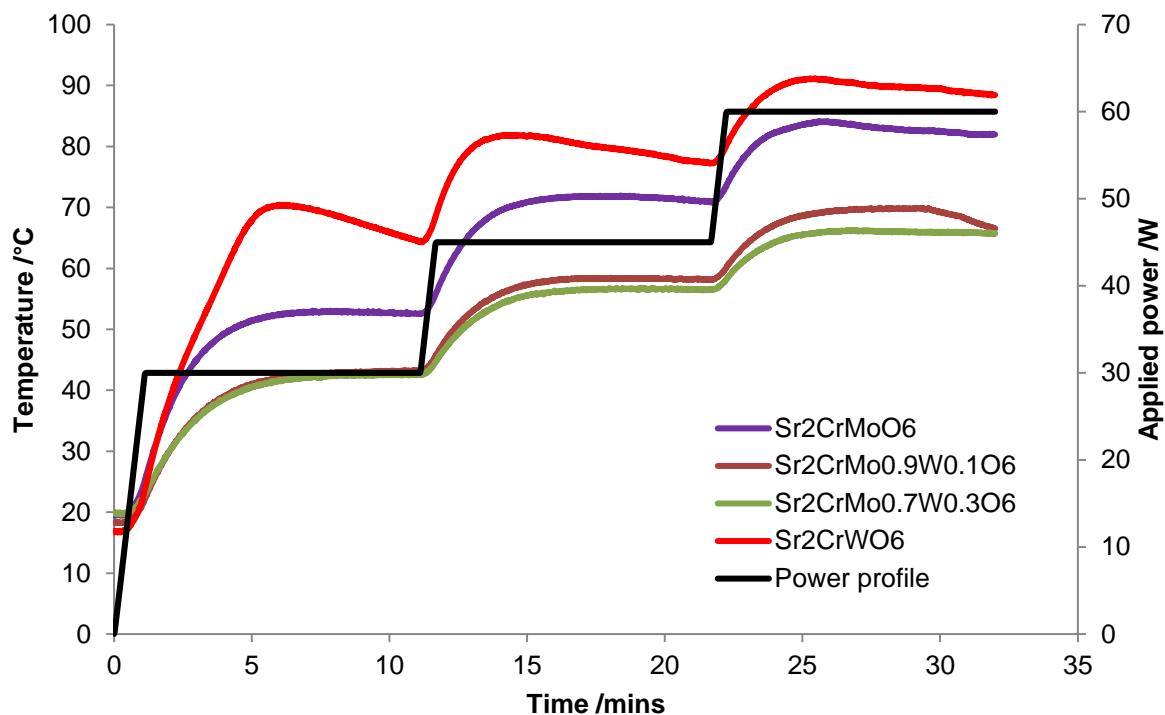
Table 5.17. Temperature difference between the power ramps of the $\text{Sr}_2\text{FeMoO}_6$ series in the H-field of the MWTA instrument.

Composition	Temperature difference °C (T2-T1)	Temperature difference °C (T2-T3)
$\text{Sr}_2\text{FeMoO}_6$	14	6
$\text{Sr}_2\text{FeMo}_{0.75}\text{W}_{0.25}\text{O}_6$	16	8
$\text{Sr}_2\text{FeMo}_{0.6}\text{W}_{0.4}\text{O}_6$	11	5
$\text{Sr}_2\text{FeMo}_{0.5}\text{W}_{0.5}\text{O}_6$	11	6
$\text{Sr}_2\text{FeMo}_{0.4}\text{W}_{0.6}\text{O}_6$	15	6
$\text{Sr}_2\text{FeMo}_{0.25}\text{W}_{0.75}\text{O}_6$	13	12
Sr_2FeWO_6	21	13

Fig. 5.31 Double perovskite series $\text{Sr}_2\text{FeMo}_{1-x}\text{W}_x\text{O}_6$ results from H-field of microwave.

5.11.2 $\text{Sr}_2\text{CrMo}_{1-x}\text{W}_x\text{O}_6$

The double perovskite system $\text{Sr}_2\text{CrMo}_{1-x}\text{W}_x\text{O}_6$ was studied due to Sr_2CrWO_6 previously



being reported as having T_c at room temperature.¹⁷⁶ The series was researched to enable a comparison of the substitution of Fe with Cr on the B site. The percentage of Mo to W was slightly different to the $\text{Sr}_2\text{FeMoW}_x\text{O}_6$ series, as these samples were synthesised as part of a separate project running alongside this research.

Table 5.18. Temperature difference between the power ramps of the $\text{Sr}_2\text{CrMoO}_6$ series in the E-field of the MWT A instrument.

Composition	Temperature difference °C (T2-T1)	Temperature difference °C (T2-T3)
$\text{Sr}_2\text{CrMoO}_6$	18	11
$\text{Sr}_2\text{CrMo}_{0.9}\text{W}_{0.1}\text{O}_6$	4	8
$\text{Sr}_2\text{CrMo}_{0.7}\text{W}_{0.3}\text{O}_6$	14	9
Sr_2CrWO_6	13	11

Fig. 5.32 below shows the MWT A thermogram for the SCMWO series and Table 5.18 gives the maximum temperature reached by each composition.

Fig. 5.32 Double perovskite series $\text{Sr}_2\text{CrMo}_{1-x}\text{W}_x\text{O}_6$ results from E-field of microwave.

Previous research investigating the magnetic properties of the Sr_2CrWO_6 discovered that this perovskite had a T_C of 450 K (177 C).¹⁷⁷ Research also suggest that this compound is attracted to a magnet at room temperature¹⁰⁵ and although this was not a noticeable effect with the samples synthesised for this research, it was felt that analysing the samples in both the MWTA and IHTA systems may show magnetic behaviour previously undiscovered. Table 5.18 shows the maximum temperatures reached by the series when in the E-field of the microwave. It can be seen from both table 5.18 and fig 5.32, that three of the samples coupled better in the E-field than the others. These compositions were $\text{Sr}_2\text{CrMoO}_6$, $\text{Sr}_2\text{CrMo}_{0.5}\text{W}_{0.5}\text{O}_6$ and Sr_2CrWO_6 . It was expected that the Sr_2CrWO_6 sample may interact well in the microwave, as research suggests that this composition has some electrical properties similar to $\text{Sr}_2\text{FeMoO}_6$. There were no expectations with the other samples as there are very few literature sources containing the various compositions discussed in this thesis. It is interesting to note that the 50:50 sample shows some coupling within the E-field, as it is unknown whether this composition has been studied for its magnetic and electrical properties prior to this research. The unusual trace from the Sr_2CrWO_6 sample is obvious in comparison to the other samples. This steady reduction in coupling during the isothermal hold has been noted in another sample, WO_3 . This behaviour, and the literature T_C not being observed, may suggest there is a high impurity level within this sample. It could also be attributed to adsorbed moisture within the sample.

When the series was examined in the H-field (fig. 5.33) it was determined that while the $\text{Sr}_2\text{CrMoO}_6$ and Sr_2CrWO_6 coupled slightly better than the other five samples, reaching temperatures of 42 °C and 51 °C respectively, this interaction was negligible (Table 5.19). It was expected that the Sr_2CrWO_6 would couple better than the other samples due to previous research¹¹⁷ suggesting that HM-FM properties had been observed as with $\text{Sr}_2\text{FeMoO}_6$, but the same level of interaction within the microwave was not observed. Although the interaction in the H-field was negligible, the series was still analysed in the IHTA system. These results will be discussed further in Section 5.12.

Table 5.19. Temperature difference between the power ramps of the $\text{Sr}_2\text{CrMoO}_6$ series in the H-field of the MWTA instrument.

Composition	Temperature difference °C (T2-T1)	Temperature difference °C (T2-T3)
$\text{Sr}_2\text{CrMoO}_6$	8	6

$\text{Sr}_2\text{CrMo}_{0.9}\text{W}_{0.1}\text{O}_6$	7	5
$\text{Sr}_2\text{CrMo}_{0.7}\text{W}_{0.3}\text{O}_6$	8	5
Sr_2CrWO_6	11	7

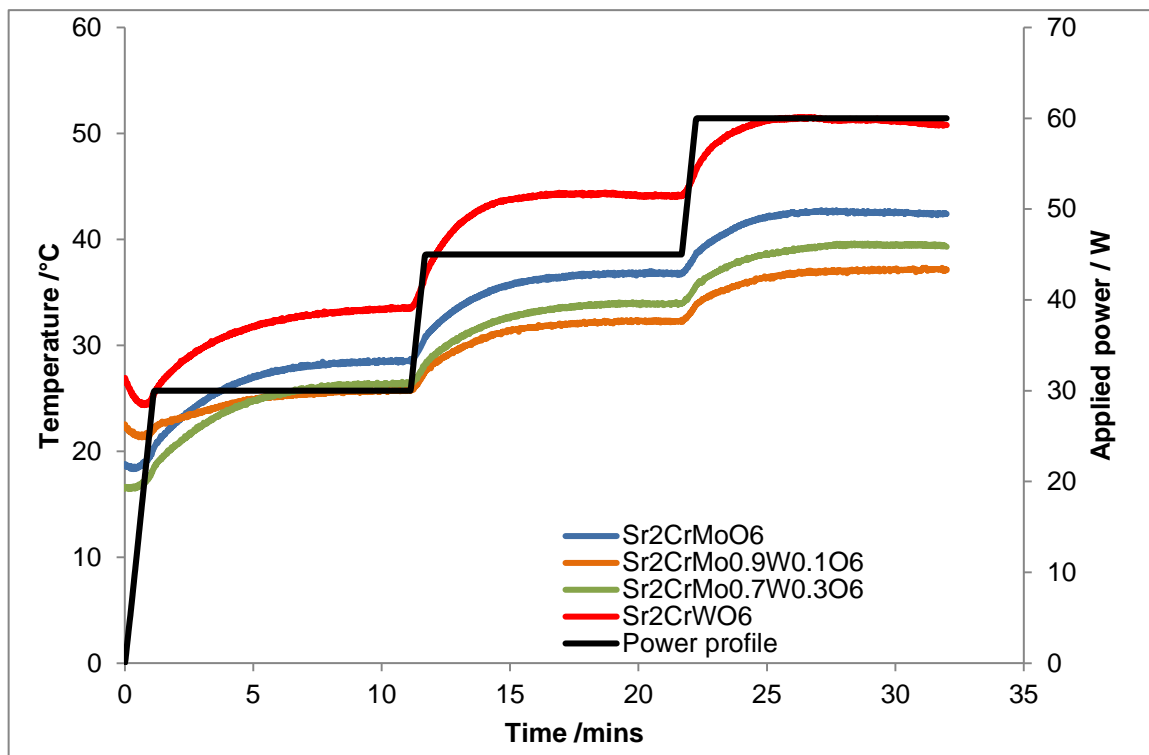


Fig. 5.33 Double perovskite series $\text{Sr}_2\text{CrMo}_{1-x}\text{W}_x\text{O}_6$ results from H-field of microwave.

5.11.3 $\text{Sr}_{2-x}\text{La}_x\text{FeMoO}_6$

This series was investigated as research has discovered that substituting Sr for La on the A-site can increase T_C and the magnetic properties of these double perovskites.^{41,178} Hussain *et al* suggest that La-doping where La mole percent >0.2 increases the anti-site disorder which decreases the magnetic capabilities of the compounds. Therefore, this research has focussed on the series $\text{Sr}_{2-x}\text{La}_x\text{FeMoO}_6$ where $0 \leq x \leq 0.2$.

Figure 5.34 and table 5.20 overleaf show the results from the samples in the E-field of the microwave. The series was expected to couple well with the E-field and achieve a high degree of heating, but it was uncertain whether this series would interact better than the $\text{Sr}_2\text{FeMoO}_6$ sample.

It is apparent from fig 5.34 that the $\text{Sr}_{0.90}\text{La}_{0.10}\text{FeMoO}_6$ couples with the E-field better and heats more readily than the $\text{Sr}_2\text{FeMoO}_6$ sample. This was unexpected, but does agree with the literature research which indicates that the properties of this series can be changed by doping with a La^{3+} ion.⁶¹

Table 5.20 overleaf shows the temperature difference for each sample. All the samples obtain a temperature above 50 °C, only the $\text{Sr}_{1.90}\text{La}_{0.10}\text{FeMoO}_6$ sample reaches a temperature in excess of 100 °C.

Table 5.20. Temperature difference between the power ramps of the $\text{Sr}_{2-x}\text{La}_x\text{MoO}_6$ series in the E-field of the MWTA instrument.

Composition	Temperature difference °C (T2-T1)	Temperature difference °C (T2-T3)
$\text{Sr}_2\text{FeMoO}_6$	21	8
$\text{Sr}_{1.95}\text{La}_{0.05}\text{FeMoO}_6$	21	16
$\text{Sr}_{1.90}\text{La}_{0.10}\text{FeMoO}_6$	12	6
$\text{Sr}_{1.85}\text{La}_{0.15}\text{FeMoO}_6$	20	18
$\text{Sr}_{1.80}\text{La}_{0.20}\text{FeMoO}_6$	29	20

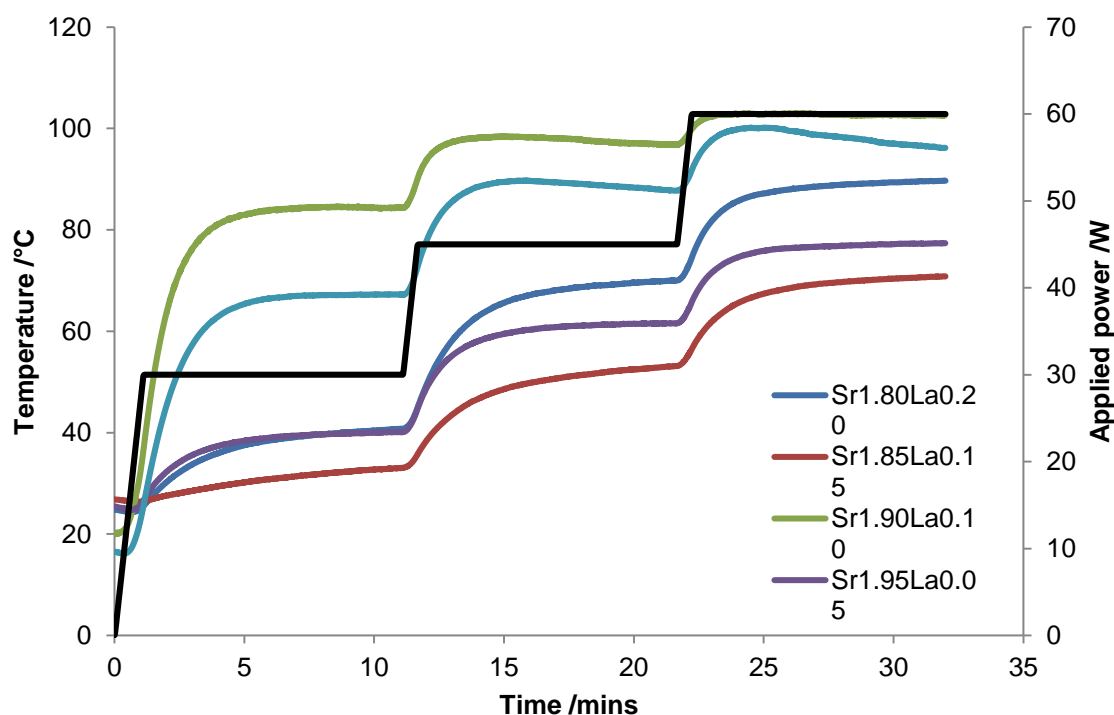


Fig. 5.34 Double perovskite series $\text{Sr}_{2-x}\text{La}_x\text{FeMoO}_6$ results from E-field of microwave.

Figure 5.35 overleaf shows the temperatures reached by the series in the H-field of the microwave. It is immediately obvious that the results are different to the analysis obtained from the E-field heating. $\text{Sr}_{1.90}\text{La}_{0.10}\text{FeMoO}_6$ again reached a high temperature but table 21 shows that as the power increases at each step, the level of coupling, and therefore the heating, begins to decrease. The difference in temperature (table 5.21) indicates that

although the initial coupling in the H-field for the $\text{Sr}_{1.90}\text{La}_{0.10}\text{FeMoO}_6$ was high, as the power was continually increased, there was less and less magnetic interaction with the applied field. $\text{Sr}_{1.80}\text{La}_{0.20}\text{FeMoO}_6$ however, continually interacted with the applied field, and the final maximum temperature reached by this sample was higher. Again, these results in the H-field agree with previous research, in that the different compositions of this series doped with a La ion can increase the magnetic susceptibility of the sample^{41,178}. These results also suggest that particular compositions are required for the properties to be increased, as the other samples in the series ($\text{Sr}_{1.95}\text{La}_{0.05}\text{FeMoO}_6$ and $\text{Sr}_{1.85}\text{La}_{0.15}\text{FeMoO}_6$) have a decreased interaction with the magnetic field in comparison to $\text{Sr}_2\text{FeMoO}_6$. These samples were all analysed with the IHTA system, which will be discussed in Section 5.12. There is the possibility that there are impurities within the sample, as with the $\text{Sr}_2\text{FeMoO}_6$, SrMoO_4 may also be present within the lanthanum doped samples.

Table 5.21. Temperature difference between the power ramps of the $\text{Sr}_{2-x}\text{La}_x\text{MoO}_6$ series in the E-field of the MWTA instrument.

Composition	Temperature difference °C (T2-T1)	Temperature difference °C (T2-T3)
$\text{Sr}_2\text{FeMoO}_6$	14	6
$\text{Sr}_{1.95}\text{La}_{0.05}\text{FeMoO}_6$	24	10
$\text{Sr}_{1.90}\text{La}_{0.10}\text{FeMoO}_6$	5	3
$\text{Sr}_{1.85}\text{La}_{0.15}\text{FeMoO}_6$	26	12
$\text{Sr}_{1.80}\text{La}_{0.20}\text{FeMoO}_6$	28	10

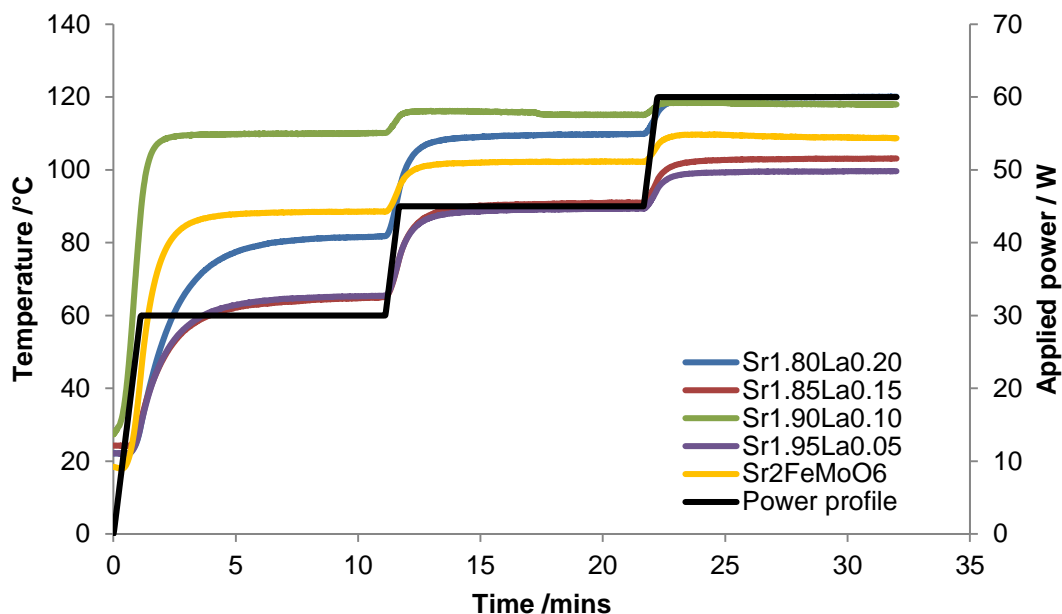


Fig. 5.35 Double perovskite series $\text{Sr}_{2-x}\text{La}_x\text{FeMoO}_6$ results from H-field of microwave.

This series of samples in the H-field show well-behaved data. There are no obvious fluctuations within the steps and the temperatures appear to be converging (step one temperature difference = 45 °C and step three temperature difference = 17 °C), which again supports the theory (mentioned previously) that there may be a maximum temperature that can be reached with these samples. The sequence also changes for $\text{Sr}_{1.8}$, where the temperature increases up to a similar temperature as $\text{Sr}_{1.9}$, but the others do not behave like this and keep their temperature paths in comparison to starting points.

5.12 IHTA

5.12.1 $\text{Sr}_2\text{FeMo}_x\text{W}_{1-x}\text{O}_6$

The coupling of this series in the MWTA system was dependent on the composition of the sample. The data gathered from the microwave suggest that three of the samples should couple better in the IHTA than the others. It is expected that the $\text{Sr}_2\text{FeMoO}_6$, $\text{Sr}_2\text{FeMo}_{0.6}\text{W}_{0.4}\text{O}_6$ and $\text{Sr}_2\text{FeMo}_{0.4}\text{W}_{0.6}\text{O}_6$ will heat readily with the IHTA as they reached the highest temperatures while in the H-field of the microwave. The results from the IHTA experiments can be seen on the next two pages in figs 5.36 and 5.37. The applied power needed to heat the samples to a set temperature are also tabulated below and can be seen in Table 5.22.

The samples were analysed using two different amounts (0.5 g and 1.0 g) to ascertain whether more or less power would be required depending on the amount of sample within

the holder. This was mentioned previously in Chapter 3, when examining the applied power with iron oxide samples during method development of the IHTA instrument.

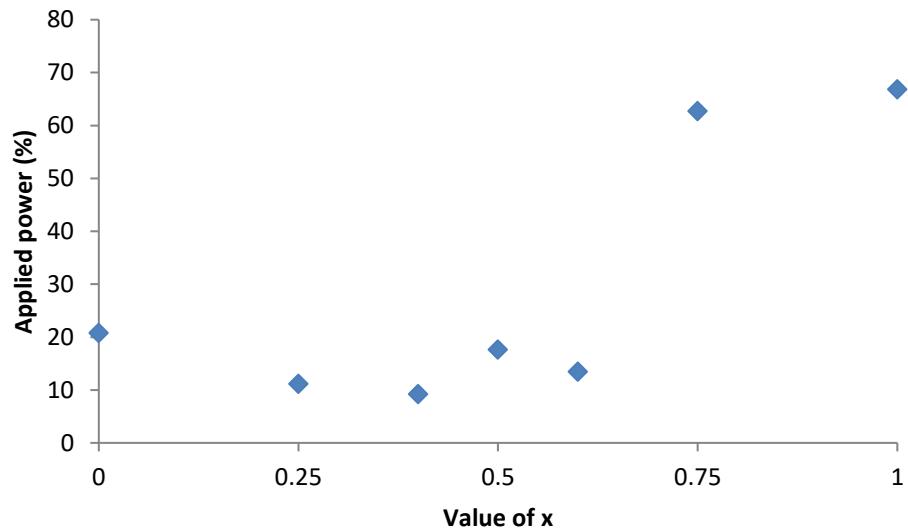
Table 5.22 Comparison of power needed to heat the different compositions to a set temperature of 60 °C.

Value of x	0.5 g $\text{Sr}_2\text{FeMo}_{1-x}\text{W}_x\text{O}_6$ Applied power (%)	1.0 g $\text{Sr}_2\text{FeMo}_{1-x}\text{W}_x\text{O}_6$ Applied power (%)
0	32	21
0.25	11	11
0.40	18	9
0.50	33	18
0.60	24	13
0.75	59	63
1.00	62	67

As Table 5.22 shows, in the case of $x = 0, 0.40, 0.50$ and 0.60 , the power required to heat the samples are greatly reduced when the sample weight is doubled. However, with the compositions of $x = 0.75$ and $x = 1.00$, the increase in sample weight has also resulted in an increase of applied power. This increase in power could be due to the induced current being the greatest on the outside layer of the sample,¹⁷⁹ and this has required more power to be applied to the larger sample for the same temperature to be acquired. The compositions with the larger W component are also antiferromagnetic which reduces the amount of Joule heating that can occur within the sample.

Figures 5.36 below and 5.37, below and overleaf, show a visual representation of the data in Table 5.22. The samples that heat more readily within the IHTA instrument are easily distinguishable from the other data points. With regard to the induction heater being

comparable to the MWTA instrument, two of the samples that were expected to heat well in the induction heater ($\text{Sr}_2\text{FeMo}_{0.6}\text{W}_{0.4}\text{O}_6$ and $\text{Sr}_2\text{FeMo}_{0.4}\text{W}_{0.6}\text{O}_6$) due to their coupling in the H-field of the microwave, did require less power to reach the desired temperature than the other samples. The third sample ($\text{Sr}_2\text{FeMoO}_6$) heated less well than was expected. The



sample that was least expected reach the set temperature, due to only reaching a temperature of 55.94 °C in the MWTA H-field, was the $Sr_2FeMo_{0.25}W_{0.75}O_6$, and the IHTA analysis is in agreements with the MWTA H-field analysis. Both the samples where $x = 0$, 0.75 and 1.00 require the highest power level to reach the set temperature, indicating low interaction with the induced magnetic field.

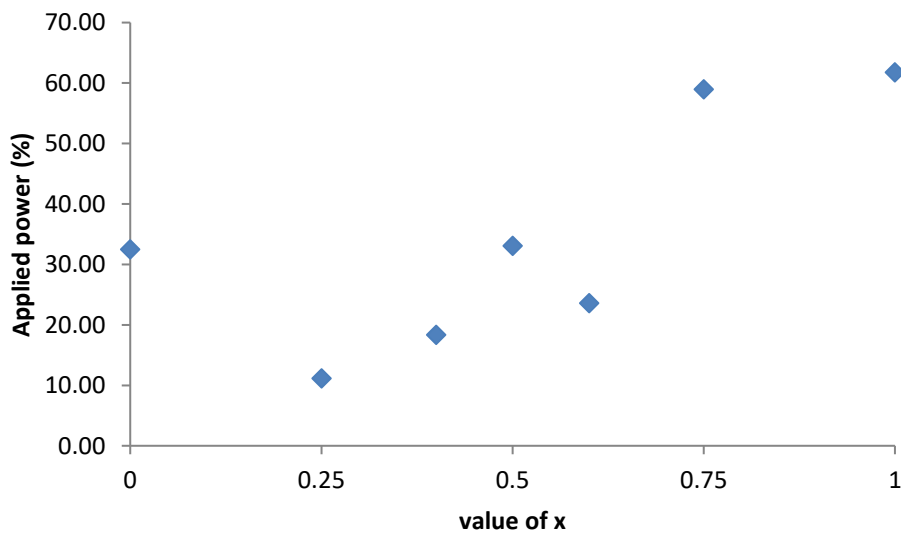


Fig. 5.36 IHTA of $Sr_2FeMo_{1-x}W_xO_6$ - 0.5 g sample

Fig. 5.37 IHTA of $Sr_2FeMo_{1-x}W_xO_6$ - 1.0 g sample

The increased sample weight reduces the power required for heating to 60 °C, specifically for samples where $x = 0$, 0.50 and 0.60. In fig. 5.8 above, this can be seen as the samples

a show much more linear trend ($0 \leq x \leq 0.6$) than in figure 5.7. The interesting thing about these figures is that the same trend can be observed even after doubling the mass, including the clear step in how well the series heats inductively at $x=0.75$. This is a good sign that the IHTA could be quantitative.

Research by Iranmanesh *et al.* suggests that where $x = 0.4$ almost perfect ordering (rock salt ordering) is present¹⁸⁰ which could be a possible explanation to the magnetic interactions for this sample in the induction heater. The results for $x = 0.75$ and 1.00 also agree with the literature¹⁸⁰ which found that at 80 % substitution of Mo with W showed a drop in magnetic hysteresis, indicating a transition from the FM to AFM state. This is possibly due to a structural change in this series, as a change from tetragonal to monoclinic has been documented by Iranmanesh *et al.*¹⁸⁰ and the refinements shown in section 2.2 seemed to agree with the literature values and structures.

5.12.2 $\text{Sr}_2\text{CrMo}_{1-x}\text{W}_x\text{O}_6$ series

Fig. 5.38 shows the difference in maximum power needed to reach 60 °C between the $\text{Sr}_2\text{CrMo}_{1-x}\text{W}_x\text{O}_6$ samples. Table 5.22 shows the numerical values for the maximum applied power required by the samples. For this series, the samples all behaved similarly within the induction heater. All the samples within the series reached the set temperature of 60 °C, and the power input differences were negligible. The sample which required the least power to reach the set temperature was the Sr_2CrWO_6 . This was expected due to the heating of the same sample when in the H-field of the microwave system. The other samples behaved in a similar way, the exception being $\text{Sr}_2\text{CrMoO}_6$. This sample reached a temperature of 81.98 °C in the H-field of the microwave (second to Sr_2CrWO_6 which reached 88.44 °C),

Composition	Max. Applied power (%)
$\text{Sr}_2\text{CrMoO}_6$	61.4
$\text{Sr}_2\text{CrMo}_{0.9}\text{W}_{0.1}\text{O}_6$	59.5

but

$\text{Sr}_2\text{CrMo}_{0.7}\text{W}_{0.3}\text{O}_6$	58.4
$\text{Sr}_2\text{CrMo}_{0.5}\text{W}_{0.5}\text{O}_6$	56.0
$\text{Sr}_2\text{CrMo}_{0.3}\text{W}_{0.7}\text{O}_6$	63.4
$\text{Sr}_2\text{CrMo}_{0.1}\text{W}_{0.9}\text{O}_6$	64.5
Sr_2CrWO_6	52.7

required the highest percentage of applied power in order for it to heat up to 60 °C. It could be assumed that this behaviour is due to the ordering of the sample with this composition, as research suggests that while the perfect $\text{Sr}_2\text{CrMoO}_6$ shows half metallic nature, this can be easily lost due to oxygen vacancies.¹⁸¹ This phenomenon may be more obvious when analysed in the induction heater due to the heating being restricted to the outside layer,¹⁶⁶ preventing the deeper penetration of the sample which could be possible within the H-field of the microwave.

Table 5.22 Comparison of power needed to heat the different $\text{Sr}_2\text{CrMo}_{1-x}\text{W}_x\text{O}_6$ compositions to a set temperature of 60 °C.

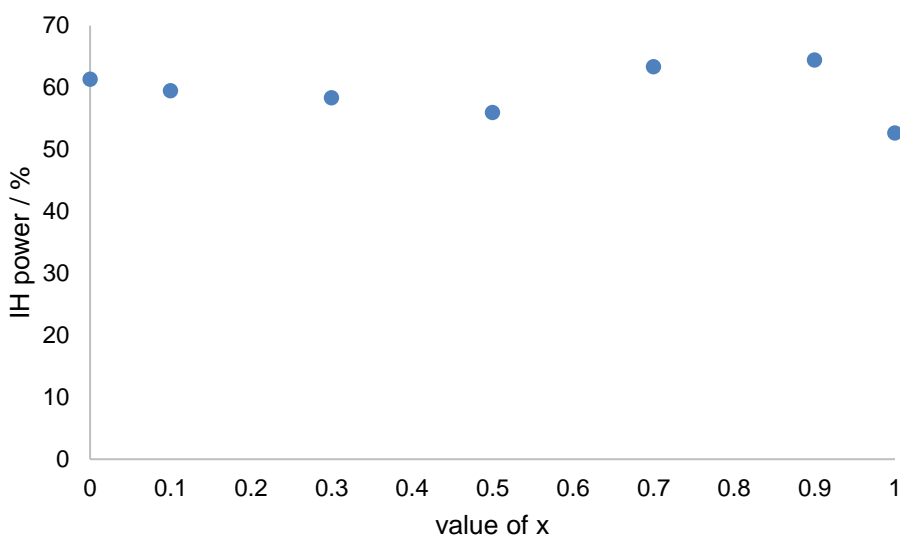


Fig. 5.38 IHTA comparison of the $\text{Sr}_2\text{CrMo}_{1-x}\text{WxO}_6$ series of samples – IH power (%) vs value of x

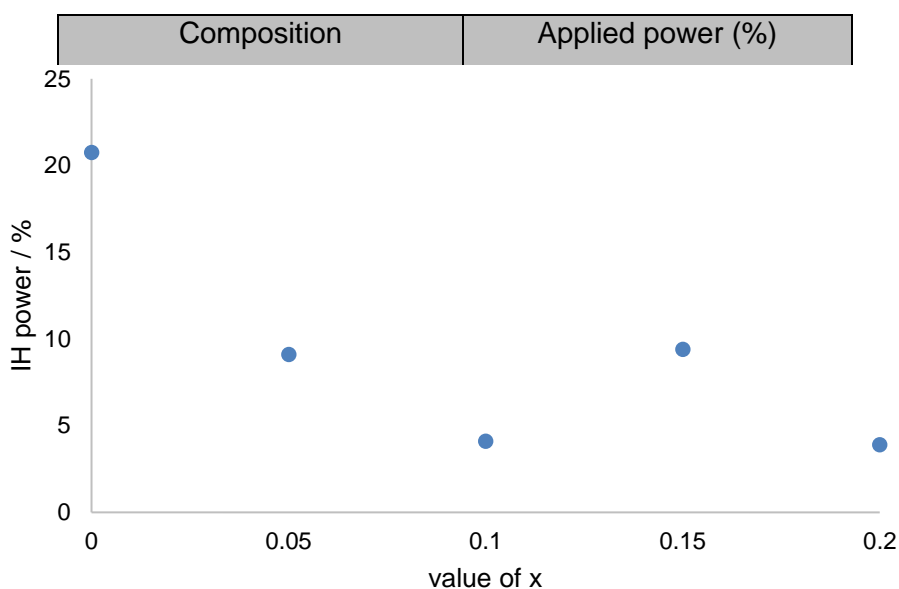
SCWO is reported to have a T_C of 390 K¹⁷⁶ and more recent research by Zhang *et al.*¹⁸² has shown that this compound has highly desirable characteristics when synthesised in a particular way. It seems that it is difficult to synthesise a pure sample and thin film experimentation has been utilised to show the magnetic capabilities of this compound. As mentioned previously, the IH automatically stopped when the sample reached 60 °C, and from fig.5.38, SCWO required the least power to reach this temperature. The new literature does help to clarify the reasoning behind this behaviour, that even though SCWO is reported to be AFM, suggestions have been made that it is a long range AFM ordering, or ferrimagnetism.¹⁸²

5.12.3 Sr_{2-x}La_xFeMoO₆

The samples in the Sr_{2-x}La_xFeMoO₆ coupled well with the H-field in the microwave, and heating was observed in all the samples, although some coupled better than others (see Section 5.11). The series was analysed using the IHTA instrument to ascertain whether these heating profiles were a product of the H-field only or whether the induced field could also heat the samples. As with Sr₂FeMoO₆, the experimental conditions used a stepwise set-point with a set temperature of 60 °C, 5 °C min⁻¹ ramp rate and a 2-minute hold between ramps. Fig 5.39 below shows the maximum power against the set temperature for this series of samples. Table 5.23 gives the numerical values corresponding to the points on the graph.

Fig. 5.39 IHTA comparison of the Sr_{2-x}La_xFeMoO₆ series of samples – value of x vs IH power (%)

Table 5.22 Comparison of power needed to heat the different Sr_{2-x}La_xMoO₆ compositions to a set temperature of 60 °C.



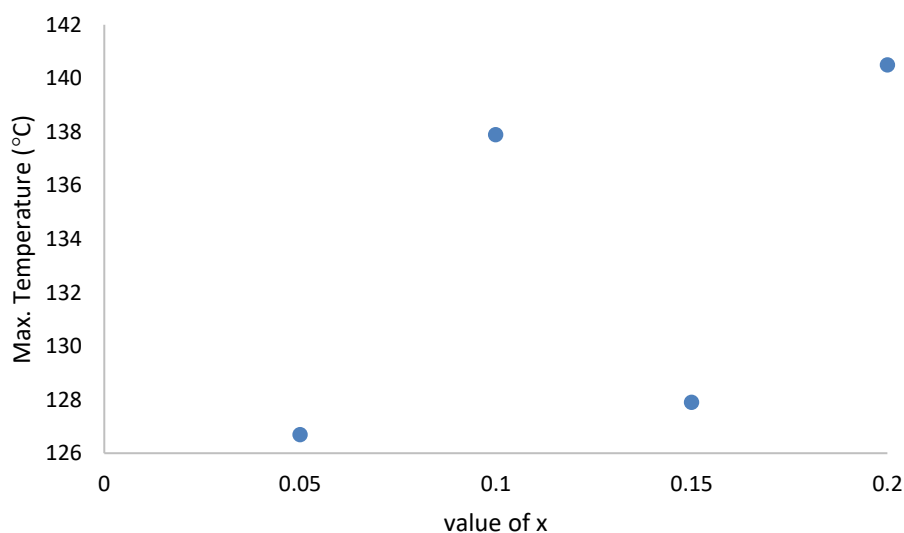
It can be seen in fig. 5.39 that the samples containing La are “paired”, depending on the amount of power required to heat to 60 °C and as observed in table 5.22, the power required to heat this series to 60 °C is extremely low, so for this reason, a second analysis was performed. This analysis had the same parameters, but the end temperature was increased to 150 °C. Fig. 5.45 and table 5.23 show the results of this experiment below.

Table 5.23 Comparison of maximum temperatures reached by the different $\text{Sr}_{2-x}\text{La}_x\text{MoO}_6$ compositions (IHTA power = 80 %)

Composition	Temperature (°C)
$\text{Sr}_{1.95}\text{La}_{0.05}\text{FeMoO}_6$	126
$\text{Sr}_{1.90}\text{La}_{0.10}\text{FeMoO}_6$	137
$\text{Sr}_{1.85}\text{La}_{0.15}\text{FeMoO}_6$	127
$\text{Sr}_{1.80}\text{La}_{0.20}\text{FeMoO}_6$	140

Fig 5.40 shows that the samples again “pair up” depending on their ability to heat in the induced magnetic field. None of the samples reached the set temperature of 150 °C, so the power stopped being applied at 80 %, however, it can be seen that two of the compositions ($x = 0.10$ and 0.20) reach a higher temperature than the other two ($x = 0.05$ and 0.15). The numerical values can be seen in table 5.23.

Fig. 5.40 IHTA comparison of the $\text{Sr}_{2-x}\text{La}_x\text{FeMoO}_6$ series of samples – value of x vs temperature (°C)



All the samples also reached a higher temperature within the IHTA instrument than they did

within the MWTA H-field, although (see table 5.24) they correspond to the heating profiles seen in the H-field i.e. the same compositions reached the higher temperatures. This does not agree with the results found with the rock salt samples, where the sample that heated least in the H-field, heated most when in the induction heater. Further research is required

to explain what type of heating is taking place within the samples and to try and explain why some samples heat well and others do not.

Table 5.24 Comparison of the maximum temperatures reached by the $\text{Sr}_{2-x}\text{La}_x\text{FeMoO}_6$ samples in the MWTA H-field and the IHTA.

Composition	H-field Max. Temp (°C)	IHTA Max. Temp (°C)	ΔT (°C)
$\text{Sr}_{1.95}\text{La}_{0.05}\text{FeMoO}_6$	89	126	37
$\text{Sr}_{1.90}\text{La}_{0.10}\text{FeMoO}_6$	115	137	22
$\text{Sr}_{1.85}\text{La}_{0.15}\text{FeMoO}_6$	91	127	36
$\text{Sr}_{1.80}\text{La}_{0.20}\text{FeMoO}_6$	109	140	30

When analysed in the E-field of the microwave, the series did not reach the higher temperatures seen in the H-field, and again, when heated in a purely magnetic field, the maximum temperatures again increased. This difference in temperature could possibly be due to the E-field having a negative effect on the coupling of the samples when in the H-field of the microwave, although this has yet to be fully determined and requires further research.

These samples coupled well in both the H-field of the microwave and in the induction heater so the samples were analysed on the IHTA using a linear experiment (see Chapter 4) and the data plotted with the data from the MWTA instrument.

It is apparent from all four of the power graphs that the power input from both instruments is directly comparable when observing the behaviour of this series. Table 4.28 below gives the values for the maximum temperatures (T_{max}) reached by each of the samples. In the cases of the linear heating (LH), the maximum power input of the microwave is 120 W, and the maximum power of the induction heater is 75%.

Table 5.25 Comparison of the maximum temperatures reached by the $\text{Sr}_{2-x}\text{La}_x\text{FeMoO}_6$ samples in the MWTA H-field and the IHTA – Linear heating.

Composition	LH MWTA T_{max} (°C)	LH IHTA T_{max} (°C)
-------------	-------------------------------	-------------------------------

$\text{Sr}_{1.95}\text{La}_{0.05}\text{FeMoO}_6$	117	119
$\text{Sr}_{1.90}\text{La}_{0.10}\text{FeMoO}_6$	116	131
$\text{Sr}_{1.85}\text{La}_{0.15}\text{FeMoO}_6$	122	120
$\text{Sr}_{1.80}\text{La}_{0.20}\text{FeMoO}_6$	137	132

It can be seen here that there is a slight anomaly to the trend of T_{max} reached by one of the samples. It was expected that $\text{Sr}_{1.90}\text{La}_{0.10}\text{FeMoO}_6$ would heat to around 130 °C, in line with the temperatures reached both by the induction heater and the $\text{Sr}_{1.80}\text{La}_{0.20}\text{FeMoO}_6$ sample. This sample was analysed three times with identical results and is thought that there was an impurity within the sample which was causing the reduced temperature. Further investigation is required to ascertain why this sample is behaving differently at this point.

The four graphs on the next page are to show the similarities and differences in the power input for the IHTA and the MWTA.

Due to the difference in frequencies of the MWTA and the IHTA instruments, power profiles have been included as an example to show that while the coupling capability of the samples in the IHTA are not directly comparable to the coupling within the MWTA, it can be observed that the power profiles for the two instruments are very similar when compared directly (fig. 5.41-5.44). The maximum temperature reached by the samples may differ due to the power input of the instrument. The wattage of the two systems is not dissimilar - 300 W for the MWTA and ~240 W for the IHTA.

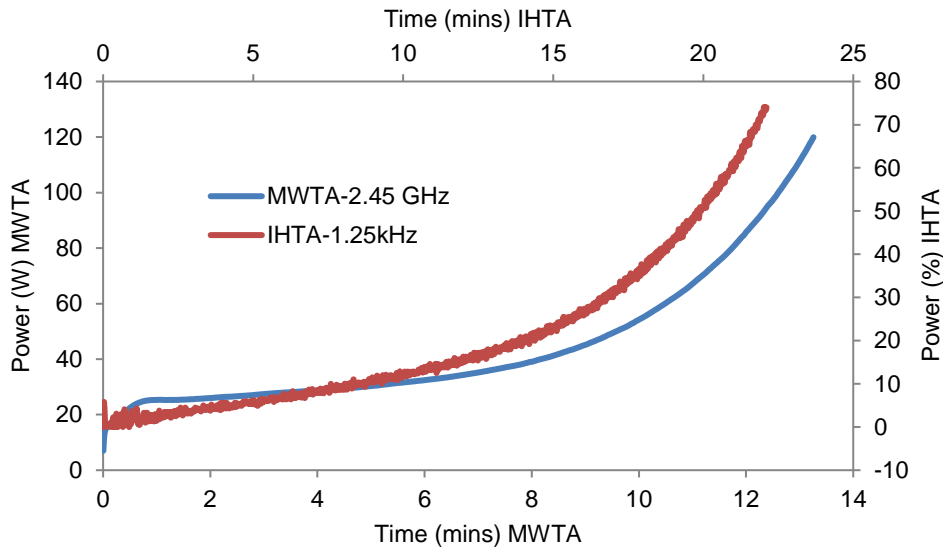


Fig. 5.41 IHTA/MWTA comparison of the $Sr_{1.80}La_{0.20}FeMoO_6$ time vs power

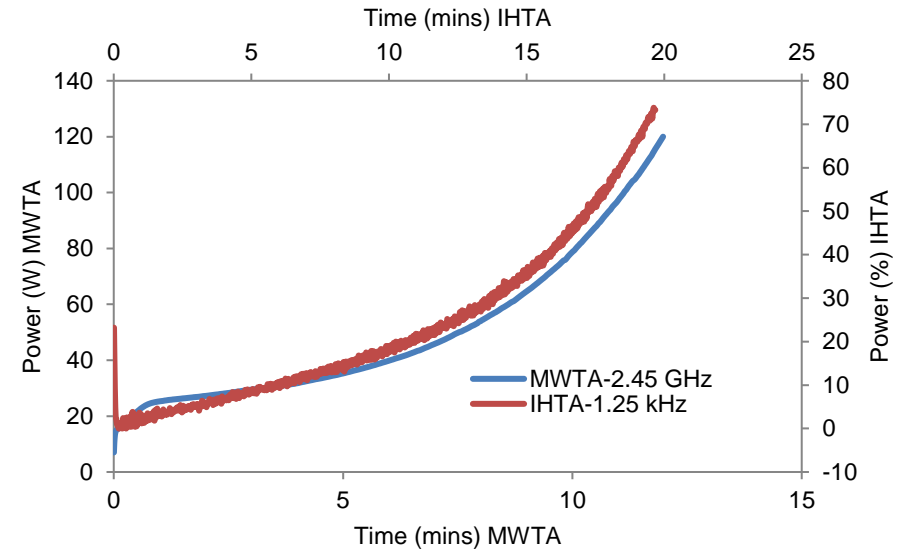


Fig. 5.42 IHTA/MWTA comparison of the $Sr_{1.85}La_{0.15}FeMoO_6$ time vs power

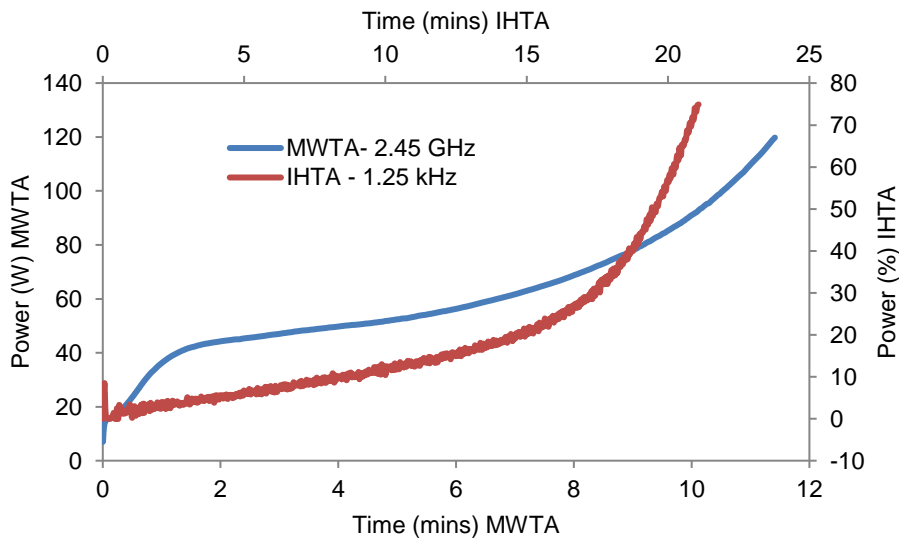


Fig. 5.43 IHTA/MWTA comparison of the $Sr_{1.90}La_{0.10}FeMoO_6$ time vs power

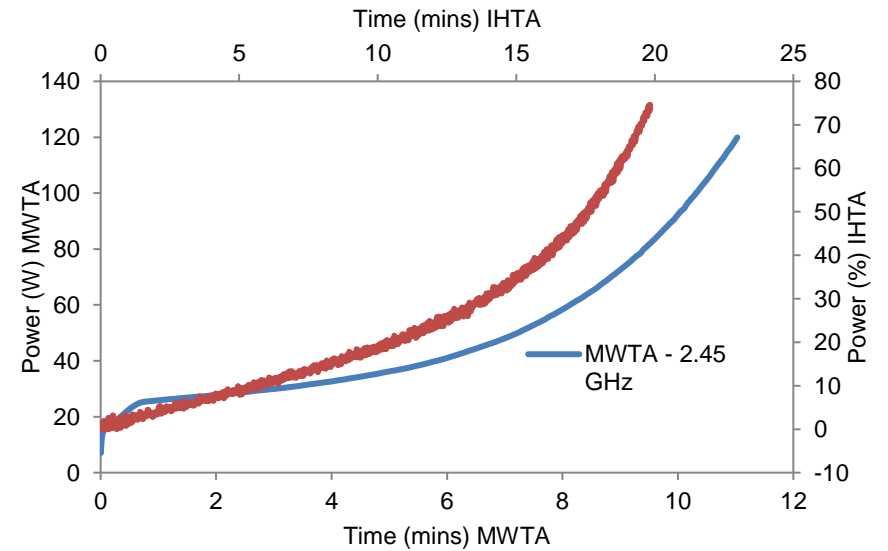


Fig. 5.44 IHTA/MWTA comparison of the $Sr_{1.95}La_{0.15}FeMoO_6$ time vs power

Chapter 6

6.0 Conclusions and Further Work

6.1 Conclusion

Using induction heating as a thermal analysis technique is a novel approach, with unique instrumentation that requires a lot of further research. However, the results gathered are extremely promising and will hopefully allow for much better characterisation of magnetic properties in the future. The most promising technique is being able to determine the T_C of a material, and this can easily be confirmed using literature values or in conjunction with TGA or DSC and it is regrettable that this was not the primary focus during this research. This technique allows a cheap alternative to the more expensive SQUID analysis and could allow users to determine magnetic characteristics before using a SQUID for confirmation – again the instrumentation is to be used in conjunction with other known analysis techniques, but gives a unique insight into the properties of new and existing materials.

6.1.1 MWTA

The adaptations made to the previous instrument and cell design have shown that it is possible to change the position of the sample within the microwave field, allowing analysis of sample interaction with the H-field. This difference in interaction and coupling of the various samples is evident in the results as the temperature differences are measured in both fields.

Fig. 5.10 in chapter 5 shows how the different metal oxides interact in both the E- and H-fields, and while it cannot be guaranteed that one field is the primary heating mode, because some compounds heat well in the E-field and not the H-field, it seems that there is a good separation of the fields within the microwave cavity.

The results from the microwave analysis, in particular the H-field data, were used to determine suitable compounds with which to test the novel IHTA instrumentation.

6.1.2 IHTA

Using a novel induction heating thermal analysis instrument, previously developed at the University of Huddersfield, the work carried out in this project has been able to demonstrate the potential for magnetic and electrical analysis of numerous materials. Using well characterised samples has enabled a direct comparison with the results shown in this work and has given a clear indication that the IHTA instrument can be utilised for investigation into T_C 's, quantitative analysis and electrical and magnetic coupling. The main development

of the instrument has taken place with the simpler metal oxides, which have shown that discrepancies in mass and volume can have an effect on the analysis, along with impurities in samples, which can change how well the samples couple in the H-field. This research could also be beneficial to industry, where induction heating is used as a manufacturing technique. Being able to determine how different materials behave within the H-field, and being able to analyse this on a smaller scale before manufacture could save a lot of time and expense to these industries.

Initial testing showed that the mass of a sample has an effect of how well the sample interacts (fig. 5.22), and subsequently heats, within the induction coil. At this point in the research, the sample size is fixed at a maximum amount, and this is dependent on the density of the sample.

Expectations were made whereby if the compound heated well within the H-field of the microwaves, it *should* heat well in the induction heater. It was found that most did heat to a set maximum temperature, but it was the power levels that were the limiting factor. The power levels were kept low for safety reasons and to protect the integrity of the instrument.

This research has also shown that the IHTA can be used in T_C determination and even though still in its infancy, has the potential to be a strong tool in conjunction with other thermal analysis techniques.

The quantitative aspect of the IHTA has been investigated with Fe_3O_4/Fe_2O_3 as initial testing with the MWTA showed Fe_3O_4 coupled well in both the E- and H-field, whereas Fe_2O_3 didn't heat at all. Similar results were found when the compounds were placed in the IHTA, with Fe_3O_4 interacting strongly with the magnetic fields, and Fe_2O_3 hardly interacting at all. Fig. 5.25 shows how well the quantitative determination of a mixture of compounds can be achieved. It is thought that it may eventually be possible to determine a weight% of Fe within a sample utilising this technique.

This novel method of thermal analysis is easily and cheaply available to build within academic institutions and industry, enabling research to continue into this analytical technique.

6.2 Further work

Due to time constraints within this research, there are a lot of aspects of the IHTA investigations which could not be explained fully.

The instrument is a completely new concept to be used within thermal analysis, and as mentioned in previous sections, the full potential of the instrument was not investigated to maintain integrity of the components. It may be possible to increase the power output of the instrument to examine previously unobserved interactions.

While the MWTA instrument has been used to determine suitable compounds for investigation with the IHTA instrument, the two are not directly comparable due to the differences in power (MWTA = 2.45 GHz, IHTA = 1.25 kHz). Where one compound may have heated well in the H-field of the MWTA, but not in the IHTA it may be due to this difference and does require further investigation as the instrument is developed further.

Curie point transitions were investigated briefly for CrO₂ and NiO. Initial analysis showed that the IHTA gave a good indication of T_C for these metal oxides but further investigations need to be conducted on a wider range of samples to determine if these trends are consistent. This is the same with the quantitative aspect of the IHTA instrument. While good trends have been found within different mixtures of Fe₃O₄/Fe₂O₃, further work is required to determine whether this trend can be replicated with different mixtures and different compounds. It would have been more beneficial to the current research to continue analysing the T_C of known materials as a direct comparison. This would have also validated the new instrument as an accurate technique for T_C determination.

Further work is required on the sample cells for both the MWTA and the IHTA. The MWTA cell for E- and H-field analysis doesn't allow for a mass to be used, only a volume, which can alter the interactions of the sample within the cavity. This needs further investigation as the IHTA has shown the mass of the sample has a direct effect on the sample interaction and therefore heating, which may affect the H-field heating of the samples in the MWTA. The cells developed for the IHTA do not always allow for smaller sample sizes, as the thermocouple is required to be in the centre of the sample to detect any heating which arises. Further development on the IHTA sample cell would address this issue and enable a wider range of samples to be analysed.

It also requires noting that some of the more complex samples behaved differently depending on the composition of the sample. These compounds, particularly the Sr_{2-x}La_xFeMoO₆ (where x = 0.05, 0.1, 0.15 and 0.2) series, may be quite susceptible to impurities within the sample. These compounds were difficult to characterise fully due to

issues with the XRD instruments which weren't available for use for an extended period of time.

As mentioned in the thesis, the frequencies on the MW and the IH are very different, and it is unknown what effect this would have when attempting to use the instruments in conjunction with one another. It would be beneficial to get the IH frequency closer to that of the microwave, if components allow, as this would give a much fairer indication of couple capabilities of the materials being analysed.

It is also worth noting that there is not a full set of refinements for the synthesised compounds due to the same issues with the analytical equipment. As part of the further work required on this research it would be beneficial to get a full set of refinements. This would enable the detection of any atom positioning that may contribute to the magnetic and electrical properties.

While this research focussed on the analysis of stock and synthesised samples, development of the instrumentation is limited as this was completed separately.

Finally and a key point to make, is the level of impurity in the synthesised samples. For future development, it is suggested that synthesis routes take the path of least impurity such as the sol-gel method. This would greatly increase the understanding of properties from the samples as it is still unknown the affect the impurities are having on the analysis, and no definitive conclusion can be made regarding the IH and MW H-field coupling capabilities.

7.0 References

- 1 B. E. Erickson, *Anal. Chem.*, 1999, **71**, 689A-692A.
- 2 D. Noble, *Anal. Chem.*, 1995, **67**, 323A-327A.
- 3 L. Voress, *Anal. Chem.*, 1994, **66**, 1035A.
- 4 D. M. P. Mingos and D. R. Baghurst, *Chem. Soc. Rev.*, 1991, **20**, 1–47.
- 5 *Microwave Processing of Materials*, The National Academies Press, 1994.
- 6 R. Appleyard, *Electr. Commun.*, 1927, **6**, 63–77.
- 7 M. I. Skolnik, History of Radar, <https://www.britannica.com/technology/radar/History-of-radar>.
- 8 Raytheon, Raytheon U.K. History.
- 9 Raytheon, Raytheon Company: History, <https://www.raytheon.com/ourcompany/history>.
- 10 A. C. Metaxas, R. J. Meredith and I. of E. Engineers, *Industrial microwave heating*, Peregrinus on behalf of the Institution of Electrical Engineers, London, 1983.
- 11 L. Waters, S. Bedford and G. B. Parkes, *AAPS PharmSciTech*, 2011, **12**, 1038–1043.
- 12 T. Zerner, Phys. Microw. Ovens.
- 13 SimScale, What is Joule heating?
- 14 G. M. B. Parkes, P. A. Barnes, E. L. Charsley and G. Bond, *J. Therm. Anal. Calorim.*, 1999, **56**, 723–731.
- 15 G. Rupprecht and R. O. Bell, *Phys. Rev.*, 1962, **125**, 1915–1920.
- 16 N. Standish, H. K. Worner and D. Y. Obuchowski, *Powder Technol.*, 1991, **66**, 225–230.
- 17 M. Tanaka, M. Ignatenko, H. Kono, K. Maruyama and Y. Zempo, in *Materials Science and Technology Conference and Exhibition 2010, MS and T'10*, 2010, vol. 4, pp. 2903–2906.
- 18 M. Tanaka, H. Kono and K. Maruyama, *Phys. Rev. B - Condens. Matter Mater. Phys.*, , DOI:10.1103/PhysRevB.79.104420.
- 19 M. Hayashi, Y. Yokoyama and K. Nagata, *J. Microw. Power Electromagn. Energy*, 2010, **44**, 198.
- 20 C. A. Crane, M. L. Pantoya, B. L. Weeks and M. Saed, *Powder Technol.*, 2014, **256**, 113–117.
- 21 E. Karmazsin, R. Barhoumi, P. Satre and F. Gaillard, *J. Therm. Anal.*, 1985, **30**, 43–47.
- 22 E. Karmazsin, *Thermochim. Acta*, 1987, **110**, 289–295.
- 23 G. M. B. Parkes, P. A. Barnes, E. L. Charsley and G. Bond, *Anal. Chem.*, 1999, **71**, 5026–5032.
- 24 G. M. B. Parkes, G. Bond, P. A. Barnes and E. L. Charsley, *Rev. Sci. Instrum.*
- 25 I. Hamilton, University of Huddersfield, 2009.
- 26 V. Rudnev, D. Loveless, R. Cook and M. Black, *Handbook of Induction Heating*, Marcel Dekker, Inc., New York, 2003.
- 27 S. Zinn and S. L. Semiatin, *Elements of Induction Heating*, Carnes Publication Services, 1988.
- 28 GH Group, GH IA Induction Heating Guide.

- 29 GH Induction Atmospheres, What is induction heating?, http://www.gh-ia.com/induction_heating.html.
- 30 R. E. Haimbaugh, *Practical Induction Heat Treating*, A S M International, 2001.
- 31 G. D. Ngantso, A. Benyoussef, A. El Kenz and S. Naji, *J. Supercond. Nov. Magn.*, 2015, **28**, 2589–2596.
- 32 J.-W. G. Bos and J. P. Atfield, *Chem. Mater.*, 2004, **16**, 1822–1827.
- 33 S. Benci, M. Manfredi and G. C. Salviati, *Solid State Commun.*, 1980, **33**, 679–682.
- 34 T. S. Chan, R. S. Liu, S. F. Hu and J. G. Lin, *Mater. Chem. Phys.*, 2005, **93**, 314–319.
- 35 R. J. D. Tilley, 2016.
- 36 T. Saitoh, M. Nakatake, H. Nakajima, O. Morimoto, A. Kakizaki, S. Xu, Y. Moritomo, N. Hamada and Y. Aiura, *J. Electron Spectros. Relat. Phenomena*, 2005, **144–147**, 601–603.
- 37 S. R. Popuri, D. Redpath, G. Chan, R. I. Smith, O. Cespedes and J.-W. G. Bos, *Dalt. Trans.*, DOI:10.1039/C4DT03307H.
- 38 D. M. Smyth, *Solid State Ionics*, 2000, **129**, 5–12.
- 39 F. Sher, A. Venimadhav, M. G. Blamire, B. Dabrowski, S. Kolesnik and J. P. Atfield, *Solid State Sci.*, 2005, **7**, 912–919.
- 40 J. E. Pask, D. J. Singh, I. I. Mazin, C. S. Hellberg and J. Kortus, , DOI:10.1103/PhysRevB.64.024403.
- 41 G. Narsinga Rao, S. Roy, C.-Y. Mou and J. W. Chen, *J. Magn. Magn. Mater.*, 2006, **299**, 348–355.
- 42 B. Ertug, *Am. J. Eng. Res.*, 2013, **2**, 1–7.
- 43 B. Jaffe, R. S. Roth and S. Marzullo, *J. Appl. Phys.*, 1954, **18**, 809–810.
- 44 J. . G. and J. . Longo, *Magnetic Properties · Magnetic and Other Properties of Oxides and Related Compounds · Part A*, Springer-Verlag, 1970.
- 45 M. Tanaka, H. Kono and K. Maruyama, .
- 46 F. Maca, J. Kudrnovsky, V. Drchal and G. Bouzerar, , DOI:10.1063/1.2936858.
- 47 M. Bibes and A. Barthelemy, *IEEE Trans. Electron Devices*, 2007, **54**, 1003–1023.
- 48 E. Bordes-Richard and P. Courtine, in *Metal Oxides*, CRC Press, 2005, pp. 319–352.
- 49 C. N. R. Rao and B. Raveau, *Transition metal oxides*, VCH, New York, 1995.
- 50 K. Conder, *Lab. Dev. methods, Paul Scherrer Inst.*
- 51 S. J. Pearton, W. H. Heo, M. Ivill, D. P. Norton and T. Steiner, *Semicond. Sci. Technol.*, 2004, **19**, R59–R74.
- 52 Y.-H. Chou, A. J. Morgan, N. S. Hondow, R. Brydson and R. E. Douthwaite, *Dalt. Trans.*, 2010, **39**, 6062–6066.
- 53 P. A. Cox, *Transition metal oxides: an introduction to their electronic structure and properties*, Clarendon, Oxford, 1992, vol. 27.
- 54 N. Nuraje, R. Asmatulu and S. Kudaibergenov, *Curr. Inorg. Chem.*, 2012, **2**, 124–146.

- 55 C. N. R. Rao and G. V. Subba Rao., *Transition Metal Oxides*, Washington, 1974.
- 56 A. Wold and K. Dwight, *Solid State Chemistry: Synthesis, Structure and Properties*, Chapman and Hall, 1993.
- 57 B. V Lotsch, *Angew. Chemie Int. Ed.*, 2014, **53**, 635–637.
- 58 U. Muller, *Inorganic Structural Chemistry*, Wiley, Chichester, 2007.
- 59 M. Johnsson and P. Lemmens, *Handb. Magn. Adv. Magn. Mater.*
- 60 R. H. Mitchell, *Perovskites: Modern and Ancient*, Almaz Press Incorporated, 2002.
- 61 A. Kahoul, A. Azizi, S. Colis, D. Stoeffler, R. Moubah, G. Schmerber, C. Leuvrey and A. Dinia, *J. Appl. Phys.*, 2008, **104**.
- 62 E. Burzo, I. Balasz, M. Valeanu and I. G. Pop, *J. Alloys Compd.*, 2011, **509**, 105–113.
- 63 K. I. Kobayashi, T. Kimura, H. Sawada, K. Terakura and Y. Tokura, *Nature*, 1998, **395**, 677–680.
- 64 D. D. Sarma, E. V Sampathkumaran, S. Ray, R. Nagarajan, S. Majumdar, A. Kumar, G. Nalini and T. N. Guru Row, *Solid State Commun.*, 2000, **114**, 465–468.
- 65 T. Saha-Dasgupta, *J. Supercond. Nov. Magn.*, 2013, **26**, 1991–1995.
- 66 R. S. Roth, *J. Res. Nat. Bur. Stand*, 1957, **58**, 75–88.
- 67 E. A. WOOD, *Acta Cryst*, 1951, **4**, 353.
- 68 G. H. Jonker and J. H. Van Santen, *Physica*, 1950, **16**, 337–349.
- 69 C. Zener, *Phys. Rev.*, 1951, **82**, 403–405.
- 70 C. Zener, *Phys. Rev.*, 1951, **81**, 440–444.
- 71 2691738, 1954.
- 72 D. Lybye, F. W. Poulsen and M. Mogensen, *Solid State Ionics*, 2000, **128**, 91–103.
- 73 J. Valasek, *Phys. Rev.*, 1921, **17**, 475–481.
- 74 A. von Hippel, R. G. Breckenridge, F. G. Chesley and L. Tisza, *Ind. Eng. Chem.*, 1946, **38**, 1097–1109.
- 75 G. A. Rossetti Jr, L. E. Cross and J. P. Cline, *J. Mater. Sci.*, 1995, **30**, 24–34.
- 76 M. J. Polking, A. P. Alivisatos and R. Ramesh, *MRS Commun.*, 2015, **5**, 27–44.
- 77 B. O'Regan and M. Gratzel, *Nature*, 1991, **353**, 737–740.
- 78 M. T. Anderson, K. B. Greenwood, G. A. Taylor and K. R. Poeppelmeier, *Prog. Solid State Chem.*, 1993, **22**, 197–233.
- 79 C. J. Howard and H. T. Stokes, *Acta Crystallogr. Sect. B*, 1998, **54**, 782–789.
- 80 G. King and P. M. Woodward, *J. Mater. Chem.*, 2010, **20**, 5785–5796.
- 81 B. P. Burton and E. Cockayne, *Phys. Rev. B - Condens. Matter Mater. Phys.*, 1999, **60**, R12542–R12545.
- 82 D. Sarma, *Curr. Opin. Solid State Mater. Sci.*, 2001, **5**, 261–268.
- 83 S. Stramare, V. Thangadurai and W. Weppner, *Chem. Mater.*, 2003, **15**, 3974–3990.
- 84 A. Arulraj, K. Ramesha, J. Gopalakrishnan and C. N. R. Rao, *J. Solid State Chem.*, 2000, **155**,

233–237.

- 85 M. W. Lufaso, P. W. Barnes and P. M. Woodward, *Acta Crystallogr. Sect. B*, 2006, **62**, 397–410.
- 86 J. N. Lalena and D. A. Cleary, *Principles of Inorganic Materials Design*, John Wiley & Sons Inc, US, 2010, vol. 2nd; 2; 2n.
- 87 P. M. Woodward, *Acta Crystallogr. Sect. B*, 1997, **53**, 44–66.
- 88 A. M. Glazer, *Acta Crystallogr. Sect. B*, 1972, **28**, 3384–3392.
- 89 A. R. Von Hippel, *Dielectric materials and applications: papers by twenty-two contributors*, Published jointly by the Technology Press of M. I. T. ; Wiley, Cambridge : New York, 1954.
- 90 M. Thirumal, I. N. Jawahar, K. P. Surendiran, P. Mohanan and A. K. Ganguli, *Mater. Res. Bull.*, 2002, **37**, 185–191.
- 91 S. Hirano, T. Hayashi and A. Hattori, *J. Am. Ceram. Soc.*, 1991, **74**, 1320–1324.
- 92 H. Tamura, *J. Eur. Ceram. Soc.*, 2006, **26**, 1775–1780.
- 93 A. Belous, O. Ovchar, D. Durylin, M. Valant, M. Macek-Krzmanec and D. Suvorov, *J. Eur. Ceram. Soc.*, 2007, **27**, 2963–2966.
- 94 H. Su and S. Wu, *Mater. Lett.*, 2005, **59**, 2337–2341.
- 95 A. Dias, G. Subodh, M. T. Sebastian, M. M. Lage and R. L. Moreira, *Chem. Mater.*, 2008, **20**, 4347–4355.
- 96 Y. Q. Lin and X. M. Chen, *J. Am. Ceram. Soc.*, 2011, **94**, 782–787.
- 97 V. Ting, Y. Liu, L. Norén, R. L. Withers, D. J. Goossens, M. James and C. Ferraris, *J. Solid State Chem.*, 2004, **177**, 4428–4442.
- 98 S. M. Said, M. F. M. Sabri and F. B. T.-R. M. in M. S. and M. E. Salleh, Elsevier, 2017.
- 99 C. R. Nave, Ferromagnetism, <http://hyperphysics.phy-astr.gsu.edu/hbase/hph.html>.
- 100 Boundless Chemistry, Diamagnetism and Paramagnetism.
- 101 D. Serrate, J. M. De Teresa and M. R. Ibarra, *J. Phys. Condens. Matter*, 2007, **19**, 23201.
- 102 R. E. Cohen, *Nature*, 1992, **358**, 136–138.
- 103 J. Longo and R. Ward, *J. Am. Chem. Soc.*, 1961, **83**, 2816–2818.
- 104 A. W. Sleight, J. Longo and R. Ward, *Inorg. Chem.*, 1962, **1**, 245–250.
- 105 F. K. Patterson, C. W. Moeller and R. Ward, *Inorg. Chem.*, 1963, **2**, 196–198.
- 106 E. O. Wollan, *Phys. Rev.*, 1960, **117**, 387–401.
- 107 T. K. Mandal, C. Felser, M. Greenblatt and J. Kubler, , DOI:10.1103/PhysRevB.78.134431.
- 108 C. L. Yuan, S. G. Wang, W. H. Song, T. Yu, J. M. Dai, S. L. Ye and Y. P. Sun, *Appl. Phys. Lett.* , 1999, **75**, 3853.
- 109 T. Sugahara, M. Ohtaki and K. Suganuma, *J. Asian Ceram. Soc.*, 2013, **1**, 282–288.
- 110 M.-R. Li, M. Retuerto, Z. Deng, P. W. Stephens, M. Croft, Q. Huang, H. Wu, X. Deng, G. Kotliar, J. Sanchez-Benitez, J. Hadermann, D. Walker and M. Greenblatt, *Angew. Chemie*, 2015, **127**, 12237.

- 111 P. Majewski, S. Geprägs, A. Boger, M. Opel, A. Erb, R. Gross, G. Vaitheeswaran, V. Kanchana, A. Delin, F. Wilhelm, A. Rogalev, L. Alff, M. Tillämpad, Kth, M. Skolan för industriell teknik och and Materialvetenskap, *Phys. Rev. B - Condens. Matter Mater. Phys.*
- 112 M. Sparks, *Google Patents US1367124*.
- 113 J. R. Woodyard, *Google Patents US2530110*.
- 114 S. Shirasaki, *Solid State Commun.*, 1971, **9**, 1217–1220.
- 115 M. T. Buscaglia, M. Viviani, V. Buscaglia, C. Bottino and P. Nanni, *J. Am. Ceram. Soc.*, 2002, **85**, 1569–1575.
- 116 A. Pelaiz-Barranco, Y. Mendez-Gonzalez, D. C. Arnold, D. J. Keeble and P. Saint-Gregoire, .
- 117 J. Philipp, P. Majewski, L. Alff, A. Erb, R. Gross, T. Graf, M. Brandt, J. Simon, T. Walther, W. Mader, D. Topwal and D. Sarma, *Phys. Rev. B*, , DOI:10.1103/PhysRevB.68.144431.
- 118 A. SALEM, M. MOKHTAR and G. ELSHOBAKY, *Solid State Ionics* , 2004, 170, 33–42.
- 119 A. R. Denton and N. W. Ashcroft, *Phys. Rev. A*, 1991, **43**, 3161–3164.
- 120 R. Shirley, The CRYSFIRE System for Automatic Powder Indexing, <http://www.ccp14.ac.uk/tutorial/crys/index.html>.
- 121 A. C. Larson Von Dreele, R.B, General Structure Analysis System (GSAS), <http://www.ccp14.ac.uk/solution/gsas/>.
- 122 P. J. Haines and G. R. Heal, 2002.
- 123 W. C. Roberts-Austen, *Proc. Inst. Mech. Eng.*, 1899, **56**, 35–102.
- 124 Norton, F.,H., *J. Am. Ceram. Soc.*, 1939, **22**, 54–64.
- 125 Boersma, S., L., *J. Am. Ceram. Soc.*, 1955, **38**, 281–284.
- 126 G. M. B. Parkes, P. A. Barnes, G. Bond and E. L. Charsley, *Thermochim. Acta*, 2000, **356**, 85–96.
- 127 R. Gedye Smith, F., Westaway, K., *J. Microw. Power Electromagn.*, 1991, **26**, 3–17.
- 128 S. Z. De Ferranti, 1910.
- 129 O. A. Colby, 1921.
- 130 F. A. Kjellin, 1905.
- 131 Kevin.F, Effect of Increasingly High Frequency on Induction Heating.
- 132 O. Lucía, P. Maussion, E. J. Dede and J. M. Burdío, *IEEE Trans. Ind. Electron.*, 2014, **61**, 2509–2520.
- 133 C. Gómez-Polo, S. Larumbe, L. F. Barquín and L. R. Fernández, *J. Nanoparticle Res.*, 2016, **18**, 1–9.
- 134 Powder X-ray Diffraction, http://chemwiki.ucdavis.edu/Analytical_Chemistry/Instrumental_Analysis/Diffraction/Powder_X-ray_Diffraction.
- 135 B. L. and C. Dutrow C.M., X-Ray Powder Diffraction (XRD), <http://serc.carleton.edu/18400>.
136. Haynes W, M, *CRC handbook of chemistry and physics*, 2011.

- 137 A. S. Garde, *ASCE*, 2014, **3**, 18.
- 138 I. A. Garifullin, N. N. Garif'yanov, V. Y. Maramzin and G. G. Khaliullin, *Solid State Commun.*, 1993, **85**, 1001–1004.
- 139 V. I. Anisimov, M. A. Korotin and E. Z. Kurmaev, *J. Phys. Condens. Matter*, 1990, **2**, 3973.
- 140 A. R. West, *Solid State Chemistry and Its Applications*, John Wiley & Sons Inc, Chichester, vol. 2nd; Secon.
- 141 N. C. Mallick, P., Mishra, *J. Mater. Sci.*, 2012, **2**, 66–71.
- 142 E. Antoini, *J. Mater. Sci.*, 1992, **27**, 3335–3340.
- 143 N. F. Mott, *Proc. Phys. Soc. Sect. A*, 1949, **62**, 416.
- 144 M. Lenglet, F. Hochu, J. Dürr and M. H. Tuilier, *Solid State Commun.*, 1997, **104**, 793–798.
- 145 J. Zaanen, G. A. Sawatzky and J. W. Allen, *Phys. Rev. Lett.*, 1985, **55**, 418–421.
- 146 F. H. H. and N. F. W. and Y. Z. T. and Y. S. C. and M. P. Houn, *J. Phys. D. Appl. Phys.*, 2013, **46**, 275104.
- 147 A. R. West, *Basic solid state chemistry*, Wiley, Chichester, 1999.
- 148 J. Cheng, R. Roy and D. Agrawal, *Mater. Res. Innov.*, 2002, **5**, 170–177.
- 149 J. Sun, W. Wang and Q. Yue, *Mater.*, 2016, 9.
- 150 D. Agrawal, J. Cheng, R. D. Peelamadu and R. Roy, in *Proc. Of Intl. Symp. On Microwave Science and its Application to Related Fields, Nara (Japan)*, 2002, pp. 8–9.
- 151 I. Kuryliszyn-Kudelska, W. D. Dobrowolski, Ł. Kilanski, B. Hadžić, N. Romčević, D. Sibera, U. Narkiewicz and P. Dziawa, *J. Phys. Conf. Ser.*, 2010, **200**, 72058.
- 152 H.-J. Lee, S.-Y. Jeong, C. R. Cho and C. H. Park, *Appl. Phys. Lett.*
- 153 C. N. R. Rao and F. L. Deepak, *J. Mater. Chem.*, 2005, **15**, 573–578.
- 154 J. I. Di Cosimo, V. K. Diez, C. Ferretti and C. R. Apesteguia, in *Catalysis: Volume 26*, The Royal Society of Chemistry, 2014, vol. 26, pp. 1–28.
- 155 I.-C. Ho, Y. Xu and J. D. Mackenzie, *J. Sol-Gel Sci. Technol.*, 1997, **9**, 295–301.
- 156 J.-Y. Chen, W.-H. Hsu and C.-L. Huang, *J. Alloys Compd.*, 2010, **504**, 284–287.
- 157 J. Cheng, R. Roy and D. Agrawal, *J. Mater. Sci. Lett.*, 2001, **20**, 1561–1563.
- 158 Z. P. and J.-Y. H. and M. Andriese, *Appl. Phys. Express*, 2012, **5**, 27304.
- 159 N. Cusack, *The Electrical and Magnetic Properties of Solids: An Introductory Textbook*, 1958.
- 160 C. Kittel, *Introduction to solid state Physics*, Wiley, 1996.
- 161 P. Samarasekara, *GESJ Phys.*, 2010, **2**, 3–8.
- 162 R. S. Bhalerao-Panajkar, M. M. Shirolkar, R. Das, T. Maity, P. Poddar and S. K. Kulkarni, *Solid State Commun.*, 2011, **151**, 55–60.
- 163 G. V Subba Rao, B. M. Wanklyn and C. N. R. Rao, *J. Phys. Chem. Solids*, 1971, **32**, 345–358.
- 164 V. G. Bhide and R. H. Dani, *Physica*, 1961, **27**, 821–826.
- 165 S. Gallego, J. I. Beltrán, J. Cerdá and M. C. Muñoz, *J. Phys. Condens. Matter*, 2005, **17**,

L451–L457.

- 166 P. Kapranos, in *Light Metal Age [H.W. Wilson - AST]*, H.W. Wilson - Applied Science & Technology Abstracts, 1996, vol. 54, p. 72.
- 167 S. Roberts, *Phys. Rev.*, 1951, **83**, 1078.
- 168 S. Sawaguchi, E., Maniwa, H., Hoshino, *Phys. Rev.*, 1951, **83**, 1078.
- 169 I. N. Apostolova, A. T. Apostolov, S. G. Bahoosh and J. M. Wesselinowa, *J. Appl. Phys.*, 2013, **113**, 4–7.
- 170 V. A. Chaudhari and G. K. Bichile, *Smart Mater. Res.*, 2013, 2013, 1–9.
- 171 J. B. and J. A. R. and A. Reznik, *J. Phys. Condens. Matter*, 2013, **25**, 475801.
- 172 C. Lee, P. Ghosez and X. Gonze, *Phys. Rev. B*, 1994, **50**, 13379–13387.
- 173 M.-T. Wang, T.-H. Wang and J. Y. Lee, *Microelectron. Reliab.*, 2005, **45**, 969–972.
- 174 AZO Materials, Zirconia - ZrO₂, Zirconium Dioxide.
- 175 E. Carvajal, O. Navarro, R. Allub, M. Avignon and B. Alascio, *Eur. Phys. J. B - Condens. Matter Complex Syst.*, 2005, **48**, 179–187.
- 176 J. B. Philipp, D. Reisinger, M. Schonecke, A. Marx, A. Erb, L. Alff, R. Gross and J. Klein, *Appl. Phys. Lett.*
- 177 J. B. Philipp, P. Majewski, L. Alff, A. Erb, R. Gross, T. Graf, M. S. Brandt, J. Simon, T. Walther, W. Mader, D. Topwal and D. D. Sarma, *Phys. Rev. B*, 2003, **68**, 144431.
- 178 I. Hussain, M. S. Anwar, J. W. Kim, K. C. Chung and B. H. Koo, *Ceram. Int.*, 2016, **42**, 13098–13103.
- 179 C. M. P. Kapranos, R.C. Gibson, D.H. Kirkwood, Sellars, in *4th International Conference on Semi-Solid Processing of Alloys and Composites*, ed. P. Kirkwood, D.H. and Kapranos, Sheffield, 1996, p. 148.
- 180 M. Iranmanesh, M. Lingg, M. Stir and J. Hulliger, *RSC Adv.*, 2016, 6, 42069–42075.
- 181 Q. F. L. and X. F. Z. and L. F. Chen, *J. Phys. Condens. Matter*, 2008, **20**, 255230.
- 182 J. Zhang, W.-J. Ji, J. Xu, X.-Y. Geng, J. Zhou, Z.-B. Gu, S.-H. Yao and S.-T. Zhang, *Sci. Adv.*, , DOI:10.1126/sciadv.1701473.